Characterisation and modelling of stress-dependent permeability and flow in shallow fractured rock aquifers

Luke Mortimer
B.Sc. (Hons)

As a requirement in full for the degree of
Doctor of Philosophy in the
School of the Environment
Faculty of Science and Engineering
Flinders University

September 2011

A groundwater observation well at the Wendouree Winery, Clare Valley, South Australia.

Table of Contents

List of Tables

List of Figures

Summary

In situ stress can exert a significant control on fluid flow patterns in fractured rocks with relatively low matrix permeability. In addition to overall reduction in rock mass permeability, fracture deformation results in preferential flow along fractures oriented orthogonal to the minimum principal stress direction (due to low normal stress) or inclined ~30^{o} to the maximum principal stress direction (due to dilation). As fracture void geometries and the connectivity of a flow network change in response to changing *in situ* stress, the storage, permeability and flow pattern should also be expected to change in magnitude, heterogeneity and/or anisotropy. These influences of *in situ* stress on the absolute and relative magnitudes and spatial distribution of the components of the permeability tensor are well documented for applications at depth but have received little attention at shallow to near surface settings. Groundwater flow modelling of shallow (<200 m) fractured rock aquifers is typically conducted under the assumption that permeability is independent of the stress state i.e. fluid flow is taking place within an effectively non-deforming medium. The potential influence of stress on fracture permeability at shallow depths might also be considered weak owing to the relatively low overburden pressures. This is perhaps the main reason why the effects of stress fields are largely ignored in shallow depth hydrogeological investigations. The question as to what extent this assumption holds at shallow to near surface depths is the main focus of this body of research.

Stress-related effects on groundwater flow at shallow depths are difficult to identify and characterise due to the complex interactions between all of the inherent properties of a fractured rock aquifer. These properties include the factors that dominantly control groundwater flow: fracture network density, geometry, connectivity and infill. Furthermore, surface processes such as weathering, erosion and unloading alter the original hydraulic nature (connectivity, transmissivity) of fractured rock masses resulting in higher degrees of spatial heterogeneity within shallow flow systems. These processes and interactions often mask the influence of *in situ* stress fields on fracture network permeability and groundwater flow. The multitude of the influential factors means that no one method can adequately map the spatial distribution of hydraulic properties that control advective groundwater flow at

shallow depths. Therefore, any stress-dependent fracture permeability investigations require a multi-parameter, multi-disciplinary methodology including hydromechanical (HM) modelling.

This research began with a detailed geological and hydrogeological characterisation of fractured rock aquifers within the Clare Valley, South Australia. The study area is situated within a near horizontal, WNW-ESE directed regional compressional stress field that is seismically active and undergoing uplift and erosion. This area was the subject of several previous geological, geophysical and hydrogeological investigations that provided invaluable background field observations which improved model constraints and reduced the level of uncertainty. This research built on these previous studies through an integrated analysis of local area fracture networks from outcrop mapping, geotechnical drill core logging, surface and borehole geophysical surveys, borehole groundwater flow analyses and representative HM models. It demonstrated how *in situ* stress affects groundwater flow in shallow (<200 m) fractured rock aquifers and to what extent fracture hydraulic aperture distributions, fracture network connectivity and groundwater flow rates are modified via fracture deformation processes. The inclusion of representative HM models was important as field techniques such as outcrop mapping, borehole hydraulic and geophysical surveys do not fully account for sub-surface fracture deformation and HM response of a fracture network as a whole. In particular, comparison between deformed (stressed state) and undeformed (zero stress state) HM models enabled the effects of *in situ* stress to be qualified and quantified through evaluation of the measurable changes in the groundwater flow system of the original (pre-existing) versus deformed (contemporary) state of a fracture network.

This research adopted a unique philosophy and approach that demonstrates how to generate information complementary to standard hydrogeological observations, especially in areas where field hydrogeological data are limited. This concept was extended to preliminary fault stress state modelling to improve the probability of identifying zones of enhanced fault permeability, which in turn, could potentially increase productivity and reduce the uncertainty in locating fault-related fluid production targets, particularly in early stage exploration projects or in areas of unknown or complex geology.

Ultimately, this research contributes to the knowledge and understanding of the role *in situ* stress plays and of its interactions with other influential factors in determining groundwater flow in fractured rock aquifers. It also provides guidance on what are the critical datasets and how they can be measured and practically applied in the field as well as incorporated within groundwater flow models over local to regional scales.

Declaration of Originality

I certify that this thesis does not incorporate without acknowledgment any material previously submitted for a degree or diploma in any University; and that to the best of my knowledge and belief it does not contain any material previously published or written by another person except where due reference is made in the text

---

Luke Mortimer

Acknowledgements

I would like to express my deepest gratitude to my two main supervisors, Professor Craig Simmons and Associate Professor Adnan Aydin. I am deeply indebted not just for their continual academic support and guidance but also for their personal mentoring, encouragement and highly professional example. Of particular significance to me, Professor Simmons was forever enthusiastic and inspiring whilst Associate Professor Aydin voluntarily offered his time and expertise simply in his belief in me and this research project. I also wish to thank Dr Andrew Love whose early involvement, insight, support and guidance got this research project off the ground. Without them this research project would not have been possible.

I wish to thank Professor Graham Heinson for his excellent support and involvement which was of great benefit to our second journal paper.

Thanks to the staff and students of the National Centre for Groundwater Research and Training. Particular thanks go to my fellow PhD students whose company made it a great experience both academically and personally. Special thanks go to James Ward who helped me with numerous computing and programming problems.

Thanks go to my family and friends who not only encouraged me but also repeatedly asked “when are you going to finish?”. Special thanks go to Terry and Lorraine Dixon for accommodating my dog and I at their Clare Valley homestead during the field campaigns. They made field work very easy. Thanks also go to Mike Coulthard who helped me with numerous UDEC issues.

I wish to thank several institutions that supported this research. Namely Flinders University, (former) Department of Water Land and Biodiversity Conservation, Geological Survey of South Australia, University of Hong Kong and the University of Mississippi. I wish to specifically mention Tania Wilson, Brian Traegar, Don Freebairn and Wolfgang Preiss for their great support.

Further acknowledgements of specific financial and personal support are included at the end of each chapter in the same form as they appeared in each publication.

1 Introduction

1.1 Objectives

In situ stress fields are ubiquitous within the Earth's crust regardless of geological setting. Stress (σ) arises at all scales in the Earth's crust from several sources including the weight of overlying rocks, tectonic forces, fluid pressures, thermal loading and other geological phenomena such as volcanic activity, igneous intrusions etc (Engelder 1993, Hobbs *et al.* 1976, NRC 1996). In general, stress fields are inhomogeneous and defined by three mutually orthogonal principal axes of stress, which generally lie in the vertical (σ_V) and the maximum (σ_H) and minimum (σ_h) horizontal planes. In practice, far-field crustal stress regimes are classified using the Andersonian scheme, which relates the three major styles of faulting in the crust to the three major arrangements of the principal axes of stress (Anderson 1951). These stress regimes are: (a) normal faulting ($\sigma_V > \sigma_H > \sigma_h$); (b) strike-slip faulting ($\sigma_H > \sigma_V > \sigma_h$); and (c) reverse faulting ($\sigma_H > \sigma_h > \sigma_V$).

Stress acting on a fracture plane can be resolved into normal and shear stresses, which are the components of stress that act normal and parallel to a plane, respectively. In a fractured rock mass, these stresses are highly coupled and can cause fractures to deform. It is well documented that these processes occur at depth, in the order of kilometres, under conditions of high confining pressures and are often accounted for in petroleum, geothermal, nuclear repository and rock engineering studies (e.g. Barton *et al.* 1995, Finkbeiner *et al.* 1997, Gentier *et al.*, 2000; Hillis *et al.*, 1997; Hudson *et al.* 2005; Rutqvist and Stephansson 2003). However, the potential rate of fracture deformation is considered to be greatest at shallow depths where lower confining pressures result in a lesser amount of contact between fracture walls (fracture stiffness) (NRC 1996). This concept of nonlinear fracture stiffness implies that stress-dependency of fracture permeability may be expected to be greatest at shallow depths where groundwater is typically extracted. Whether this dependency would result in discernible changes in fracture permeability at the relatively low stresses prevailing at shallow depths is a complex issue that has largely been ignored in hydrogeological investigations. Presently, groundwater flow

modelling of shallow fractured rock aquifers is typically conducted under the assumption that permeability is independent of the stress state (i.e. fluid flow is taking place within a non-deforming medium) but this assumption at shallow to near surface depths remains to be fully investigated.

The influence of *in situ* stress on groundwater flow in shallow fractured rock aquifers is difficult to characterise due to the inherent complexities in fracture network geometries, densities, connectivity, infill and weathering. These intrinsic factors dominate and may, in some cases, mask any evidence of the effects of the stress field at least at depths of <200 m below the surface. The multitude of the influential factors means that no one method can adequately map the spatial distribution of hydraulic properties that control advective groundwater flow at shallow depths. Therefore, this research investigated stress-dependent fracture permeability at shallow depths through a multi-parameter, multi-disciplinary methodology including hydromechanical (HM) modelling.

This research project is based upon the fractured rock aquifers of the Clare Valley, South Australia. This is an ideal field site as it is situated within a near horizontal, WNW-ESE directed regional compressional stress field that is seismically active and undergoing uplift and erosion. Importantly, this area has been the subject of several previous geological, geophysical and hydrogeological investigations that provided invaluable background field observations which improved model constraints and reduced the level of uncertainty.

The research described in Chapters 2 and 3 demonstrate how the effects of *in situ* stress is ubiquitous and always plays some role in the behaviour of groundwater systems at shallow (<200 m) depths. Specifically, Chapters 2 and 3 are based on the same detailed integrated analysis of local area fracture networks, borehole geophysical logs, borehole groundwater yields and HM models that demonstrate that *in situ* stress does affect groundwater flow in shallow (<200 m) fractured rock aquifers by altering fracture hydraulic aperture distributions, fracture network connectivity and groundwater flow rates via fracture deformation processes. Critically, field observations are explained through the use of representative, stochastic, HM models which characterise the key physical processes involved. A

comparison between deformed (stressed state) and undeformed (zero stress state) HM models enabled the effects of *in situ* stress to be qualified and quantified through evaluation of the measurable changes in the groundwater flow system of the original (pre-existing) versus deformed (contemporary) state of a fracture network. Both chapters present a logical and robust basis for identifying, measuring, modelling and quantifying the effects of *in situ* stress at shallow depths from single well- to regional-scale datasets.

The research outcomes of Chapters 2 and 3 benefitted from the fact that their respective investigations were based upon one fractured stratigraphic unit located at one well instrumented field site. Chapter 4 builds upon these outcomes by further applying the concept of mechanical stratigraphy to an intercalated fractured sedimentary sequence to describe how stress-dependent fracture permeability differs within individual stratigraphic units and how, ultimately, this affects local groundwater flow behaviour. This is achieved through an analysis of outcrop data in conjunction with a conceptual, stochastic HM model which differentiate between the influences of the primary (or inherent) fracture network versus that of the present-day *in situ* stress field and their respective effects on bulk rock mass permeability.

This research developed a unique philosophy and approach that demonstrated how to generate structural and geomechanical information complementary to standard hydrogeological observations, especially in areas where field hydrogeologic data are limited. Chapter 5 shows how this methodology may be practically applied to preliminary fault stress state modelling that aims to improve the probability of identifying zones of enhanced, stress-related, fault permeability. Although this particular chapter focuses on a practical application of this methodology to the specific problem of geothermal fluid exploration it is just as applicable for any subsurface fluid regardless of depth.

This research contributes to the knowledge and understanding of the role *in situ* stress plays in determining groundwater flow in fractured rock aquifers through:

1. Specifically answering the complex question to what extent *in situ* stress affects groundwater flow in shallow (<200 m) fractured rock aquifers.

2. Identifying the critical datasets and how they can be best measured, practically applied and numerically modelled.
3. Differentiating the role of the inherent fracture network permeability (e.g. fracture orientation, spacing etc) versus the modifying effects of secondary processes such as subsurface fracture deformation, weathering, uplift and unloading.
4. Applying the concept of mechanical stratigraphy to describe contrasting HM effects on groundwater flow within an intercalated fractured sedimentary sequence.
5. Developing a methodology based upon structural and geomechanical datasets complimentary to standard hydrogeological field data which has many practical benefits in areas of unknown or complex geology irrespective of geological setting or depth below the surface.

This thesis is comprised of three journal papers (Chapters 2, 3 and 4) and one conference proceeding (extended abstract; Chapter 5). Each chapter contains pertinent literature reviews within their introductory sections. In their chapter order these publications are referenced as follows:

Mortimer L, Aydin A, Simmons CT, Love AJ (2011) Is *in situ* stress important to groundwater flow in shallow fractured rock aquifers? Journal of Hydrology, 399 (3-4): 185-200 [Chapter 2].

Mortimer L, Aydin A, Simmons CT, Heinson G and Love AJ (2011) The role of *in situ* stress in determining hydraulic connectivity in a fractured rock aquifer. Hydrogeology Journal, DOI 10.1007/s10040-011-0760-z [Chapter 3].

Mortimer L, Aydin A, Simmons CT, Love AJ (in prep.) Role of mechanical stratigraphy in determining groundwater flow in fractured sedimentary successions. Submitted to Hydrogeology Journal 30 June 2011 [Chapter 4].

Mortimer L, Aydin A, Simmons CT, Love AJ (2010) Targeting Faults for Geothermal Fluid Production: Exploring for Zones of Enhanced Permeability. Proceedings Australian Geothermal Conference 2010, November 16-19, 2010, Adelaide, Australia [Chapter 5].

1.2 Outline of remaining chapters

The following abstracts, directly extracted from their respective journal and conference papers, provide an outline of the content from each of the five chapters.

Chapter 2: Is *in situ* stress important to groundwater flow in shallow fractured rock aquifers?

In situ stress affects the permeability tensor of fractured rock masses at depth but its effect on shallow to near-surface fractured rock aquifers has received little attention. This is partly because stress-related effects on groundwater flow at shallow depths are difficult to identify and characterise due to the complex interactions between all of the inherent properties of a fractured rock aquifer. These properties include the factors that dominantly control groundwater flow: fracture network density, geometry, connectivity and infill. Furthermore, surface processes such as weathering, erosion and unloading alter the original hydraulic nature (connectivity, transmissivity) of fractured rock masses resulting in higher degrees of spatial heterogeneity within shallow flow systems. These processes and interactions often mask the influence of *in situ* stress fields on fracture network permeability and groundwater flow. In this study, an integrated analysis of local area fracture networks, borehole geophysical logs, borehole groundwater yields and hydromechanical models demonstrate that *in situ* stress does affect groundwater flow in shallow (<200 m) fractured rock aquifers by altering fracture hydraulic aperture distributions, fracture network connectivity and groundwater flow rates via fracture deformation processes. In particular, a comparison between representative models of deformed (stressed state) and undeformed (zero stress state) fracture networks showed that below 100 m depth, groundwater flow rates could decrease several fold under the influence of the contemporary stress field. This prediction was highly consistent with the field observations. In contrast, groundwater flow modelling of shallow fractured rock aquifers is typically conducted under the assumption that

permeability is independent of the state of stress. A key finding of this study is that *in situ* stress may be a more important control on both local and regional scale shallow groundwater flow systems than previously recognised. The methodology applied in this study also offers an alternative approach to investigating groundwater flow in fractured rock masses where field hydrogeological data are limited.

Chapter 3: The role of *in situ* stress in determining hydraulic connectivity in a fractured rock aquifer.

Fracture network connectivity is a spatially variable property that is difficult to quantify from standard hydrogeological datasets. This critical property is related to the distributions of fracture density, orientation, dimensions, intersections, apertures and roughness. These features that determine the inherent connectivity of a fracture network can be modified by secondary processes including weathering, uplift and unloading and other mechanisms that lead to fracture deformation in response to *in situ* stress. This study focussed on a fractured rock aquifer in the Clare Valley, South Australia, and found that fracture network connectivity could be discriminated from several geological, geophysical and hydrogeological field datasets at various scales including single well and local- to regional-scale data. Representative hydromechanical models of the field site were not only consistent with field observations but also highlighted the strong influence of *in situ* stress in determining the distribution of fracture hydraulic apertures and the formation of hydraulic chokes that impede fluid flow. The results of this multi-disciplinary investigation support the notion that the hydraulic conductivity of a fracture network is limited to the least hydraulically conductive interconnected fractures, which imposes a physical limit on the bulk hydraulic conductivity of a fractured rock aquifer.

Chapter 4: Role of mechanical stratigraphy in determining groundwater flow in fractured rock successions.

Fractured sedimentary rock successions can be subdivided in terms of mechanical stratigraphy, which defines a subdivision of rock into discrete intervals according to the mechanical properties which determines the deformational behaviour of each interval to an applied force. This study focussed on fractured rock aquifers of the Clare Valley, South Australia, and found that the key determinant of groundwater flow is the inherent permeability of the mechanical stratigraphy and to a lesser extent

the effects of *in situ* stress. Conceptual hydromechanical modelling demonstrated that mechanical stratigraphy governs subsurface fracture deformation processes which ultimately results in a reduction in the magnitudes of the permeability tensor of individual mechanical stratigraphy units and accordingly the bulk rock mass permeability. Mechanical decoupling and poor hydraulic connection between significantly contrasting mechanical stratigraphy could potentially modify and even inhibit cross-bed flow. Methods that map and subdivide fractured rock aquifers which capture relative fracture network permeability and heterogeneity from structural and geomechanical datasets have many practical benefits in terms of the targeting of wells and management of catchment-wide groundwater resources.

Chapter 5: Targeting faults for geothermal fluid production: exploring for zones of enhanced permeability.

Faults can potentially deliver increased geothermal fluid production by boosting the bulk permeability and fluid storage of a production zone. However, the hydromechanical properties of faults are inherently heterogeneous and anisotropic, thereby, making it challenging to distinguish between permeable and impermeable faults. This discussion paper outlines the key features that determine fault permeability and shows how the probability of locating zones of enhanced fault permeability can be improved by preliminary fault stress state modelling. It is proposed that such modelling (with appropriate level of complexity commensurate with the availability, nature and quality of data) can reduce the uncertainty and risk of exploring for fault-related geothermal targets, particularly in early stage exploration projects or in areas of unknown or complex geology.

2 Is *in situ* stress important to groundwater flow in shallow fractured rock aquifers?

2.1 Introduction

The influence of *in situ* stress on the permeability of deep-seated, fractured rock masses is well documented in studies relating to hydrocarbon and geothermal reservoirs and the siting of nuclear repositories (e.g. Gentier *et al.* 2000; Hillis *et al.* 1997; Hudson *et al.* 2005). However, the possible influence of *in situ* stress on groundwater flow at shallow to near surface depths (<200 m) is less well known. Presently, groundwater flow modelling of shallow fractured rock aquifers is typically conducted under the assumption that permeability is independent of the stress state (i.e. fluid flow is taking place within a non-deforming medium) but this assumption at shallow to near surface depths remains to be fully investigated.

In situ stress can exert a significant control on fluid flow patterns, particularly, in fractured rocks with low matrix permeability. In a key study of deep (>1.7 km) boreholes, Barton *et al.* (1995) found that stress-dependent fracture permeability manifests itself as fluid flow focussed along fractures, which are favourably aligned within the *in situ* stress field and if fractures are critically stressed, this could impart a significant permeability anisotropy to a fractured rock mass. In particular, preferential flow occurs along fractures that are oriented orthogonal to the minimum principal stress direction (due to low normal stress) or inclined ~30° to the maximum principal stress direction (due to dilation) (Barton *et al.* 1995). As fracture void geometries and the connectivity of a flow network change in response to changing *in situ* stress, the storage, permeability and flow pattern should also be expected to change in magnitude, heterogeneity and/or anisotropy.

Since the principle of stress-dependent fracture permeability was established, there have been few investigations into whether this phenomenon can be detected and predicted in the shallow to near-surface environment and what the consequences are for groundwater flow analyses. These studies have covered a range of geological environments including the three major tectonic stress regimes (normal, strike-slip

and reverse), flat and mountainous terrains and lithologies ranging from volcanic, granitic, sedimentary and metamorphic rock types (e.g. Banks *et al.* 1996; Ferrill *et al.* 1999; Henriksen and Braathen 2006; Morin and Savage 2003, Neves and Morales 2007). All of these investigations were based upon knowledge of the contemporary stress field from earthquake data and/or *in situ* borehole measurements together with fracture network characterisation from surface outcrop and/or borehole geophysical logs. These studies relied heavily on the identification of anisotropic permeability orientations from standard field techniques such as aquifer pump tests and borehole yields because anisotropic permeability orientations are considered indicative of stress-dependent permeability (e.g. Barton *et al.* 1995; Ferrill *et al.* 1999).

The majority of these previous studies did find a coincidence between orientations of the permeability anisotropy and those of favourably oriented faults and fractures with respect to the contemporary stress field (e.g. Ferrill *et al.* 1999; Henriksen and Braathen 2006; Morin and Savage 2003; Neves and Morales 2007). For example, Ferrill *et al.* (1999) outlined a method of inferring the potential permeability of faults based on their 3D geometry within the *in situ* stress field at Yucca Mountain, Nevada. This study involved an integrated approach of *in situ* borehole stress measurements, fault mapping, 3D fault stress state modelling and the identification of critically stressed (and potentially permeable) faults. Subsequent aquifer pumping tests showed that the maximum permeability direction is controlled by favourably oriented faults although this conclusion is complicated as this direction is also near coincident with the dominant fault trend in the region. However, all of these previous studies concluded that *in situ* stress fields only partially control the hydraulic conductivity of fractures with anisotropic permeability orientations largely dominated by inherent fracture network properties such as fracture density, geometry, connectivity and infill. For example, Banks *et al.* (1996) assessed groundwater yields from shallow (~40-80 m) boreholes but did not find any conclusive correlation between the directions of maximum fracture permeability and maximum principal stress despite encountering unusually high magnitudes of stress in the near surface environment. They found the hydraulic properties of fracture zones difficult to predict due to significant amounts of mineralization (*in situ* clays) within the fractures. This suggests that at shallow depths the dominant inherent properties of a fractured rock aquifer can obscure or mask the possible effects of

stress fields. The key deficiencies of these previous studies is that they do not fully account for the integrated effects of subsurface fracture deformation processes on fracture network hydraulics or adequately define to what extent groundwater flow is controlled by inherent fracture network properties versus the effect of the *in situ* stress field.

The aim of this study is to investigate the extent to which *in situ* stress fields can influence groundwater flow within shallow (<200 m) fractured rock aquifers at both local and regional scales. This study differs from the previous studies in that it explicitly links structural and geomechanical processes to groundwater flow through (a) detailed structural and hydraulic characterisation of local and regional scale fracture networks; (b) construction of representative hydromechanical (HM) models to interpolate subsurface fracture deformation and resultant groundwater flow patterns; and (c) a comparison between these models with *in situ* borehole fracture hydraulic activity data, borehole geophysical, environmental isotope and hydraulic depth profiles and regional-scale groundwater yield trends. The approach of the HM models is to demonstrate that deformation of representative, fracture network models under shallow depth conditions could provide a reasonable correlation with known groundwater flow observations. A particular objective is to gauge the potential impact of including or excluding the effects of stress fields in shallow groundwater models. This is achieved through a direct comparison between undeformed (zero stress state) and deformed (stressed state) HM models to evaluate the changes in the groundwater flow system of the original (pre-existing) versus deformed (contemporary) state of the fracture network.

2.2 Background

Stress (σ) arises at all scales in the Earth's crust from several sources including the weight of overlying rocks, tectonic forces, fluid pressures, thermal loading and other geological phenomena such as volcanic activity, igneous intrusions etc (Hobbs *et al.* 1976). In general, stress fields are inhomogeneous and defined by three mutually orthogonal principal axes of stress, which generally lie in the vertical (σ_V) and the maximum (σ_H) and minimum (σ_h) horizontal planes. In practice, far-field crustal

stress regimes are classified using the Andersonian scheme, which relates the three major styles of faulting in the crust to the three major arrangements of the principal axes of stress (Anderson 1951). These stress regimes are: (a) normal faulting ($\sigma_V > \sigma_H > \sigma_h$); (b) strike-slip faulting ($\sigma_H > \sigma_V > \sigma_h$); and (c) reverse faulting ($\sigma_H > \sigma_h > \sigma_V$).

Stress acting on a fracture plane can be resolved into normal and shear stresses, which are the components of stress that act normal and parallel to a plane, respectively. In a fractured rock mass, these stresses are highly coupled and can cause fractures to deform with the potential rate of fracture deformation considered to be greatest at shallow depths where lower confining pressures result in a lesser amount of contact between fracture walls (fracture stiffness) (NRC 1996). This concept of nonlinear fracture stiffness implies that stress-dependency of fracture permeability may be expected to be greatest at shallow depths where groundwater is typically extracted. However, whether this dependency would result in discernible changes in fracture permeability at the relatively low stresses prevailing at shallow depths is a complex issue that has been largely ignored in hydrogeological investigations.

Fracture deformation results in changes in permeability and storage because the ability of a fracture to transmit a fluid is extremely sensitive to its aperture as demonstrated by the "Cubic Law" that defines the hydraulic conductivity of an individual fracture idealized as an equivalent parallel plate opening. For an isolated test interval within a borehole, it is expressed as:

$$K_b = \frac{(2b)^3}{2B}\frac{\rho g}{12\mu} \qquad (2.1)$$

Where K_b is the bulk hydraulic conductivity ($m.s^{-1}$) (where K_b = Transmissivity/test interval length), $2b$ is the fracture aperture width (m), $2B$ is the fracture spacing (m), ρ is the fluid density ($kg.m^{-3}$), g is gravitational acceleration ($m.s^{-2}$) and μ is the dynamic viscosity of the fluid (Pa.s).

2.3 Methodology

The field site chosen for this investigation is the Wendouree Winery located within the Clare Valley, South Australia (Figure 2.1). It is an ideal field site as it is underlain by a fractured rock aquifer terrain situated within a near horizontal, WNW-ESE directed regional compressional stress field that is seismically active and undergoing uplift and erosion (Sandiford 2003). The Wendouree field site is located approximately 2 km SSE of the township of Clare and it is a well-instrumented, multi-piezometer site located within the steeply dipping, overturned, western limb of the large "Hill River Syncline" structure. It contains several observation wells ranging in depths from 60-222 m which are all located within low porosity and permeability, thinly laminated (mm to cm), carbonaceous siltstones and dolomites of the Auburn Dolomite unit (Saddleworth Formation) over an area of ~0.1 km^2 (Figure 2.2; Love 2003).

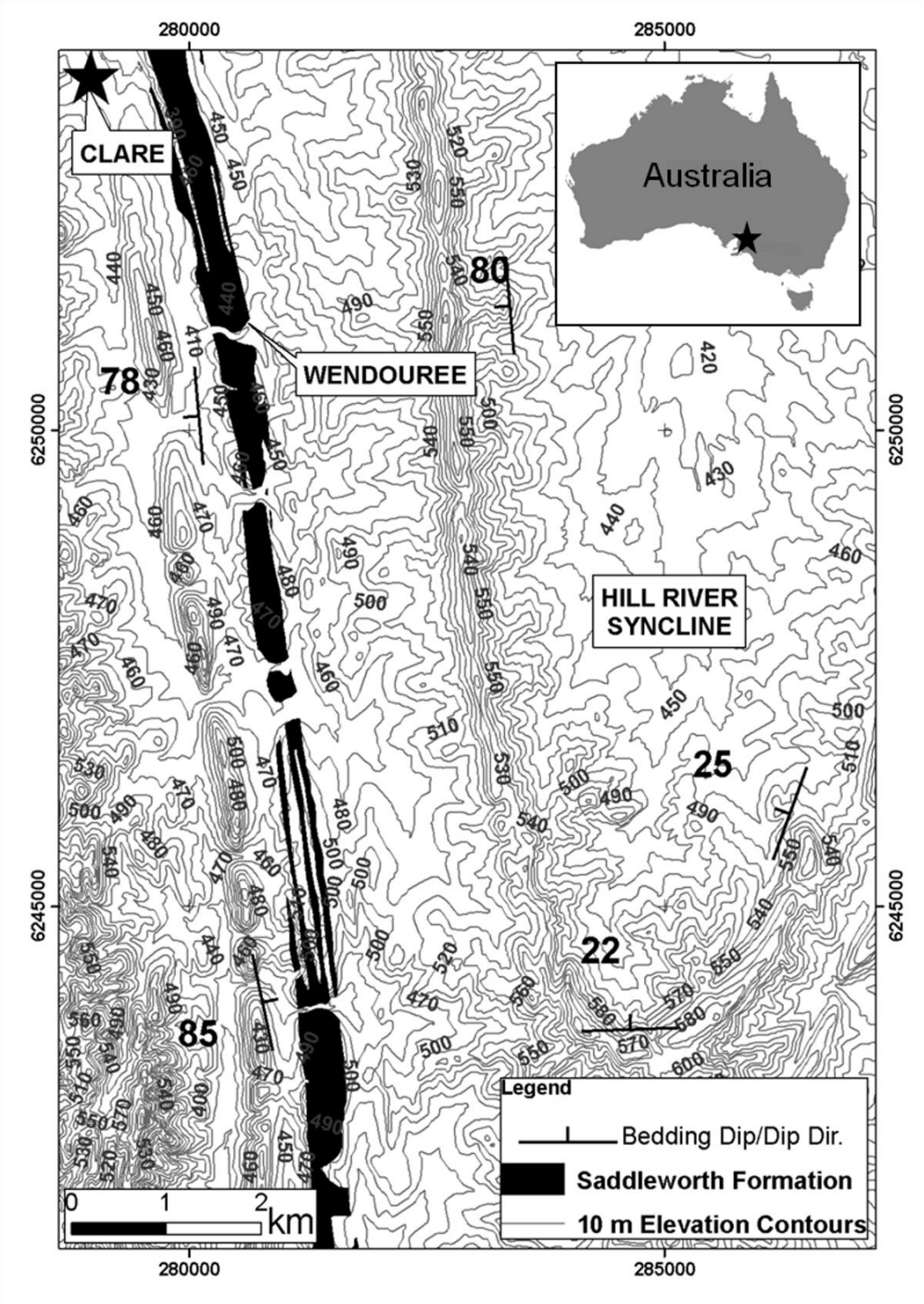

Figure 2.1 Location of the Neoproterozoic (~730 Ma) Saddleworth Formation and Wendouree field site in the Clare Valley catchment with 10 m topographic contours. The basement geology is comprised of a layered sedimentary sequence that has been folded into the large "Hill River Syncline". The Wendouree site is located on the overturned, western limb of this syncline (Geological Survey of South Australia 2001).

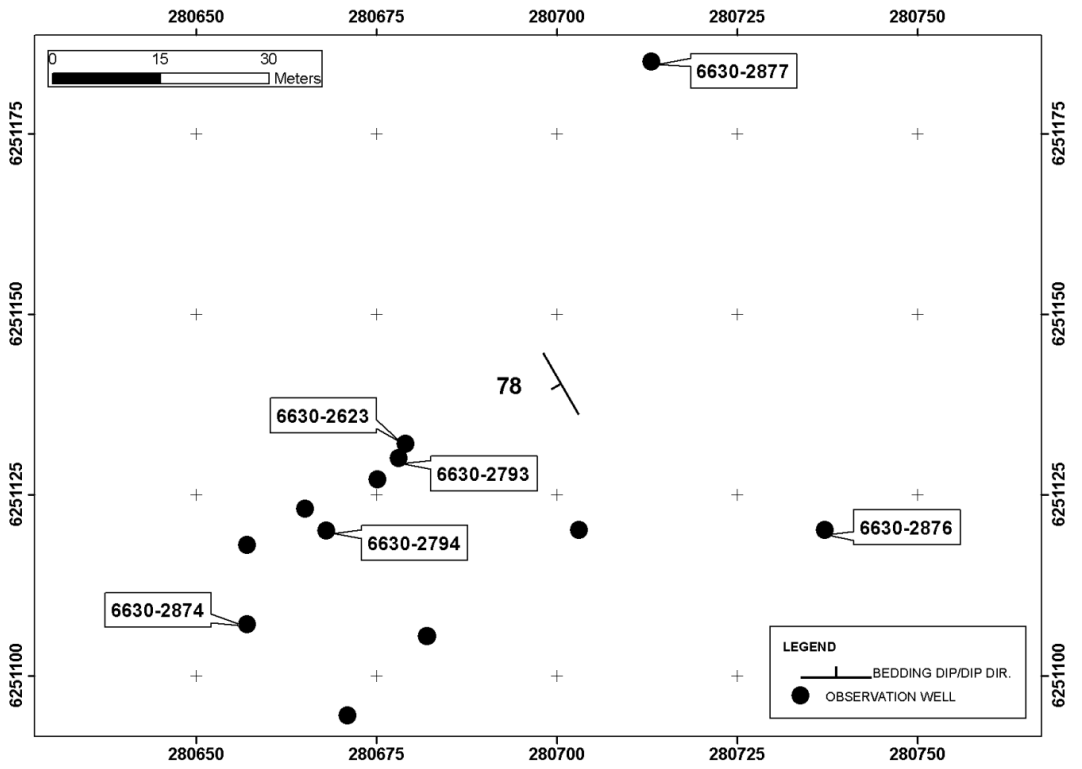

Figure 2.2 The Wendouree multi-piezometer field site in the Clare Valley showing the locations of the wells (Unit Nos.) discussed in this study (PIRSA 2009).

This study adopted a multi-disciplinary approach involving the following four key steps:

1. Geological and hydrogeological setting.

A summary review of existing data and knowledge of the local- to regional-scale geology and hydrogeology.

2. Fracture network characterisation.

As part of this study, the general style and timing of joint formation within the Hill River Syncline was first determined from mapping of selected outcrop. At Wendouree, an ALT ABI140 acoustic borehole televiewer (BHTV) which can image fractures of widths ≥1 mm was used to image *in situ* fractures within four open wells (6630-2794, -2874, -2876 and -2877) ranging from 90 to 222 m depth (Figure 2.2). Down hole temperature profiles were also collected from the same wells using a Seabird SBE39 Temperature Probe accurate to 0.001°C with temperature readings collected approximately every 3-4 cm. This data was used to calculate temperature

gradient (dT/dx) and temperature gradient difference (T-{dT/dx}) logs, which are the most useful for identifying distinct, localised, thermal anomalies. Potentially hydraulically active fractures were identified based upon the coincidence of BHTV-imaged fractures with temperature anomalies indicative of advective groundwater flow in or out of a well. In a well close to thermal equilibrium with its host rocks, high-resolution temperature profiles are useful because any distinct, localised positive or negative thermal anomalies relative to the background geothermal gradient indicate the location of groundwater flow along relatively permeable structures (Barton *et al.* 1995; Ge 1998). An evaluation of the population distribution and orientations of the interpreted hydraulically active fractures is used to identify whether an observable anisotropic fracture permeability orientation exists within the fracture network. Other rock mass and fracture parameters were gained from limited drill core samples (well 6630-3068; Figure 2.2) and pre-existing scanline fracture mapping data (T Halihan, Flinders University, unpublished data, 1999).

3. Conceptual model.

The results of Steps 1 and 2 above are used to develop a conceptual geological and hydrogeological model of the Wendouree site.

4. Hydromechanical (HM) models.

To investigate the potential effects of the contemporary stress field, representative stochastic 2D Universal Distinct Element Code (UDEC) HM models of the conceptual Wendouree model. The modelling approach is not designed to produce a precise match to the field data but rather to help demonstrate how the process of subsurface fracture deformation alters fracture network hydraulics and connectivity. UDEC represents the rock mass as an assembly of discrete deformable, impermeable blocks separated by discontinuities (faults, joints etc) and can reproduce fully coupled HM behaviour (Itasca 2004). The basic HM model predicts the physical response of a fractured rock mass to an imposed stress field and the stress-displacement relationship of the medium, while satisfying the conservation of momentum and energy in its dynamic simulations with fluid flow calculations derived from Darcy's Law (for a comprehensive review of the UDEC governing equations see Itasca 2004). In these models, rock mass deformation was defined by the Mohr-Coulomb model and fracture behaviour was defined by the Coulomb-Slip

criterion that assigns elastic stiffness, tensile strength, frictional, cohesive and dilational characteristics to a fracture (Itasca 2004).

In recent years, several researchers have successfully used UDEC to investigate the link between rock deformation and fluid flow within fractured rock masses over a range of crustal depths, stress regimes, geological settings and fracture network geometries (e.g. Cappa *et al.* 2005; Gaffney *et al.* 2007; Min *et al.* 2004b; Zhang and Sanderson 1996; Zhang *et al.* 1996). Generally, HM modelling investigations use detailed "Discrete Fracture Network" (DFN) models that test key parameters such as fracture length, density, orientation, stiffness etc over a range of values derived from observed statistical distributions (e.g. Min *et al.* 2004a, Zhang *et al.* 1996). This approach requires numerous random model simulations but provides a framework for understanding the relative influence of each parameter and their specific effect on observed processes and relationships. However, the computational limitations for codes such as UDEC restrict their practical application to either detailed small-scale (<50 m) studies or stochastic representations of larger scale problems. For example, Blum *et al.* (2009) used FRAC2D and UDEC to derive the effective permeability tensors of small scale (10 m x 10 m) DFN models, which were subsequently upscaled and used in a larger continuum model of the regional-scale (1 km x 5 km) fractured rock sequence. For this Clare Valley study, we use a stochastic geometrical model based upon real (but simplified) data inputs as the overall goal is to identify groundwater flow trends and the key features and processes that have the most influence.

2.4 Geological and hydrogeological setting

The Clare Valley catchment (~500 km^2) is located approximately 100 km north of Adelaide, South Australia, and lies within the northern Mount Lofty Ranges (Figure 2.1). The Mount Lofty Ranges forms part of the Adelaide Geosyncline, which is a Neoproterozoic to Cambrian age (~827–500 Ma), thick (>10 km), rift-related, sedimentary basin complex comprising of thinly laminated (mm) to thick (m) layered sedimentary strata (Preiss 2000). During the Middle-Late Cambrian "Delamerian Orogeny", the rocks of the Clare Valley were subjected to low-grade, greenschist

facies metamorphism and three deformation events. This was a major episode of crustal shortening leading to strongly contractional, west-verging, thrust faulting and NNW-trending folding (Preiss 2000). From the Delamerian Orogeny until the late Miocene period the Adelaide Geosyncline remained relatively tectonically stable (Preiss 1995). As southern Australia entered the late Miocene period (<10 Ma) a new phase of tectonic activity commenced, which was initiated by coupling and/or convergence between the Pacific and Australian plates (Hillis and Reynolds 2000; Sandiford *et al.* 2004). As a consequence, the Clare Valley is currently under near horizontal, approximately WNW-ESE directed compression and related seismic activity, which correlates both spatially and temporally with ongoing fault activity along major range bounding faults of the Adelaide Geosyncline (Sandiford 2003). Evidence found on some of these major range bounding faults suggest that the vertical component of their slip rates are in excess of tens of metres Myr^{-1} over the past 5 Myr leading to widespread uplift, erosion and the present-day topography of the Mount Lofty Ranges (Sandiford 2003).

There have been no *in situ* borehole stress field data collected within the Clare Valley region, therefore, this study is based upon well documented regional, far-field earthquake focal mechanism data, which are considered reliable and consistent indicators of far-field stress regimes and their orientation (Zoback 2007). In the year 2001, the town of Clare experienced nine small earthquakes up to magnitude 2.8 whilst in 1995 the nearby township of Burra recorded a significant magnitude 5.1 earthquake (PIRSA Minerals 1999; 2001). An evaluation of the focal mechanism for this particular Burra earthquake event revealed a reverse faulting stress regime with near horizontal compression (σ_H) in a direction of 110° at a depth of 18-20 km with σ_h inferred to be mutually orthogonal at 020°. Although the region is undergoing horizontal compression at depth, the uppermost shallow crust is simultaneously experiencing widespread uplift, unloading and erosion (Sandiford 2003). That is, the uplift and unloading processes affecting the Mt Lofty Ranges are concurrent with and in direct response to the far field tectonic compression. It is not known to what depth the effects of uplift and unloading occur in this region but studies elsewhere in the world have shown that it could extend a few hundreds of metres to 1 km below the surface (Engelder 1985; Hancock & Engelder 1989). The focus of this study is on

the upper 200 m depth horizon, which is inferred to be under the influence of a normal stress regime that involves isotropic, lateral relaxation of the rock mass consistent with the effects of uplift and unloading (i.e. $\sigma_V > \sigma_H = \sigma_h$). This inference is appropriate given that relaxation of the rock mass is expected to be near complete considering that the total regional uplift has been estimated at greater than 200 m and that erosion processes are known to be occurring at a rate faster than that of uplift (Sandiford 2003).

Within the Clare Valley catchment there are relatively consistent and distinctive groundwater patterns. For example, Figure 2.3 is a plot of measured well yield (normalised against the total well depth, L/s/m) for all wells recorded within the catchment versus the total depth of the well. The large majority of these wells are open and used for domestic/agricultural purposes. Compared to near surface (0-10 m depth), median groundwater yields have decreased ~3 fold and ~4 fold at approximately 40 m and 100 m depth below the surface, respectively, suggesting the existence of a hydraulic discontinuity at ~40 m depth below the surface (Figure 2.3). This regional well yield dataset is independent of lithology and position within the overall folded sequence nor can this vertical trend be explained by near-surface weathering. A review of a significant volume (hundreds) of geological water well logs of sourced from the State Government online database show that across the catchment the depth of weathering is typically <20 m below the surface (PIRSA 2009). This suggests that this vertical yield profile is probably influenced by some other regional scale factors.

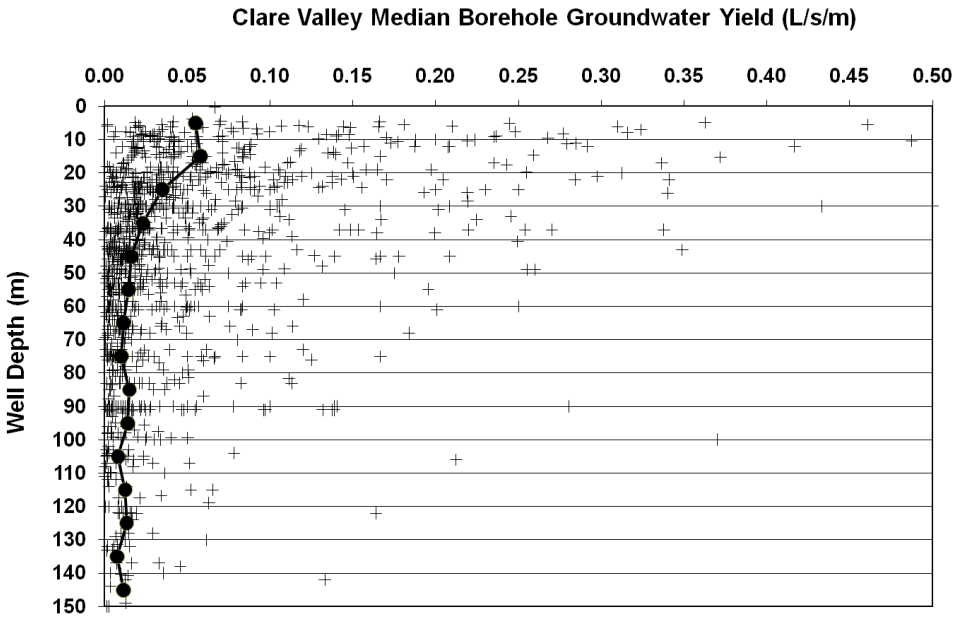

Figure 2.3 Clare Valley catchment-wide well groundwater yields whereby each well yield value was normalised against the total depth of the well then plotted against the total depth of the well (L/s/m, n=1316 drill holes). The "+" symbols represent individual data points whilst the connected solid circles represent the calculated median yield/metre for 10 m thick depth intervals below the surface (PIRSA, 2009). Note that the weathered to fresh rock transition across the catchment generally occurs at <20 m depth below the surface.

This catchment-scale trend of decreasing borehole groundwater yields with depth can also be defined in more detail within individual boreholes at the Wendouree field site. Evidence cited by Love (2003) from piezometer pumping tests and ^{222}Rn concentration depth profiles at Wendouree revealed that the hydrogeology is characterised by high spatial variances in bulk hydraulic conductivity (K_b) values and groundwater flow rates in the upper 100 m depth horizon (Figure 2.4). ^{222}Rn is produced from *in situ* decay of ^{238}U within the aquifer and because of its short half-life (3.83 days) it is used to locate zones of active groundwater flow into wells and as a proxy for lateral flow rates (Love *et al.* 2007). That is, relatively high ^{222}Rn concentrations in groundwater indicates high flow rates within fractures that rapidly transport ^{222}Rn to the well prior to it decaying below detection limits. Together, these Wendouree K_b and ^{222}Rn profiles provide an indication of transmissivities and

groundwater flow rates as a function of depth and suggest the presence of a significant discontinuity in hydraulic activity located at approximately 40 m depth below the surface that is not coincident with the known weathered to fresh rock transition located at approximately 18 m depth. The pumping test and ^{222}Rn data are supported by ^{14}C, CFC-12 and ^{3}H data collected from the same piezometers. These environmental tracers all show modern groundwater ages within the upper 40 m depth horizon indicating rapid vertical circulation whilst more ancient groundwater occurs at > 40 m depth (Love 2003). Estimates of vertical recharge rates at Wendouree from the ^{14}C groundwater age profiles were ~20 $mm.yr^{-1}$ for the upper system (<40 m depth) and <0.2 $mm.yr^{-1}$ for the lower one (>40 m depth) (Love 2003). This suggests a minimal hydraulic connection and vertical leakage between these two horizons. Regardless of depth, anomalous spikes in ^{222}Rn and ^{14}C concentrations were also found to coincide with major electrical conductivity, temperature and pH discontinuities indicating the presence of significant hydraulically active fractures and advective groundwater flow at specific down hole locations (Love 2003). However, it is clear from the data presented in Figures 2.3 and 2.4 that at shallow depths (<40 m) the system is hydraulically more active than at greater depths (>40 m).

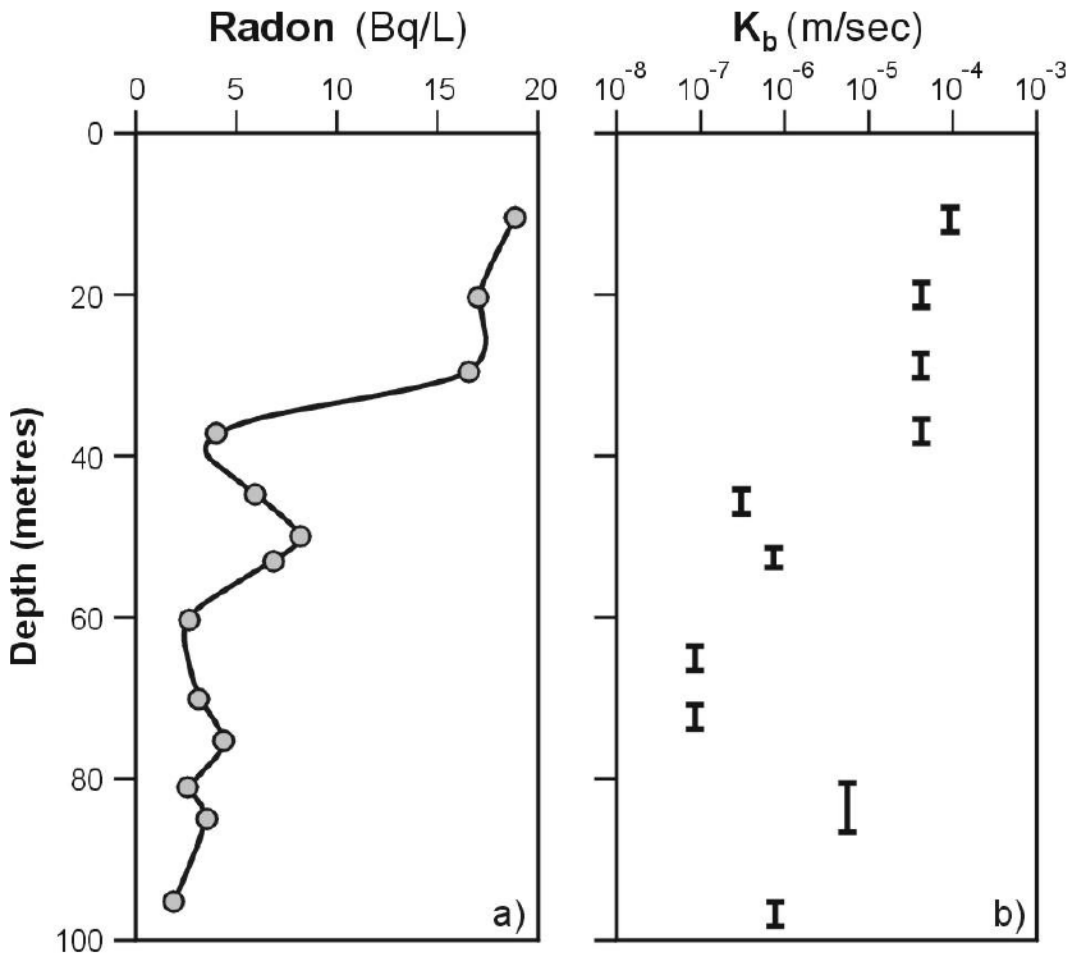

Figure 2.4 An example of ^{222}Rn and bulk hydraulic conductivity (K_b) profiles at Wendouree: (a) ^{222}Rn (Bq.L^{-1}) open well profile (well 6630-2623); and (b) K_b (m.s^{-1}) estimates from piezometer pump test (wells 6630-2623 and -2793). The vertical bars of the K_b profile represent the length of the slotted piezometer interval (Love 2003).

In a different Clare Valley study, Skinner and Heinson (2004) conducted several DC and EM surface, borehole-to-surface and borehole-to-borehole geophysical surveys at several sites including Wendouree. They used geophysical techniques to characterise fluid transport through heterogeneous fractured rocks and also concluded that there are two distinct upper and lower groundwater flow systems in the Clare Valley. In particular, they found that the most significant hydraulically conductive structures in the upper tens of metres were steeply dipping bedding planes attributed to the relaxation and enlargement of these steep structures in response to uplift and unloading. Furthermore, they found that with depth (>30 m)

vertical hydraulic conductivity was still dominant but lateral flow along a small number of extensive, low angle structures became more prevalent. Like the regional groundwater yield trend, the results of their study were consistent across all sites regardless of lithology and position within the Hill River Syncline.

2.5 Fracture network characterisation

As part of this study, outcrop mapping at several locations across the Clare Valley region found a consistent joint set pattern present within the various layered rock units of the Hill River Syncline. In addition to bedding planes, there are four joint set structures including sub-vertical "ac" (extension) joints, sub-horizontal "bc" (extension) joints and two moderately dipping conjugate "hk0" (shear) joints, which together produce a pattern typical of jointing in response to simple folding of a layered sedimentary sequence (Price 1966; van der Pluijm and Marshak 2004) during the Delamerian Orogeny. Only the joint density varied at each outcrop as determined by each rock type, thickness and position within the sequence (i.e. a stratabound joint formation pattern). It is this palaeo-stress regime and its associated deformation that is the primary control on the development of fracture networks and fracture permeability within the fractured rock aquifers of the Clare Valley.

From the four selected boreholes at Wendouree, the BHTV imaged 626 fractures, which were analysed via stereographic projection methods. This analysis revealed five distinct fracture sets as defined by ≥ 2% data density contours, labelled sets A–E (Figures 2.5a & b). This BHTV fracture dataset correlates with bedding and joint set measurements recorded from nearby outcrop and elsewhere within the Clare Valley (i.e. the five geological structures typical of the region as shown in Figure 2.6). Based upon the structural interpretation of outcrop data, the Wendouree BHTV fracture dataset is further classified in terms of their development with respect to folding (Table 2.1).

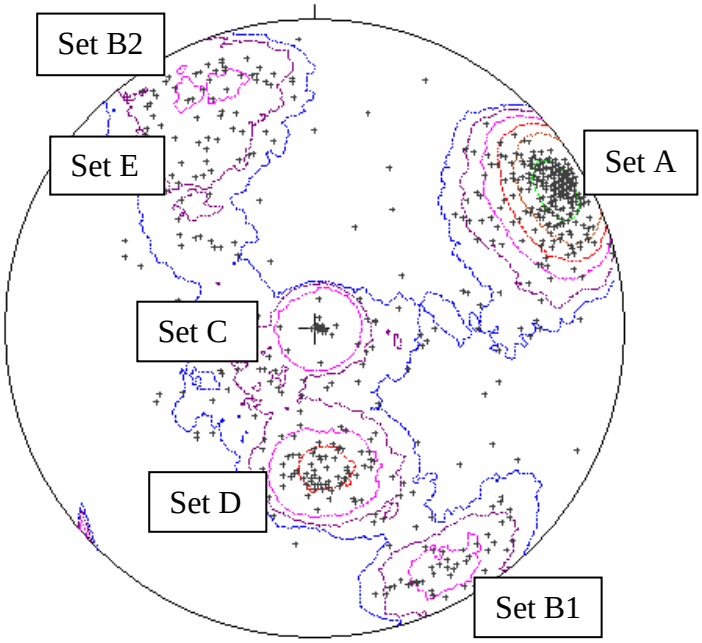

(a)

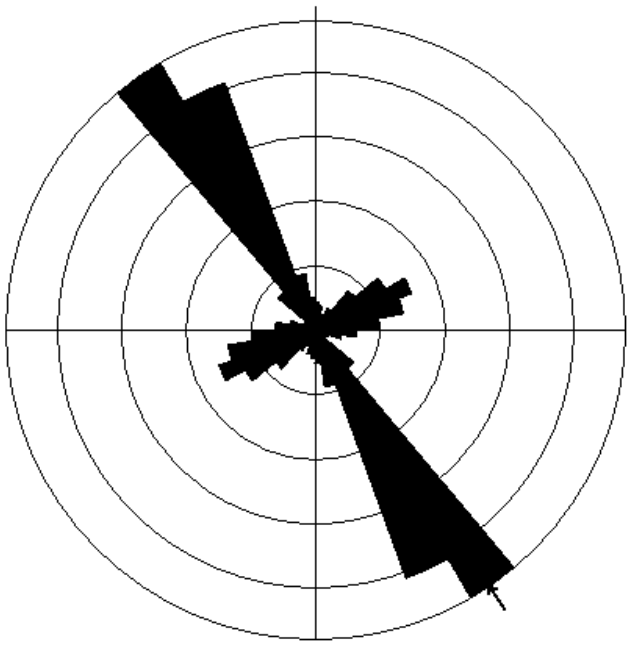

(b)

Figure 2.5 (a) Contoured, lower hemisphere, equal area stereonet of poles to all Wendouree BHTV-imaged fracture planes (Contours = Density/1% Stereonet Area; n = 626). (b) Corresponding Frequency-Azimuth rose diagram of all BHTV-imaged structures (Data Frequency = Azimuth). Produced with GEOrient© v9.2.

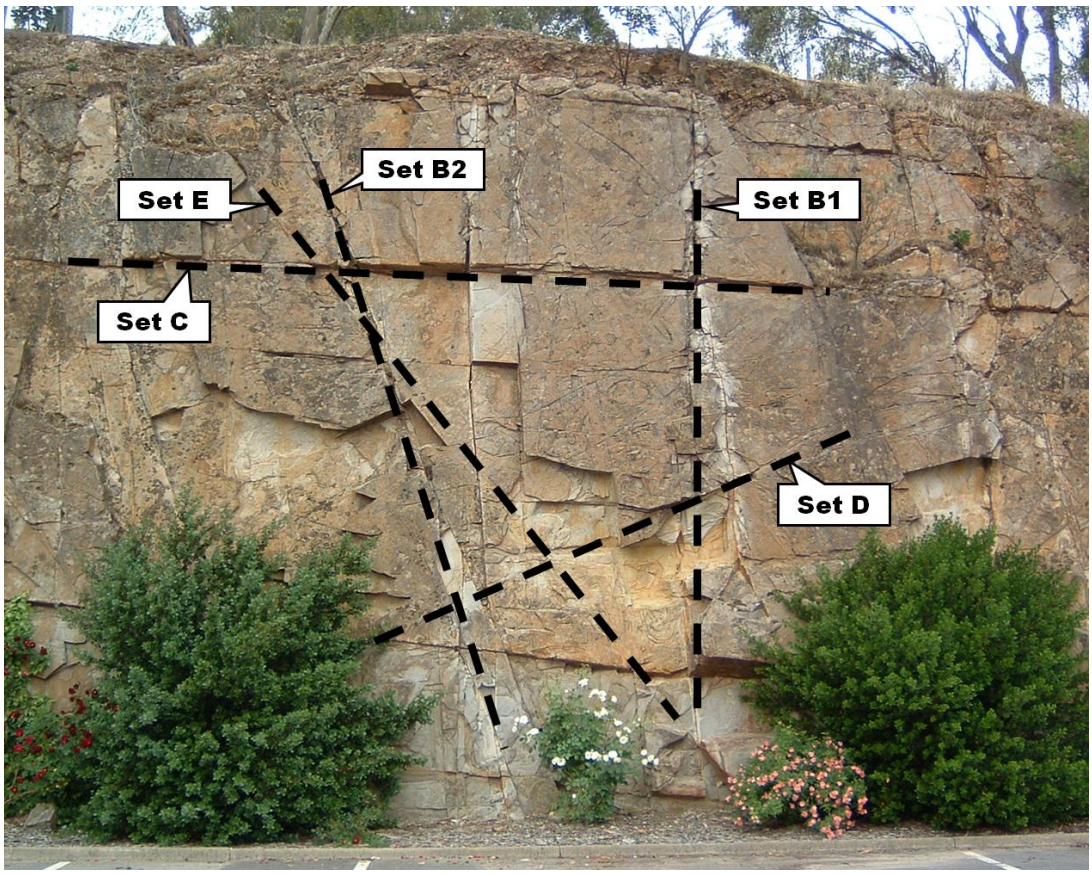

Figure 2.6 ENE-looking, longitudinal section view of a near vertical bedding plane within the Saddleworth Formation (Auburn Dolomite unit) located on the western limb of the Hill River Syncline (~5 m high rock face). This outcrop exposure contains the same rock unit and structures as that intersected in drill holes at the Wendouree site located ~2 km to the SSE. Note the five fracture sets typical of this area: bedding planes (Set A); "ac" (extension) joints (Set B1 and B2); sub-horizontal "bc" (extension) joints (Set C) and conjugate "hk0" (shear) joints (Set D and E).

Table 2.1 Mean principal orientations and characterisation of the acoustic BHTV-imaged fractures at Wendouree.

Joint Set	Mean Dip & Dip Dir.	Classification	No. Fracs.
A	78 / 240	Bedding planes ("S_0").	297
B1	78 / 331	Steep-vertical, "ac" (extension) joints.	39
B2	75 / 155	Steep-vertical, "ac" (extension) joints.	45
C	02 / 013	Sub-horizontal, "bc" (extension) joints.	43
D	38 / 356	D & E - conjugate pair of "hk0" (shear) joints.	77
E	54 / 146	D & E - conjugate pair of "hk0" (shear) joints.	17
Random		Not associated with a ≥ 2% fracture density stereonet cluster.	108

Fracture hydraulic activity interpretations at Wendouree down to a depth of ~40-50 m are problematic because previous studies (see Section 2.4) have shown this particular horizon to be weathered (to a depth of ~18 m) and relatively more fractured and transmissive, which may obscure evidence of the contemporary stress field affecting the directional permeability of the fracture network. Therefore, in this study all fracture hydraulic activity data from within the top 0-50 m depth horizon was omitted from the *in situ* fracture hydraulic activity interpretations to provide a more realistic, less "noisy" signature of any possible stress-dependent fracture permeability related to the contemporary stress field. Of the original 626 BHTV-imaged structures, a total of 147 or 23.5% were classified as potentially hydraulically active whilst the recompiled data, minus the top 0-50 m depth horizon, contained 360 fractures of which a total of 87 or 24.2% were classified as potentially hydraulically active (Table 2.2). Table 2.2 data suggest that fracture Sets A and B are the most significant hydraulically active fractures. Sets A and B are the only steep dipping structures in the entire dataset. They represent the approximately orthogonal NW-SE striking bedding plane and the NE-SW striking "ac" joint set.

Table 2.2 Proportion of potentially hydraulically active fractures within the Wendouree BHTV fracture dataset for depths >50 m below the surface.

Fracture Set	No. Fractures	No. Active Fractures	% of Active Fractures
A	194	46	52.87
B1	29	7	8.05
B2	42	10	11.49
C	15	3	3.45
D	14	3	3.45
E	14	3	3.45
Random	52	15	17.24
Total	360	87	100

The results of Table 2.2 are not conclusive due to the inherent biases of the BHTV data and insufficient diamond drill core available for reconciliation and statistical analysis. However, this interpretation is plausible given the uplift and unloading stress regime expected at these shallow depths, which should favour steep dipping structures under conditions of isotropic, lateral relaxation of the rock mass. It also agrees with the findings of Skinner and Heinson (2004). Nonetheless, there is a much less pronounced directional dependency of permeability due to the significant role of the "random" fractures that do not belong to any of the predefined joint sets as they lessen any structural/mechanical anisotropy within the rock mass (see Table 2.1).

2.6 Conceptual model

All geological and hydraulic data collected at Wendouree were combined to develop the conceptual fracture network model consisting of an upper densely fractured, clay-rich, weathered zone (0-20 m), a less fractured transitional zone (20-40 m) and a low fracture density zone (>40 m) (Figure 2.7). With increasing depth there is a trend of decreasing fracture density based upon a reduction in the numbers of joints in Sets B, C, and D & E against a persistent background of high density bedding planes (Set A). This trend has been observed within the limited amount of diamond drill core

samples available plus the BHTV logs. The primary cause of this fracture density trend is attributed to the effects of uplift and unloading. For example, the BHTV logs revealed a proportionally greater amount of sub-horizontal joints in the upper 40 m depth horizon, which is considered indicative of neotectonic joint formation in response to unloading (Hancock & Engelder 1989). Thus, the increased development of unloading-related, sub-vertical flexural and sub-horizontal sheeting (or relaxation) joints closer to the surface creates a distinct zoning of the vertical fracture density profile throughout the entire aquifer system. With increasing depth and stress magnitudes progressive fracture aperture deformation will lead to progressive changes in fracture network hydraulics and connectivity. Overall, the most significant hydraulically conductive fractures are expected to be the steeply dipping Set A and B fractures, considering that the vertical stress is the major principal stress.

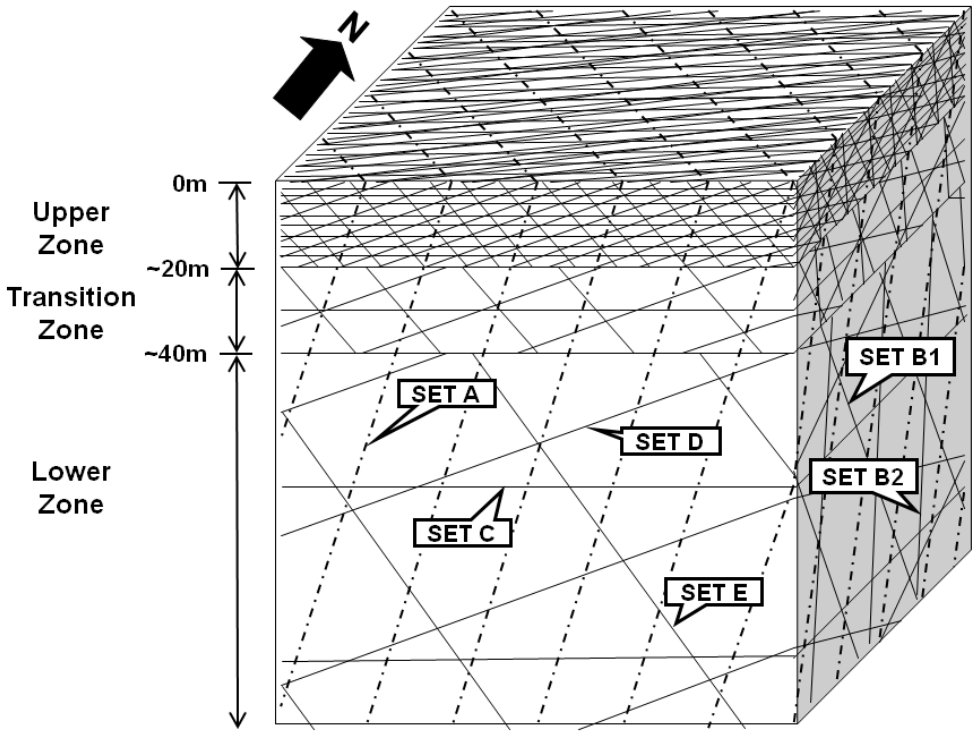

Figure 2.7 A schematic example of the Wendouree conceptual fracture network model showing decreasing joint densities between the upper, transition and lower zones. Dashed lines denote the persistent, dense, bedding planes of Set A whilst the solid lines represent joint sets B, C, D and E.

2.7 Hydromechanical models

2.7.1 Model design

The stochastic, 2D Wendouree UDEC models are based upon the conceptual model and are simple 100 m to 200 m size, cross-section (in the plane of Set B) and planar models (in the plane of Set C) built from the surface down (Figures 2.8a & b). These 2D models describe a geometrical reconstruction that consist of 2D vertical or horizontal planar slices of the conceptual fracture network model that incorporates the effects of the 3D stress field (i.e. σ_V, σ_H, and σ_h). The blocks defined by the fracture network generated within UDEC were discretized into a triangular mesh of constant strain with the nodal distances varying between 0.2 to 1.5 m in length. These models defined the Earth's surface as a free surface at zero stress with all other mechanical boundaries defined as velocity (displacement) boundaries that are either fixed (planar models) or "roller" (cross-section models) which allows for some limited block displacement. *In situ* and boundary stresses were set as either gradients (cross-section models) or fixed (planar models). *In situ* and boundary fluid pore pressures were based on an assumed hydrostatic gradient from the known water table (10 m below surface) with either fixed state (planar models) or a vertical gradient with an impermeable base (cross-section models). Fluid flow can occur in any direction within the fracture network under the imposed hydraulic gradient.

Magnitudes of stress are based upon σ_V (i.e. $\rho.g.h$) and applied as a differential stress ratio compatible with a normal stress regime involving isotropic, lateral relaxation of the rock mass consistent with the effects of uplift and unloading (i.e. $\sigma_V > \sigma_H = \sigma_h$ at a ratio of 1: 0.5: 0.5). The 2D planar and cross-section models enabled σ_H to be perpendicular to the model boundaries i.e. σ_H at 110°. The cross-section orientation is approximately parallel to the east to west hydraulic gradient recorded at the Wendouree site and used apparent dips for oblique fracture sets (Love 2003). The principal stress orientations are assumed to be the same as that determined for the far-field (deep) reverse faulting stress regime, which is a reasonable assumption as studies on shallow, neotectonic joint formation within sedimentary sequences found

unloading and release joints related to uplift and erosion strike approximately parallel and perpendicular to the regional maximum horizontal stress direction

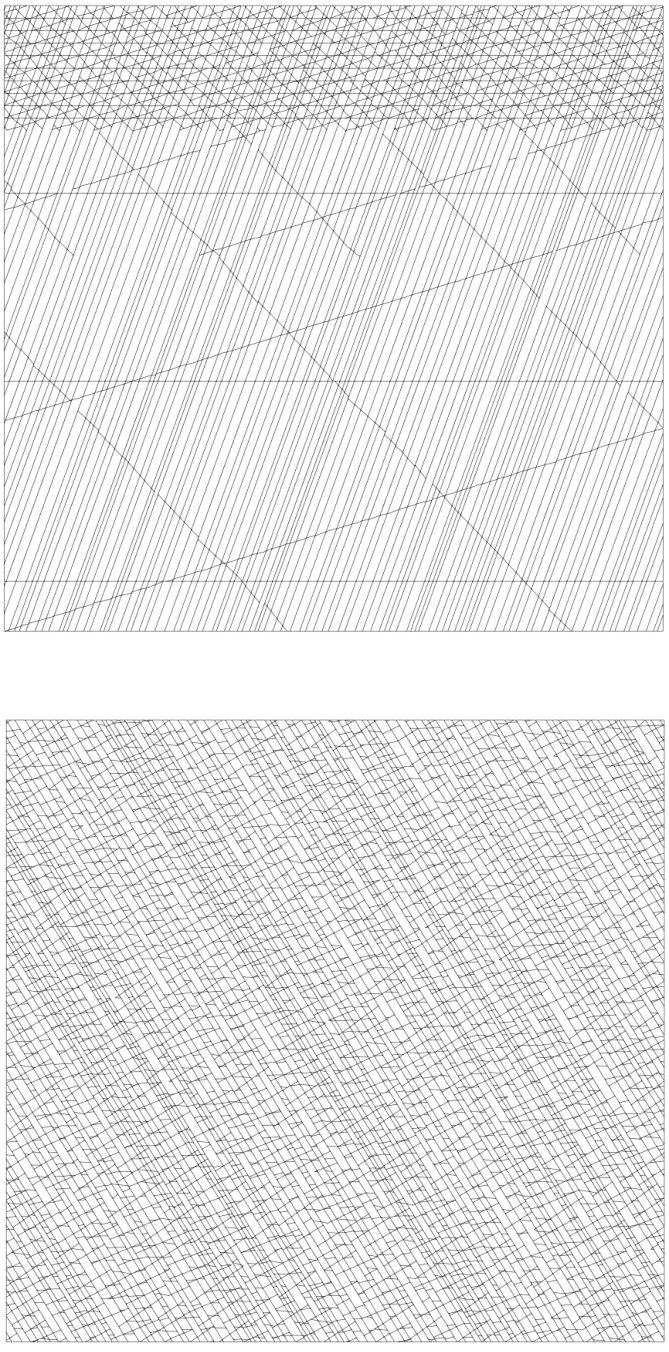

Figure 2.8 Example stochastic 2D Wendouree UDEC models: (a) the 100 m x 100 m NE-SW vertical cross-section model, in the plane of Set B, which is dominated by the dense bedding planes of Set A; and (b) the 100 m x 100 m horizontal planar model, in the plane of Set C, at 20 m depth below the surface.

(Engelder 1985; Hancock and Engelder 1989). The fracture network was based on the conceptual model (Figure 2.7) whilst other fracture parameters were taken from scanline mapping data of nearby outcrops (Table 2.3; T Halihan, Flinders University, unpublished data, 1999). The bedding plane to joint set density ratio consists of 2:1 in the upper zone, 16:1 in the transitional zone and 32:1 in the lower zone (Figure 2.8a). These joint set densities are estimates only as the precise values are unknown due to the limited and biased nature of both the vertical drill core samples and BHTV logs. However, these joint set densities are reasonably comparable to those determined from the BHTV logs and this model design resulted in a reasonable correlation with the known groundwater flow observations (see Section 2.7.3).

Table 2.3 Mean fracture orientation (std. dev.), trace (std. dev.), and spacing for the upper, transition and lower zones of the Wendouree stochastic UDEC models (see Figure 2.7). Note that the Set A fractures are designed to transect the entire model with a fixed orientation in order to represent planar, continuous bedding plane surfaces.

Fracture Set	Mean True Dip & Dip Direction	Mean Trace (m)	Mean Spacing (m)
A	78 (0) / 240 (0)	>100	0.5 - 1.5
B1	78 (9) / 331 (10)	6 (5)	2, 16, 32
B2	75 (6) / 155 (9)	6 (5)	2, 16, 32
C	2 (6) / 013 (33)	11 (18)	2, 16, 32
D	38 (4) / 356 (13)	2 (1)	2, 16, 32
E	54 (5) / 146 (9)	6 (5)	2, 16, 32

Average values of density, bulk modulus and Poisson's ratio for the intact rock material were obtained from ultrasonic velocity testing of several drill core samples which showed negligible mechanical anisotropy through tests conducted both parallel and perpendicular to the thinly laminated fabric (Table 2.4). These data were used to estimate other parameters such as the uniaxial compressive strength (UCS), tensile strength, cohesion and friction angle through Mohr circle analysis and other empirical relationships and are compatible with published values (Table 2.4;

Waltham 2002). Standard practice is to derive fracture normal (jk_n) and shear (jk_s) stiffness estimates based upon fundamental measurements of fracture surface topography profiles and the elastic properties of the intact rock material, although these estimates are affected by many factors (Bandis 1993; Barton *et al.* 1985; Barton and Choubey 1977). Normal stiffness is a critical parameter used to determine changes in fracture hydraulic conductivity via an estimate of the mechanical aperture closure under compression. For these models fracture stiffness estimates were based on joint roughness coefficient (JRC) distributions, intact rock material properties and comparison with published literature values. The estimated JRC distributions for each of the five fracture sets (Sets A–E) determined from fracture logging of oriented drill core samples were found to be highly variable (smooth to rough) with no definitive trends discernible (Figures 2.9a & b). As fracture stiffness is a function of wall contact area, the jk_n for smooth planar surfaces can approximate the value of the Young's Modulus (*E*) whereas the jk_s, for perfectly matching rough surfaces, can approximate the value of the Shear Modulus (*G*). From these relationships, estimates were derived based upon jk_n ranging from 1/2 (smooth) to 1/10 (rough) the value of *E* and jk_s ranging from 1/2 (rough) to 1/10 (smooth) the value of *G*, which are compatible with published data and those derived from empirical relationships (Table 2.4; Kulhawy and Goodman 1980; Nordlund *et al.* 1995). To reflect the highly variable JRC distributions, the range of jk_n and jk_s values were randomly populated (normal distribution) across all fractures within the model. Specifically, each individual fracture segment (0.2 to 1.5 m in length) within the model was randomly assigned jk_n and jk_s values. The objective of this approach is to account for naturally occurring fracture heterogeneity such as asperity and contact area distribution, strength etc and ultimately heterogeneity in deformation and fluid flow along individual fracture planes. Fracture friction and dilation angles were both inferred as zero as they have only a minimal impact on the overall modelling results. The fracture dilation angle is critical in investigating the role of rock mass dilation in dealing with excessive pore pressures and rock mass stability during tunnelling. However, such cases represent transient systems whereas this study is interested in modelling HM coupling under steady state conditions or after equilibrium is reached. At Wendouree, the mean fracture aperture measured from nearby outcrop was ~100-200 μm and ranged up to a maximum of 1.2 mm (Love *et al.* 2002), however, for the purposes of this modelling exercise a reference aperture of 0.5 mm at the Earth's

surface is considered appropriate to facilitate the observation of overall fracture network deformation patterns. The choice of this initial aperture value is not considered critical, as it is the relative effects of the *in situ* stress field on individual fracture sets, which is the main objective.

Table 2.4 Rock mass and fracture parameters used to construct the Wendouree UDEC HM models. Source: 1 = core sample ultrasonic velocity tests; 2 = Mohr circle analysis; 3 = core sample derived fracture JRC profiles and Elastic Moduli relationships; 4 = Inferred; and 5 = approximate values for fresh water at 20°C.

UDEC Model Parameters	Value	Units	Source
Rock Material Density (ρ)	2732	$kg.m^{-3}$	1
Poisson's Ratio (ν)	0.27	-	1
Young's Modulus (*E*)	77e6	Pa	1
Bulk Modulus (*K*)	96e9	Pa	1
Shear Modulus (*G*)	30e9	Pa	1
Cohesion (c)	19e6	Pa	2
Friction Angle (φ)	54	Degrees	2
Dilation Angle (ψ)	0	Degrees	4
Uniaxial Compressive Strength	128e6	Pa	2
Tensile Strength	8.5e6	Pa	2
Joint Normal Stiffness (jk_n)	7.7 - 35.1e9	$Pa.m^{-1}$	3
Joint Shear Stiffness (jk_s)	3.0 - 13.6e9	$Pa.m^{-1}$	3
Joint Cohesion	0	Pa	4
Joint Tensile Strength	0	Pa	4
Joint Friction Angle	0	Degrees	4
Joint Dilation	0	Degrees	4
Joint Aperture (at zero stress)	0.5	mm	4
Joint Residual Aperture	0.1	mm	4
Joint Permeability Constant (1/12μ)	83.3	$(Pa.s)^{-1}$	5
Water Density	1000	$kg.m^{-3}$	5

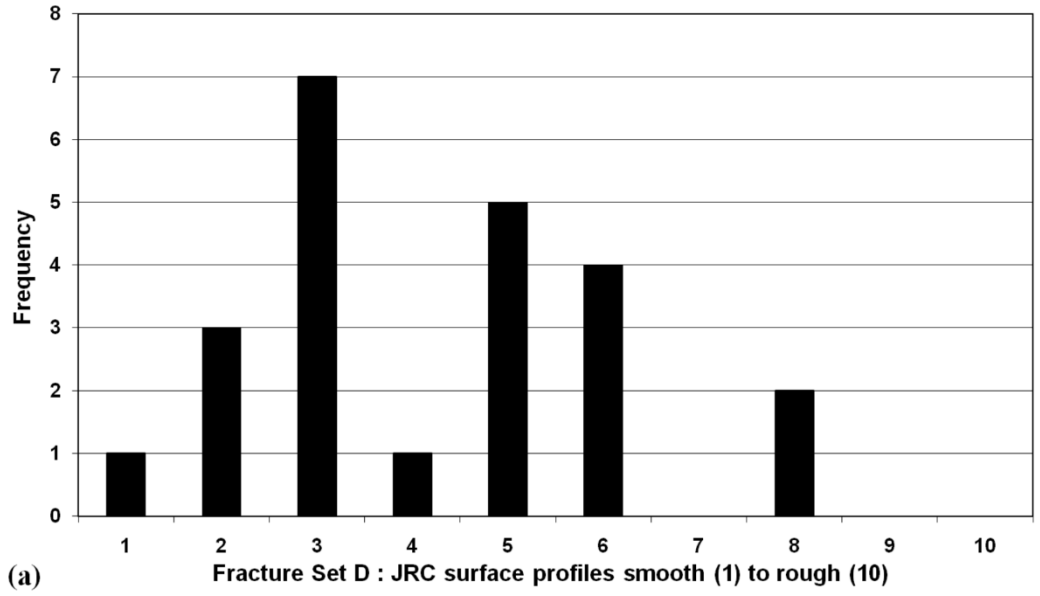

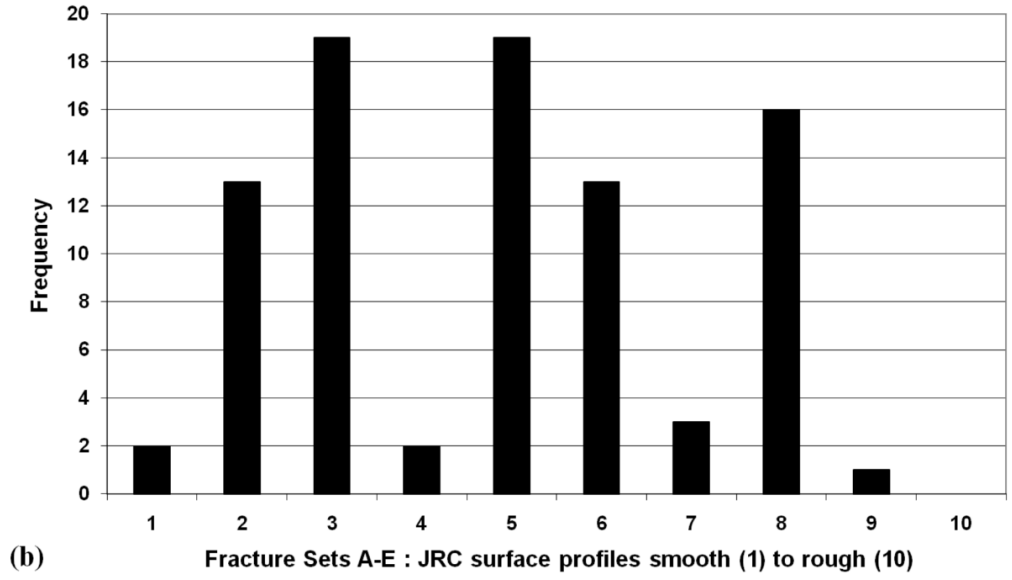

Figure 2.9 Frequency histogram of the JRC distribution recorded across drill core fracture data for (a) Set D (n=23); and (b) the entire Wendouree drill core fracture dataset (Sets A–E, n=88). JRC numbers correspond to smooth (1) to rough (10) fracture surface profiles.

2.7.2 Fracture deformation model

To assess the effect of fracture geometry within the applied normal stress regime, the amount of fracture deformation across all individual fracture sets as a function of depth was analysed for a 200 m x 200 m Wendouree NE-SW vertical cross-section (see Figure 2.8a). The deformation patterns of individual fracture sets depict the ultimate HM response of a fractured rock mass to an applied stress. UDEC calculates the effective hydraulic aperture of a fracture based upon its initial fracture aperture width at zero stress plus any normal displacement (positive or negative) that has occurred as a result of deformation. This fracture deformation data is depicted for each individual fracture set in terms of the amount of fracture closure normal to fracture walls commencing with an initial hydraulic aperture of 0.5 mm at the surface (Figure 2.10). The fracture deformation profiles of Figure 2.10 show a divergence in the relative amounts of fracture deformation occurring across the individual fracture sets commencing from approximately 50 m depth. In particular, the rate of fracture closure with depth is approximately uniform for the moderate dipping to sub-horizontal joint sets (Sets C, D & E) whilst the steep dipping bedding planes (Set A) close at a lesser rate. Using these closure estimates, the reduction in equivalent parallel-plate hydraulic conductivities for individual fractures can be derived from the Cubic Law (Equation 2.1). For example, at a depth of 185 m the average fracture hydraulic conductivities for the steep dipping bedding planes (Set A) and the moderate dipping to sub-horizontal joint sets (Sets C, D & E) are reduced by ~54% and ~62-71%, respectively. This progressive development with depth of an anisotropic permeability orientation along steep dipping fractures highlights the important role of fracture geometry in regards to stress-dependent fracture permeability. This result is attributed to the fact that the applied normal stress field simulates uplift and unloading through isotropic, lateral relaxation across the entire rock mass, which should result in less deformation occurring along steep dipping fractures. This result is consistent with the interpretations of *in situ* (borehole) fracture hydraulic conductivity and with the findings of Skinner and Heinson (2004) that steep dipping bedding planes are the most significant hydraulically active fractures at Wendouree. The local departures from the general trends are attributed to the random assignment of fracture stiffness values.

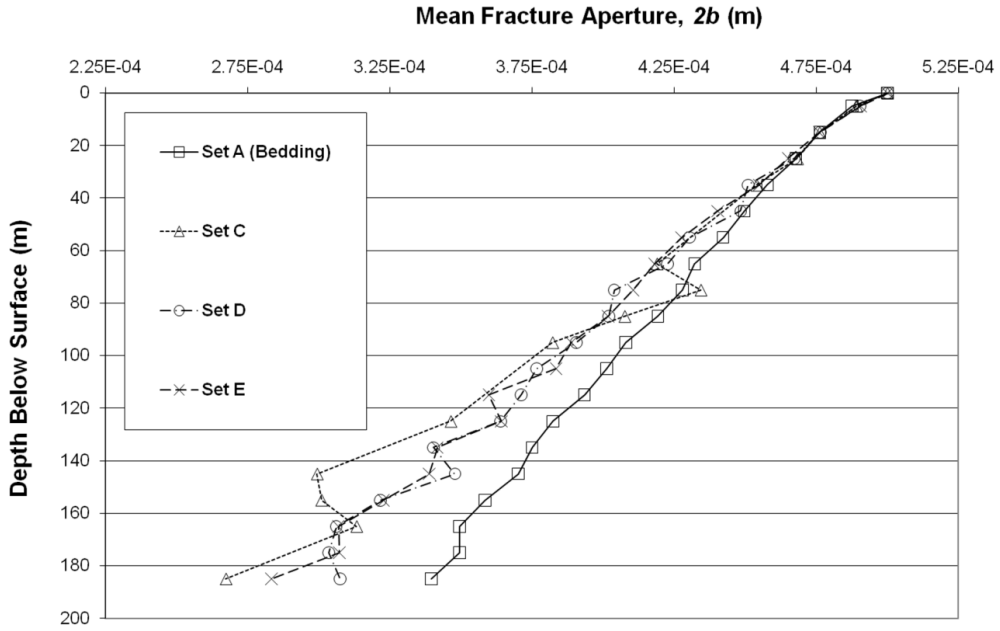

Figure 2.10 UDEC fracture deformation depth profiles of the individual fracture sets that comprise the Wendouree NE-SW cross-sectional model under a normal stress regime. The initial fracture hydraulic apertures were set at 0.5 mm with data points representing the calculated mean fracture aperture for each 10 m thick depth interval.

2.7.3 Groundwater flow models

2.7.3.1 Vertical cross-section flow model

To investigate overall fracture network hydraulics and connectivity, an analysis of groundwater flow through both the deformed (stressed state) and undeformed (zero stress state) 100 m x 100 m Wendouree NE-SW cross-sectional models was completed. For the deformed model, this process involved deforming the model under normal stress regime conditions before subjecting it to steady state, groundwater flow under an east to west oriented hydraulic head gradient of 0.01 and 0.001, which fits with the measured seasonal Wendouree hydraulic gradient of between 0.003 and 0.007 (Love 2003). Like the fracture deformation models, the initial fracture hydraulic aperture for the groundwater flow models was set at 0.5

mm. The process for the undeformed model is identical except that fracture hydraulic apertures are fixed for all depths at 0.5 mm. UDEC assigns equivalent hydraulic conductivities to each uniform aperture (parallel plate) segment of a fracture according to the Cubic Law (Equation 2.1). The flow rate through each of these segments is calculated using Darcy's Law:

$$q = \frac{(2b)^3}{12\mu}\frac{\Delta P}{L} \qquad (2.2)$$

Where q is the fracture flow rate per unit width normal to flow direction ($m^2.s^{-1}$), ΔP is the pressure difference (Pa), L is the length of each segment (m).

As the vertical depth profiles of UDEC derived fracture flow rates ($m^2.s^{-1}$) and field data such as the normalised borehole yields (L/s/m; see Figure 2.3) are not directly comparable, the following comparisons are qualitative. The results of the UDEC vertical cross-section flow models are depicted in terms of mean apertures and flow rates for all fractures within 10 m thick horizontal depth intervals with the weathered zone represented by the upper 20 m of the model (Figures 2.11a & b). Figure 2.11a shows a uniform, linear decrease in mean apertures with depth whilst the decrease in mean flow rates is non-linear and resembles the regional well groundwater yield trend depicted in Figure 2.3. When the deformed Wendouree fracture network flow model is compared against an undeformed version (Figure 2.11b), the applied normal stress regime appears to have had an effect, as the trend of decreasing mean fracture flow rates with depth in the undeformed state is distinctly different and only minimal. As both of these models use an identical fracture network model the difference between these two mean fracture flow rate profiles is attributed to stress-related, fracture deformation processes that progressively modify fracture aperture and permeability. Furthermore, this progressive fracture deformation also leads to changes in hydraulic connectivity and flow patterns within the overall fracture network, although this is difficult to ascertain from this data, particularly as the 2D cross-section model becomes dominated by the relatively higher conductivity, steeply dipping bedding planes with increasing depth.

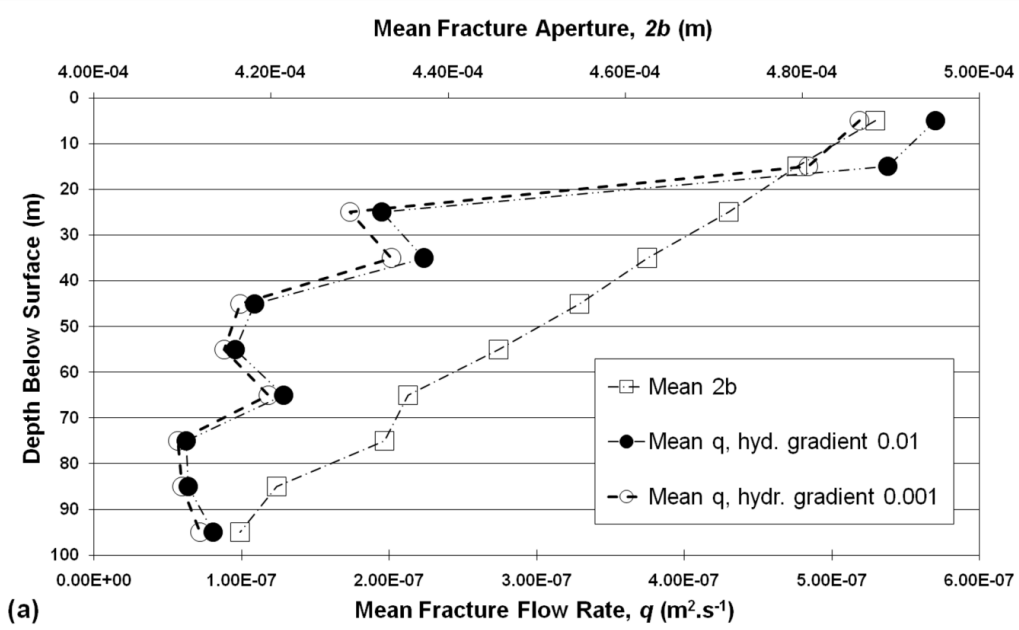

Figure 2.11a UDEC estimated mean fracture flow rates (circles, lower x-axis) and fracture apertures (squares, upper x-axis) for the Wendouree NE-SW cross-section model under a normal stress regime. Closed and open circles equal fracture flow rates calculated at hydraulic gradients of 0.01 and 0.001, respectively. The initial fracture hydraulic apertures were set at 0.5 mm.

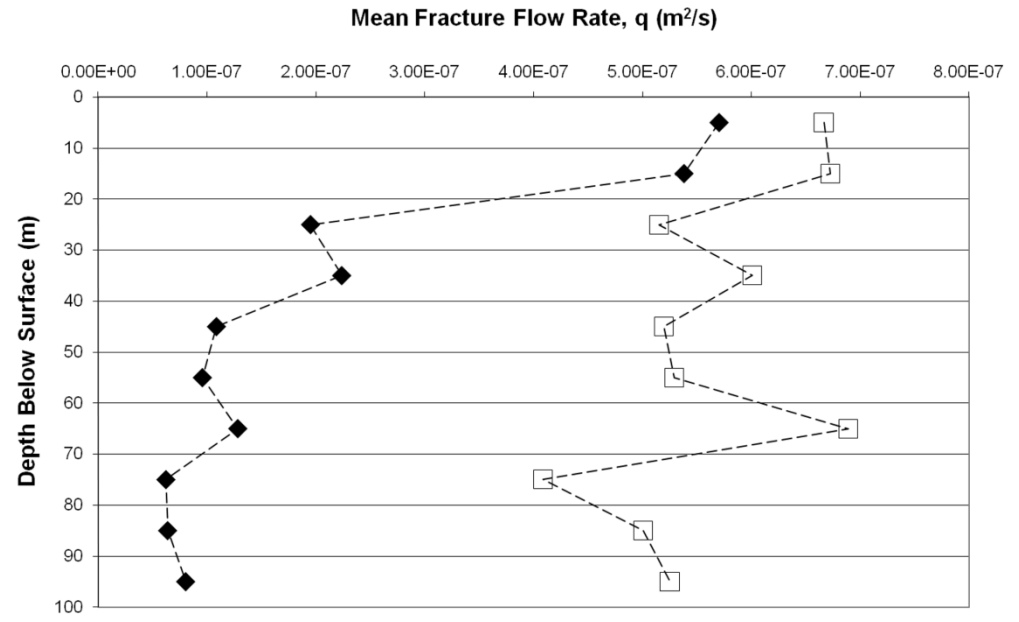

Figure 2.11b Comparison between UDEC estimated mean fracture flow rates for both the deformed (black diamonds) and undeformed (open squares) Wendouree NE-SW cross-section model under a normal stress regime and hydraulic gradient of 0.01. The initial fracture hydraulic aperture for the deformed model is 0.5 mm, which is fixed at all depths for the undeformed model.

2.7.3.2 Hydraulic conductivity ellipses

The potential influence that the imposed stress field may have on the permeability tensor of the Wendouree fracture network model was evaluated by comparing deformed and undeformed models through the estimation of 2D planar hydraulic conductivity ellipses. This process involved slicing the conceptual Wendouree fracture network model into horizontal, planar depth slices at 20 m, 40 m, 75 m and 100 m depths (see Figures 2.7 and 2.8b). These four depth slices were chosen to capture the effects of increasing stress and decreasing joint densities with depth. These planar models use a normal stress regime to simulate the effects of uplift and unloading.

UDEC has previously been used to investigate permeability tensors in discrete fracture network models (e.g. Min *et al.* 2004a; Zhang *et al.* 1996). In this study, a similar methodology was employed involving each planar model being deformed under corresponding depth-dependent magnitudes of horizontal stresses. These deformed models were then subjected to steady-state, fluid flow under an applied east to west hydraulic gradient of 0.01 with the north and south boundaries acting as impermeable, no-flow, barriers. The effective hydraulic conductivity (K) of each model is estimated using Darcy's Law below and the UDEC sum of discharge flow rates (Q) from each steady-state model:

$$Q = K A i \qquad (2.3)$$

Where Q is the sum of discharge flow rates ($m^3.s^{-1}$), K is the effective hydraulic conductivity ($m.s^{-1}$), A is the cross sectional area normal to the flow direction (m^2) and i is the hydraulic gradient.

To estimate the 2D hydraulic conductivity ellipse at a particular depth slice, the value of K is calculated for the initial fracture network model using the method described above then this entire process is repeated for 6 x 30° (i.e. 180°) horizontal rotations of the identical model. The 2D hydraulic conductivity ellipse is then constructed by plotting the value of K recorded at each 30° horizontal model rotation. For comparison, this exercise is repeated for the same fracture network models but under a zero stress field i.e. the undeformed state with fixed apertures. The initial (and zero stress) fracture aperture is set at 0.5 mm.

The model results show that at each depth slice the hydraulic conductivity ellipses are all elongated in a WNW-ESE direction (i.e. a strike direction of 300°–120°) (Figures 2.12a–d). This elongation direction represents the maximum *K* direction and is close but slightly offset to the strike of the extensive, densely spaced bedding planes (Set A, 330°–150°). The NNE-SSW direction of the minimum *K* direction approximates but slightly offset to the strike of the less dense, finite length joint sets (Sets B, D & E). This near coincidence of the maximum and minimum *K* directions with the bedding and joint planes is not a function of the 30° model rotations because one of these model rotations/gradient alignments is exactly coincident with the bedding plane direction. Overall, this ellipse elongation becomes more anisotropic with depth as the ratio between the maximum versus minimum *K* axes increases, which is attributed to the lessening influence of the decreasing joint set densities against a persistent background of dense bedding planes.

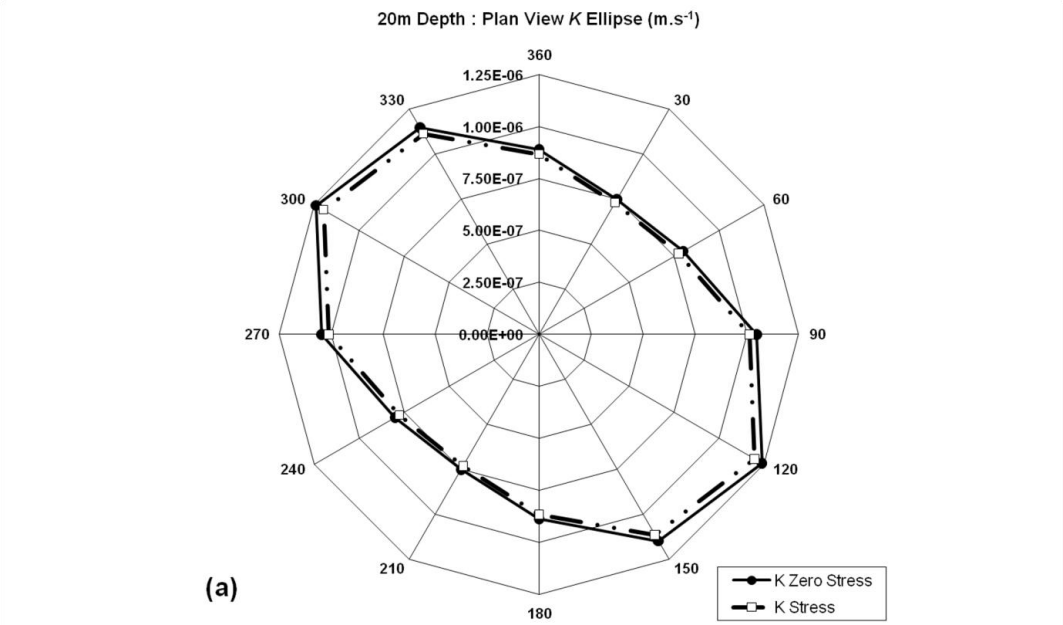

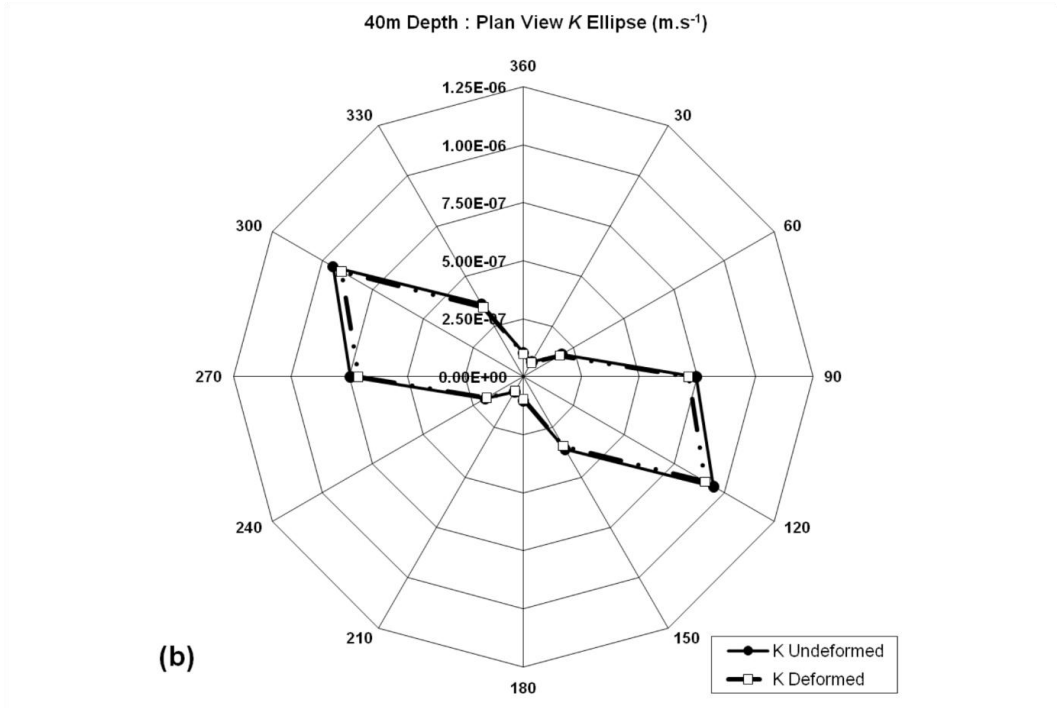

Figure 2.12 Undeformed (solid contour) versus deformed (broken contour) hydraulic conductivity (*K*) ellipses [$m.s^{-1}$] for Wendouree at (a) 20 m; and (b) 40 m depth below the surface.

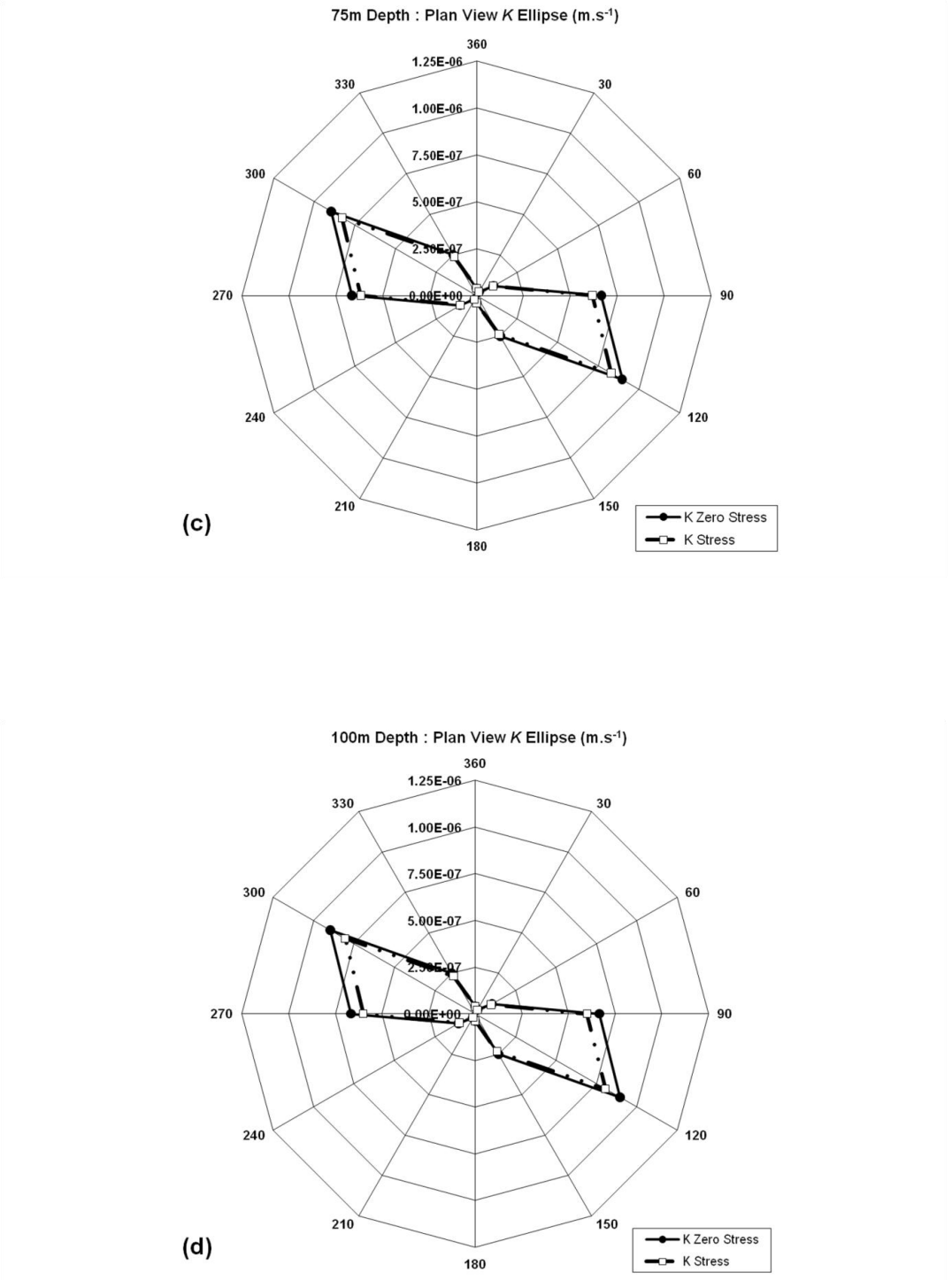

Figure 2.12 (cont.) Undeformed (solid contour) versus deformed (broken contour) hydraulic conductivity (*K*) ellipses [m.s^{-1}] for Wendouree at (c) 75 m; and (d) 100 m depth below the surface.

The overall shape of the deformed and undeformed hydraulic conductivity ellipses are near identical with the exception that the deformed models are slightly reduced in their absolute magnitudes of *K* (Figures 2.12a-d). For example, compared to the undeformed model, the maximum and minimum *K* values for the deformed model at 100 m depth are reduced by ~10% and ~2.3%, respectively. This implies that the shape and magnitude of the hydraulic conductivity ellipses are controlled by the original fracture network structure (i.e. fracture geometry and density) and only marginally influenced by the imposed normal stress regime. The UDEC *K* values are in reasonable agreement with the bulk K_b estimates derived from the Wendouree piezometer pumping tests (see Figure 2.6), particularly, commencing from >40 m depth. However, at shallower depths (0-40 m) the UDEC models underestimate the magnitude of *K* by two orders of magnitude. This difference is attributed to the effects of weathering on the apertures and densities of fractures which are difficult to define because of increased spatial heterogeneity at shallow depths. However, it is more likely that a few extensive sub-horizontal sheeting (or relaxation) joints govern flow closer to the surface owing to their generally large apertures.

2.8 Discussion

In situ stress is ubiquitous and always plays some role in the behaviour of groundwater systems regardless of their depth. The influence of *in situ* stress on groundwater flow in shallow fractured rock aquifers is difficult to characterise due to the inherent complexities in fracture network geometries, densities, connectivity, infill and weathering. These intrinsic factors dominate and may, in some cases, mask any evidence of the effects of the stress field at least at depths of <200 m below the surface.

In this study, *in situ* fracture hydraulic activity interpretations of detailed borehole geophysical logs found evidence of permeability anisotropy that favours steep dipping fractures, which is consistent with that expected for the present-day, shallow level conditions of uplift and unloading. This is supported by the UDEC fracture deformation models, which demonstrate that under a normal stress regime and at depths less than 200 m below the surface, the steep dipping bedding planes deformed

at a lower rate relative to the moderate to shallow dipping joint sets. This is due to the effect of individual fracture geometries with respect to the imposed normal stress field that simulates isotropic, lateral relaxation of the entire rock mass.

Comparing deformed and undeformed UDEC vertical cross-section flow models demonstrated that *in situ* stress fields progressively modify groundwater flow patterns commencing from the near surface via variable fracture deformation and hydraulic aperture distributions. The degree of anisotropic fracture deformation increases with depth and leads to the progressive development of hydraulic connectivity restrictions occurring within the overall fracture network (see Figure 2.10). In addition to these effects, localised bottlenecks or "chokes" within the hydraulic network will also develop through the enhanced deformation of locally, low stiffness (i.e. weak) fracture segments regardless of their fracture geometry as fracture normal and shear stiffness are never constant along a single fracture plane. For example, the UDEC models in this study were composed of numerous individual fracture segments (0.2 to 1.5 m in length) with randomly assigned jk_n and jk_s values (see Section 2.7.1) where differing amounts of fracture deformation would lead to the formation of localised hydraulic restrictions. Departures from the overall trend-lines in Figure 2.10 are attributed to this process.

In contrast, the near identical shape and increasing anisotropy of the deformed and undeformed horizontal planar Wendouree *K* ellipses with depth is attributed to the integrated effects of decreasing joint density with depth against a persistent background of dense bedding planes. The applied normal stress field appears to have had little effect on the shape of the *K* ellipses other than a minor reduction in the magnitudes of *K*. This demonstrates that the *K* ellipses are strongly controlled by the original fracture network structure but not entirely dominated by the persistent bedding plane trend, which was slightly offset to the maximum *K* direction. Unlike the vertical cross-section flow model, the stress-related reductions in *K* with depth associated with the horizontal planar models are approximately linear. This is most likely because the horizontal planar models do not include the sub-horizontal joints of Set C, which implies that these sub-horizontal fractures are critical to overall fracture network connectivity. This is supported by the Wendouree borehole-to-

borehole geophysical surveys of Skinner and Heinson (2004) that detected lateral flow along a small number of extensive, low angle structures becoming more prevalent at depths >30 m. Considering that the sub-horizontal joints are not favourably oriented (i.e. preferentially closed) with respect to the *in situ* normal stress regime, their significant role in governing groundwater flow shows their importance to overall network connectivity.

More subtle examples of stress-dependent groundwater flow in the Clare Valley can be found in other regional hydrogeological datasets. For example, regional well groundwater yield data (Figure 2.3) show a significant vertical decrease in groundwater yields commencing from approximately 40 m below the surface. This dataset is catchment wide (~500 km^2, 1316 boreholes) and independent of weathering, lithology and position within the folded sedimentary sequence. This vertical yield trend is attributed to other regional scale factors such as depth-dependent changes in fracture density, which is at least partially due to the effects of uplift and unloading, plus stress-related subsurface fracture deformation. Similarly, Love (2003) noted that the consistent pattern of increasing groundwater salinities with depth in wells across the entire Clare Valley catchment could be explained by "decreased rates of solute flushing due to the decreasing horizontal and vertical groundwater flow rates with depth". Why a hydraulic discontinuity boundary occurs at a depth of 40 m in this catchment and how we can predict the presence and depth of such boundaries elsewhere lies with an understanding of depth-dependent changes in fracture density and the effects of the *in situ* stress field.

The notable exception to the above observed groundwater patterns are the relatively deep, localised, hydraulically active fractures such as those revealed in the hydro-logging profiles of Love (2003) (see Figure 2.6, ~80-85 m). Based upon their occurrence at depths much greater than 40 m below the surface, these particular groundwater-active fractures appear to be stress-insensitive and most likely locked open as a result of earlier fracture deformation episodes (e.g. shear dislocation) or partial mineral infill and cementation (e.g. Banks *et al.* 1996; Laubach *et al.* 2004).

This study identified several limitations with its methodology, which are largely due to the complexities and uncertainties associated with data capture, representative core

samples and spatial confidence, particularly in regard to the geomechanical characterisation of *in situ* rock material and fractures. Accurate definition of key model fracture parameters (e.g. fracture density) are difficult to quantify from limited and/or biased core samples, BHTV images and outcrop. This study would have benefited from *in situ* stress measurements at the field site but this was cost prohibitive which is why in practice the *in situ* stress field is generally inferred (i.e. from earthquake focal mechanism solutions and knowledge of the period and magnitude of regional uplift). This study focussed on a fracture network pattern developed within only one stratigraphic unit although it is known that fracture density varies between different stratigraphic units as determined by rock type, thickness and position within the overall sequence. However, lithology independent datasets such as the regional well groundwater yield data (see Figure 2.3) suggest that the large-scale effects of the relatively consistent depth-dependent fracture density variations across the catchment and the *in situ* stress field play a fundamental role in regional-scale groundwater flow patterns. HM models can reflect regional scale patterns if the aquifer is homogeneous at the scale of the Representative Elementary Volume (REV), however, due to the dependence of the directional hydraulic conductivity on inherently heterogeneous properties, numerous HM models may need to be tested at various scales to ascertain its REV. The integration of local- and regional-scale field based observations into the Wendouree case study may not have dramatically changed the modelling outcomes but their inclusion improved model constraints and reduced the level of uncertainty. Regardless, this study demonstrates that a stochastic approach to HM modelling can produce results that agree with direct field observations and can offer an alternative preliminary approach to standard well hydraulic tests.

2.9 Conclusion

This study has shown that *in situ* stress fields can affect groundwater flow in fractured rock aquifers at shallow depths (<200 m). This investigation also agrees with previous researchers in that the inherent properties of a fractured rock mass such as fracture density, orientation, length and fracture infill are the dominant parameters controlling groundwater flow. That is, palaeo-stress regimes play a dominant role in

the primary development of fracture networks and fracture permeability during episodes of crustal deformation. Contemporary stress fields may superimpose a secondary influence on pre-existing fracture networks by altering aperture distributions especially through relaxation at shallow to near-surface depths. Furthermore surface processes such as weathering, erosion and unloading influence the fundamental hydraulic nature of fracture networks resulting in higher degrees of spatial heterogeneity in shallow groundwater systems.

This study has shown that the key to understanding how *in situ* stress influences groundwater flow in shallow fractured rock aquifers lies in recognition and better appreciation of subsurface fracture deformation processes, which can significantly alter fracture hydraulic aperture distributions and network connectivity. The identification of stress-related effects on groundwater flow should not rely solely on the identification of anisotropic permeability orientations, as these are complex features that can be completely controlled by the inherent properties of the fractured rock mass. An understanding of stress-dependent, subsurface, fracture deformation is also a required critical input when analysing both local and regional groundwater flow patterns. Less obvious evidence of stress-dependent fracture network permeability may be found in regional hydrogeological datasets such as regional well groundwater yield trends.

The methodology and conclusions of this study have shown that:

1) The overall philosophy and approach described herein is unique in that it provides an alternative technique that can be used to generate information complementary to standard hydrogeological observations, especially in areas where field hydrogeologic data are limited.
2) Fracture deformation processes are depth dependent: as depth increases, fracture apertures deform at different rates dependent upon their orientation within the *in situ* stress field as well as their individual geomechanical properties resulting in anisotropic permeability within the fractured rock mass.
3) The measurement of hydraulic conductivity and DFN model properties at the surface cannot be extrapolated to depth because surface measurements do not take into account sub-surface fracture deformation processes and depth-dependent variations in fracture density. This problem can be addressed through

techniques such as detailed borehole image and temperature logs and HM model simulations.

4) In the near surface environment *in situ* stress does have a discernible effect in terms of variable fracture deformation distributions, which affect overall 3D fracture network hydraulic conductivity, connectivity, anisotropy and groundwater flow rates.
5) *In situ* stress fields may be a more important control on both local and regional scale, shallow groundwater flow systems than has been previously recognised. In particular, its role in shallow groundwater flow analyses is a critical input to better understand and explain observed aquifer behaviour.

Acknowledgements

The authors gratefully acknowledge the funding and logistical support received for this research from the Centre for Groundwater Studies, the Department of Water, Land and Biodiversity Conservation South Australia and the University of Hong Kong. The authors would also like to thank Mike Coulthard, James Ward, Steve Chan and Mark Christianson for their assistance with the UDEC models, Todd Halihan for the use of his geological data and Wolfgang Preiss and Tania Wilson for additional project support and advice.

3 The role of *in situ* stress in determining hydraulic connectivity in a fractured rock aquifer

3.1 Introduction

Groundwater flow within fractured rock aquifers is dominantly controlled by fracture density, length, geometry, connectivity, infill (e.g. mineralisation, detrital clays), weathering and the effects of the present-day, *in situ* stress field. Of these seven key parameters, connectivity is possibly the most difficult parameter to identify in the field largely as it is a subjective term that can only be quantified via indirect measurements (NRC 1996). The term connectivity describes the relative amount of interconnection between finite fractures within a fracture network with the implication that higher degrees of fracture interconnection results in higher overall rock mass permeability. An understanding of the concept of connectivity within a fractured rock aquifer is important because although it is directly linked to fracture properties such as fracture density, orientation, length and aperture it is an independent factor that has a significant impact on fracture network hydraulics. For example, a densely fractured rock mass may still have a low connectivity and permeability if the fractures are of a similar orientation with few intersections.

The closest analogy to the term connectivity is the concept of percolation as defined in percolation theory, which is the study of random networks of conductors and the probability that random fractures are connected and conductive (NRC 1996). Percolation theory is used to estimate the critical fracture density required for an infinite number of connected and conductive fracture clusters or "percolation" (NRC 1996). Below this critical density threshold there are only finite sized clusters of connected fractures or no percolation (NRC 1996). However, the basis for percolation theory and hydraulic connectivity is scale-dependent and will vary with the scale of investigation. For example, Long and Witherspoon (1985) found that large scale samples of a well connected fracture network may percolate but a smaller scale sample of the same network may not. The key is whether the scale of measurement is sufficient to capture a statistically representative sample of the

fracture network but this assumes that the fractured rock mass is homogeneous (Long *et al.* 1982; Long and Witherspoon 1985).

There are many numerical modelling studies concerned with the determination of connectivity within fractured rock masses. These studies cover issues such as site characterisation and model validation, scale dependence and scale effects of fracture network permeability, relationships between permeability and fracture parameters such density, length and aperture distributions as well as appropriate modelling methodologies for applications such as flow and contaminant transport at fractured rock sites (e.g. Bour and Davy 1998; Davy *et al.* 2006; de Dreuzy *et al.* 2001; Long *et al.* 1982; Long and Witherspoon 1985; Hsieh 1998; Odling *et al.* 1997; Renshaw 1996; Renshaw 1999; Wellman and Poeter 2006). There are also numerous field-based studies, which have inferred the existence of hydraulic connections between multiple boreholes within a fractured rock aquifer site as detected via direct borehole hydraulic testing (e.g. Cook 2003; NRC 1996; Paillet 1993; Shapiro *et al.* 2007). However, these particular field-based methods largely rely on detecting interference/anomalies within observation wells, which through their own establishment may alter the natural hydraulics of the system and introduce unnatural connections within the aquifer (Paillet 1993). To avoid these unnatural connections techniques that test an aquifer without observation wells or isolate discrete well intervals (e.g. inflatable packers) are required (Paillet 1993; Shapiro *et al.* 2007). However, in field-based studies, the identification or more often the inference of processes that determine sub-surface fracture network connectivity is complex and problematic and strongly scale-dependent. Therefore, the key to understanding fracture network connectivity is observation over a wide (m to km) scale range yet this is rarely achieved largely for practicality and cost reasons.

Due to the inherent heterogeneous nature of fractured rock aquifers, field-based studies relating to fracture network connectivity require that the structural and hydraulic nature of fractured rock aquifers be characterised through a multi-disciplinary approach that incorporates several methodologies including hydrogeochemistry, geological mapping and borehole hydraulic and geophysical testing. One good example of this type of multi-disciplinary approach is presented by Shapiro *et al.* (2007) which used a wide range of field and hydrogeological

modelling techniques to characterise groundwater flow and solute transport over metre to kilometre scales in fractured crystalline rocks at the Mirror Lake site, New Hampshire. For example, Shapiro *et al.* (2007) measured the transmissivity of discrete individual and closely spaced fracture sets within 3-5m wide packer-isolated sections of single wells and found that these varied by six orders of magnitude (10^{-4} to 10^{-10} $m^2.s^{-1}$). However, when Shapiro *et al.* (2007) conducted cross-borehole hydraulic pump tests over 10's of metres, which included the presence of both high and low transmissivity fractures, the bulk rock mass hydraulic conductivity was relatively low (10^{-7} $m.s^{-1}$). This led Shapiro *et al.* (2007) to the important conclusion that the bulk rock mass hydraulic connectivity is controlled by the less conductive interconnected fractures, which act as hydraulic "bottlenecks" that impede groundwater flow. Furthermore, Shapiro *et al.* (2007) inferred that the discrete highly transmissive fracture zones were most likely not connected within the network. Their findings suggest a strong scale-dependency of the results collected from single wells (metres) versus results collected over multiple wells (10's of metres).

The key issues that are yet to be fully understood is how fracture network connectivity may change with increasing depth or be modified by secondary processes such as weathering, uplift and unloading and sub-surface fracture deformation. With a well characterised fractured rock aquifer, this study aims to: (1) describe the key elements that control hydraulic connection within a fractured rock aquifer; (2) provide examples where the effects of hydraulic connectivity can be recognised in both single well and catchment-scale hydrogeological datasets as well as surface and borehole electrical and electromagnetic geophysical surveys; and (3) demonstrate the role of *in situ* stress in modifying the inherent hydraulic connectivity of an aquifer through the use of stochastic, coupled hydromechanical (HM) models. This study is unique in that the field data is supported by representative large and small scale HM models, which demonstrate that changes in hydraulic connectivity is strongly influenced by fracture formation and deformation in response to the present-day, *in situ* stress field. The inclusion of HM models is important as techniques such as outcrop mapping, borehole hydraulic and geophysical surveys do not account for sub-surface fracture deformation and its integrated HM response on a fracture network as a whole.

This study builds on an earlier study by Mortimer *et al.* (2011) which combined local- and regional-scale field hydrogeological datasets with stochastic HM models to investigate the influence of present-day, *in situ* stress fields on groundwater flow patterns in shallow (<200 m depth) fractured rock aquifers. A key conclusion of Mortimer *et al.* (2011) is that *in situ* stress does have a discernible effect at shallow depths in terms of variable fracture deformation distributions, which affect overall 3D fracture network hydraulic conductivity, connectivity, anisotropy and groundwater flow rates. Whilst Mortimer *et al.* (2011) focussed on identifying and characterising the effects of *in situ* stress this study differs by specifically focussing on the role of *in situ* stress in determining fracture network connectivity. This study uses the same datasets and models of Mortimer *et al.* (2011) plus additional surface and borehole geophysical datasets and more detailed small scale HM models to better characterise and simulate features and processes that specifically affect fracture network connectivity.

3.2 Background

The key parameters that determine the overall connectivity of a fractured rock aquifer are the spatial distribution of fracture densities (fractures per unit volume), orientations (strike and dip), planar dimensions (area or trace extent) and hydraulic apertures (NRC 1996). Of these, fracture density is considered one of the more critical parameters for connectivity with natural fracture networks tending to have fracture densities close to the percolation threshold (Renshaw 1996). Fracture density together with orientation and dimension determine the probability of multiple fracture intersections occurring within a rock mass volume. However, this information alone is insufficient as the distribution of fracture apertures and transmissivities of individual fractures and how they are linked within the network ultimately determine the overall permeability of a fractured rock medium (Long and Witherspoon 1985; Renshaw 2000). For example, the hydraulic conductivity of a fractured rock mass is extremely sensitive to its aperture as demonstrated by the "Cubic Law". This law defines the hydraulic conductivity of an individual fracture idealized as an equivalent parallel plate opening. For an isolated test interval within a borehole, it is expressed as:

$$K_b = \frac{(2b)^3}{2B}\frac{\rho g}{12\mu} \quad (3.1)$$

Where K_b is the bulk hydraulic conductivity ($m.s^{-1}$) (where K_b = Transmissivity/test interval), $2b$ is the fracture aperture width (m), $2B$ is the fracture spacing (m), ρ is the fluid density ($kg.m^{-3}$), g is gravitational acceleration ($m.s^{-2}$) and μ is the dynamic viscosity of the fluid (Pa.s).

The Cubic Law is a reasonable approach but unrealistic as it assumes that all fractures are infinite, planar, uniform and inelastic and that the bulk hydraulic conductivity of the medium is determined by the sum of contributions of all individual fractures (Snow 1969). In reality, the degree of fracture interconnection and fracture heterogeneity determines the bulk hydraulic conductivity of a fractured rock medium, which is often less than that predicted by the Cubic Law (Long and Witherspoon 1985).

With increasing depth comes increasing magnitudes of *in situ* stress, which results in progressive deformation of fracture apertures and progressive changes in fracture network hydraulics and connectivity. In general, stress fields are inhomogeneous and defined in simplified terms by three mutually orthogonal principal axes of stress, which are assumed to lie in the vertical (σ_V) and the maximum (σ_H) and minimum (σ_h) horizontal planes. In practice, far-field crustal stress regimes are classified using the Andersonian scheme, which relates the three major styles of faulting in the crust to the three major arrangements of the principal axes of stress (Anderson 1951). These stress regimes are: (a) normal faulting ($\sigma_V > \sigma_H > \sigma_h$); (b) strike-slip faulting ($\sigma_H > \sigma_V > \sigma_h$); and (c) reverse faulting ($\sigma_H > \sigma_h > \sigma_V$). Sub-surface fracture deformation in response to *in situ* stress has been shown to have a significant effect on fracture network hydraulics and connectivity progressively with depth from the near surface (Barton *et al.* 1995; Mortimer *et al.* 2011). Stress-dependent fracture permeability manifests itself as fluid flow focussed along fractures, which are favourably aligned within the *in situ* stress field and if fractures are critically stressed, this could impart significant permeability anisotropy to a fractured rock mass. Specifically, preferential flow occurs along fractures that are oriented orthogonal to the minimum principal stress direction (due to low normal stress) or

inclined ~30^{o} to the maximum principal stress direction (due to dilation) (Barton *et al.* 1995). The amount and rate of fracture deformation depends on several factors such as the nature of the contemporary stress field, depth, rock type, strata thickness, position within the overall stratigraphic sequence, relative mechanical contrasts between adjacent rock units and fracture "stiffness" (Price 1966; van der Pluijm and Marshak 2004; Rutqvist and Stephannson 2003). Furthermore, fracture hydraulic apertures may be affected by processes such as mineralisation and detrital clay infill, which can partially or fully close fracture apertures hence altering the original transmissivity of individual fractures (Banks *et al.* 1996; Laubach *et al.* 2004).

The degree to which a fracture may deform is largely determined by its fracture stiffness, which is primarily a function of fracture wall contact area. Normal stiffness (jk_n) and shear stiffness (jk_s) of a fracture are measures of resistance to deformation perpendicular and parallel to fracture walls, respectively. Normal stiffness is a critical parameter that helps to define the hydraulic conductivity of a fracture via an estimate of the mechanical aperture as opposed to the theoretical smooth planar aperture as described in the Cubic Law. Estimates of fracture stiffness are derived by a variety of field logging or laboratory tests, which are well documented in comprehensive reviews by Bandis (1993), Barton *et al.* (1985), Barton and Choubey (1977) and Hoek (2007). Standard practice is to derive stiffness estimates based upon fundamental measurements of fracture surface topography profiles and the elastic properties of the intact rock material. Ultimately, estimates of fracture stiffness attempt to account for more realistic fracture heterogeneity, asperity contact, deformation and tortuous fluid flow.

3.3 Methodology

The field site chosen for this investigation is the Wendouree Winery located within the Clare Valley, South Australia (Figure 3.1). It is an ideal field site as it is underlain by a fractured rock aquifer terrain situated within a near horizontal, WNW-ESE directed regional compressional stress field that is seismically active and undergoing uplift and erosion (Sandiford 2003). The Wendouree field site is located approximately 2 km SSE of the township of Clare and it is a well-instrumented,

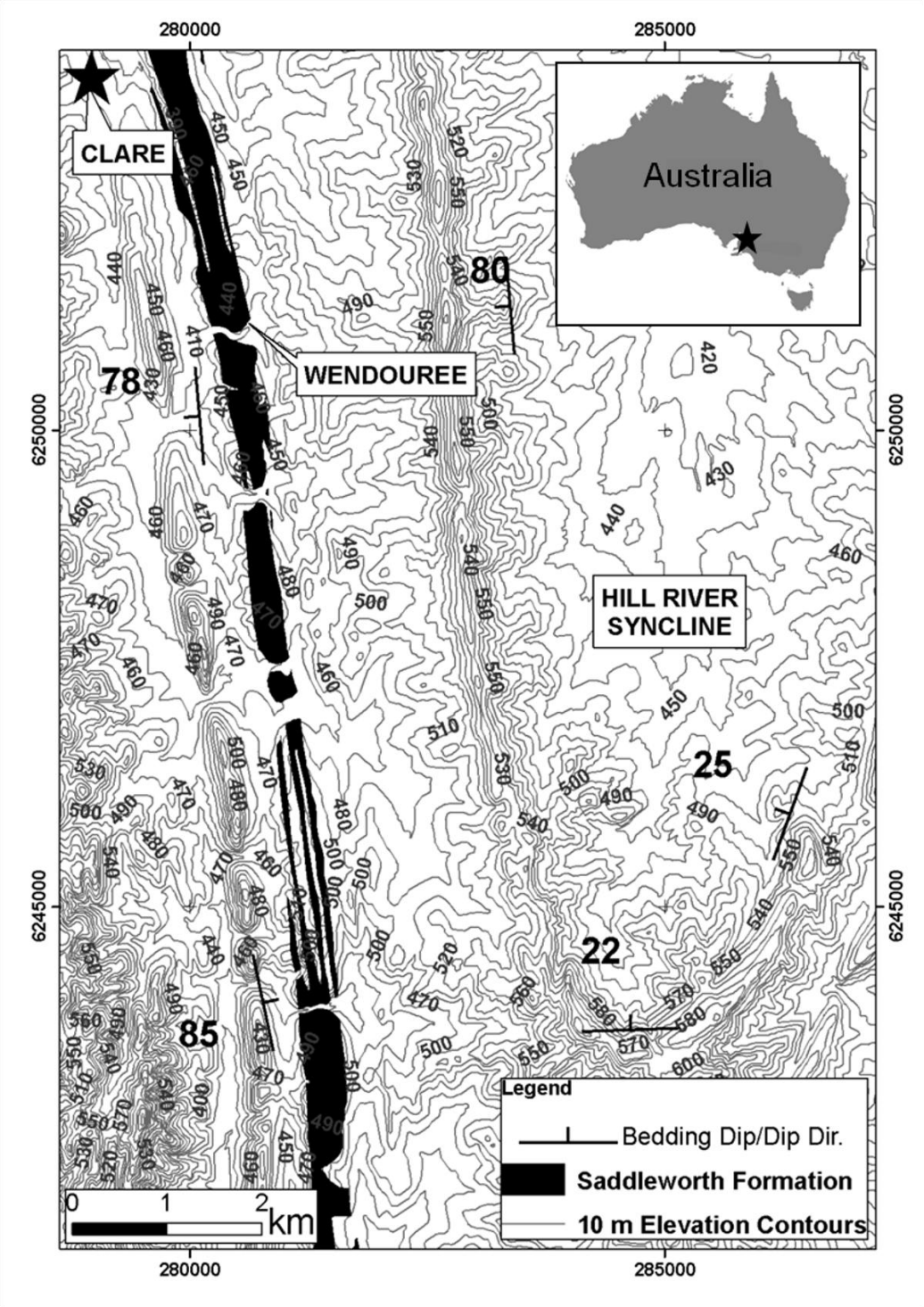

Figure 3.1 Location of the Neoproterozoic (~730 Ma) Saddleworth Formation and Wendouree field site in the Clare Valley catchment with 10 m topographic contours. The basement geology is comprised of a layered sedimentary sequence that has been folded into the large "Hill River Syncline". The Wendouree site is located on the overturned, western limb of this syncline (Geological Survey of South Australia 2001).

multi-piezometer site located within the steeply dipping, overturned, western limb of the large "Hill River Syncline" structure. It contains several observation wells ranging in depths from 60-222 m which are all located within low porosity and permeability, thinly laminated (mm to cm), carbonaceous siltstones and dolomites of the Auburn Dolomite unit (Saddleworth Formation) over an area of ~0.1 km^2 (Figure 3.2; Love 2003). Drill logs and core samples at Wendouree show that the weathered to fresh bedrock transition occurs at ~18 m depth below the surface.

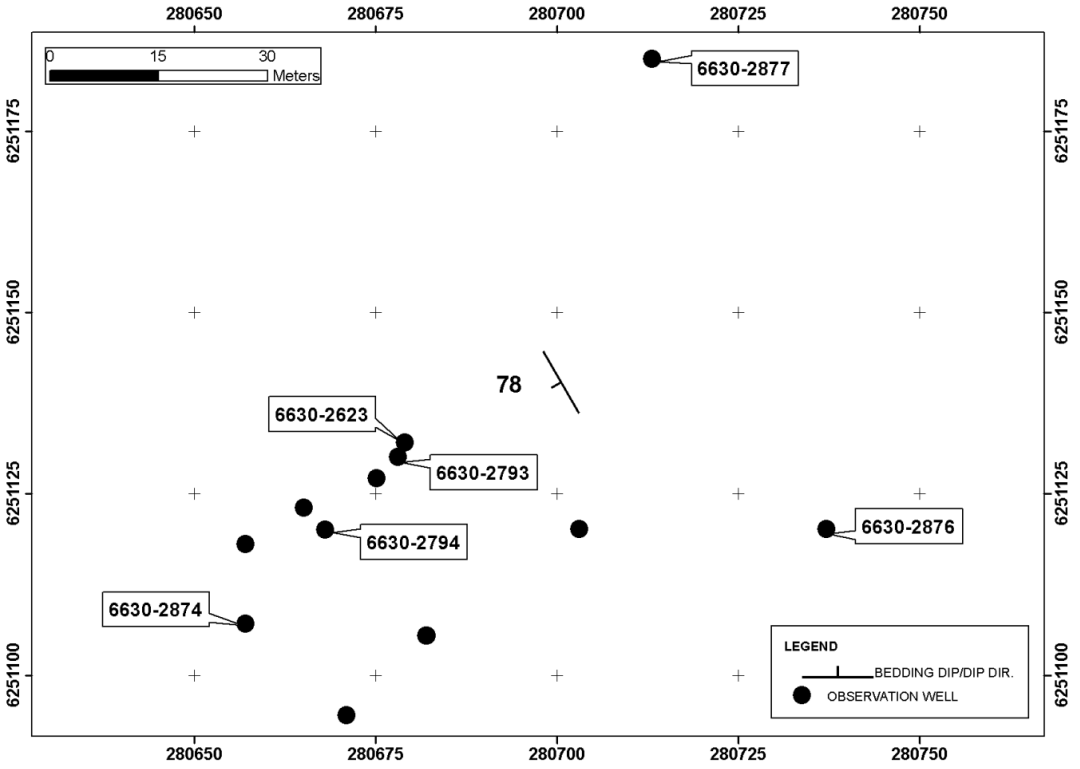

Figure 3.2 The Wendouree multi-piezometer field site in the Clare Valley showing the locations of the wells (Unit Nos.) discussed in this study (PIRSA 2009).

The methodology of this study is the same as that of Mortimer *et al.* (2011) which involves the following three key steps:

1. A synthesis of the geological and hydrogeological setting from a review of the pre-existing data and knowledge of the local- to regional-scale geology and hydrogeology. This includes fracture network characterisation results of Mortimer *et al.* (2011) which involved mapping of selected outcrops within the Hill River

Syncline, limited drill core logging and *in situ* borehole fracture mapping and hydraulic characterisation at the Wendouree site. The *in situ* characterisation of the Wendouree fracture network was derived from the interpretation of coincident acoustic borehole televiewer (BHTV) and high resolution temperature logs within four open wells (6630-2794, -2874, -2876 and -2877) ranging from 90 to 222 m depth (Figure 3.2). Similar to the methods of Barton *et al.* (1995) and Ge (1998), potentially hydraulically active fractures were identified based upon the coincidence of BHTV-imaged fractures with temperature gradient (dT/dx) anomalies indicative of advective groundwater flow in or out of a well. Other rock mass and fracture parameters were gained from limited drill core samples (well 6630-3068; Figure 3.2) and scanline fracture mapping data of (T Halihan, Flinders University, unpublished data, 1999). This study includes additional borehole electromagnetic (EM) flow meter (single inflatable packer) logs collected under pumped conditions for the same four observation wells.

2. Development of a conceptual Wendouree model based on the results of Step 1 above.

3. Stochastic hydromechanical (HM) modelling of the conceptual Wendouree model using the 2D Universal Distinct Element Code (UDEC). UDEC represents the rock mass as an assembly of discrete deformable, impermeable blocks separated by discontinuities (faults, joints etc) and can reproduce fully coupled HM behaviour (Itasca, 2004). The basic HM model predicts the physical response of a fractured rock mass to an imposed stress field and the stress-displacement relationship of the medium, while satisfying the conservation of momentum and energy in its dynamic simulations with fluid flow calculations derived from Darcy's Law (for a comprehensive review of the UDEC governing equations see Itasca, 2004). In recent years, several researchers have successfully used UDEC to investigate the link between rock deformation and fluid flow within fractured rock masses over a range of crustal depths, stress regimes, geological settings and fracture network geometries (e.g. Cappa *et al.* 2005; Gaffney *et al.* 2007; Min *et al.* 2004; Zhang and Sanderson 1996; Zhang *et al.* 1996).

In this study we use the same large scale (100-200 m) cross-sectional and horizontal planar HM models of Mortimer *et al.* (2011). These models involve stochastic geometrical models based upon real but simplified data inputs and are not designed

to produce a precise match to the field data but rather to demonstrate how sub-surface fracture deformation processes alter fracture network hydraulics and connectivity. In these models, rock mass deformation was defined by the Mohr-Coulomb model and fracture behaviour was defined by the Coulomb-Slip criterion that assigns elastic stiffness, tensile strength, frictional, cohesive and dilational characteristics to a fracture (Itasca 2004). A comparison between deformed (stressed) and undeformed (zero stress) HM models is used as the basis for identifying the key features and processes that affect fracture network connectivity. Furthermore, this study includes the addition of small scale (1 x 1 m) HM models to demonstrate how variable sub-surface fracture deformation processes play a critical role in determining the bulk hydraulic conductivity of the fractured rock mass.

3.4 Geological setting

The Clare Valley catchment (~500 km^2) is located approximately 100 km north of Adelaide, South Australia, and lies within the northern Mount Lofty Ranges (Figure 3.1). The Mount Lofty Ranges forms part of the "Adelaide Geosyncline", which is a Neoproterozoic to Cambrian age (~827–500 Ma), thick (>10 km), rift-related, sedimentary basin complex comprising of thinly laminated (mm) to thick (m) layered sedimentary strata (Preiss 2000). During the Middle-Late Cambrian "Delamerian Orogeny", the rocks of the Clare Valley were subjected to low-grade, greenschist facies metamorphism and three deformation events. This was a major episode of crustal shortening leading to strongly contractional, west-verging, thrust faulting and NNW-trending folding (Preiss 2000). From the Delamerian Orogeny until the late Miocene period the Adelaide Geosyncline remained relatively tectonically stable (Preiss 1995). As southern Australia entered the late Miocene period (<10 Ma) a new phase of tectonic activity commenced, which was initiated by coupling and/or convergence between the Pacific and Australian plates (Hillis and Reynolds 2000; Sandiford *et al.* 2004). As a consequence, the Clare Valley is currently under near horizontal, approximately WNW-ESE directed compression and related seismic activity, which correlates both spatially and temporally with ongoing fault activity along major range bounding faults of the Adelaide Geosyncline (Sandiford 2003). Evidence found on some of these major range bounding faults suggest that the

vertical component of their slip rates are in excess of tens of metres Myr^{-1} over the past 5 Myr leading to widespread uplift, erosion and the present-day topography of the Mount Lofty Ranges (Sandiford 2003).

There have been no *in situ* borehole stress field data collected within the Clare Valley region, therefore, this study is based upon well documented regional, far-field earthquake focal mechanism data, which are considered reliable and consistent indicators of far-field stress regimes and their orientation (Zoback 2007). In the year 2001, the town of Clare experienced nine small earthquakes up to magnitude 2.8 whilst in 1995 the nearby township of Burra recorded a significant magnitude 5.1 earthquake (PIRSA Minerals 1999; 2001). An evaluation of the focal mechanism for this particular Burra earthquake event revealed a reverse faulting stress regime with near horizontal compression (σ_H) in a direction of 110° at a depth of 18-20 km with σ_h inferred to be mutually orthogonal at 020°. Although the region is undergoing horizontal compression at depth, the uppermost shallow crust is simultaneously experiencing widespread uplift, unloading and erosion (Sandiford 2003). That is, the uplift and unloading processes affecting the Mt Lofty Ranges are concurrent with and in direct response to the far field tectonic compression. It is not known to what depth the effects of uplift and unloading occur in this region but studies elsewhere in the world have shown that it could extend a few hundreds of metres to 1 km below the surface (Engelder 1985; Hancock & Engelder 1989). The focus of this study is on the upper 200 m depth horizon, which is inferred to be under the influence of a normal stress regime that involves isotropic, lateral relaxation of the rock mass consistent with the effects of uplift and unloading (i.e. $\sigma_V > \sigma_H = \sigma_h$). This inference is appropriate given that relaxation of the rock mass is expected to be near complete considering that the total regional uplift has been estimated at greater than 200 m and that erosion processes are known to be occurring at a rate faster than that of uplift (Sandiford 2003).

Outcrop mapping exercises conducted at several locations across the Clare Valley found a consistent joint set pattern present within the various layered rock units of the Hill River Syncline. In addition to bedding planes, there are four joint set structures including sub-vertical “ac” (extension) joints, sub-horizontal “bc”

(extension) joints and two moderately dipping conjugate “hk0” (shear) joints, which together produced a pattern typical of jointing in response to simple folding of a layered sedimentary sequence (Price 1966; van der Pluijm and Marshak 2004) during the Delamerian Orogeny (Figure 3.3). Only the joint density varied at each outcrop as determined by each rock type, thickness and position within the sequence i.e. a stratabound joint formation pattern. It is this palaeo-stress regime and its associated deformation, which is the primary control on the development of fracture networks and fracture permeability within the fractured rock aquifers of the Clare Valley.

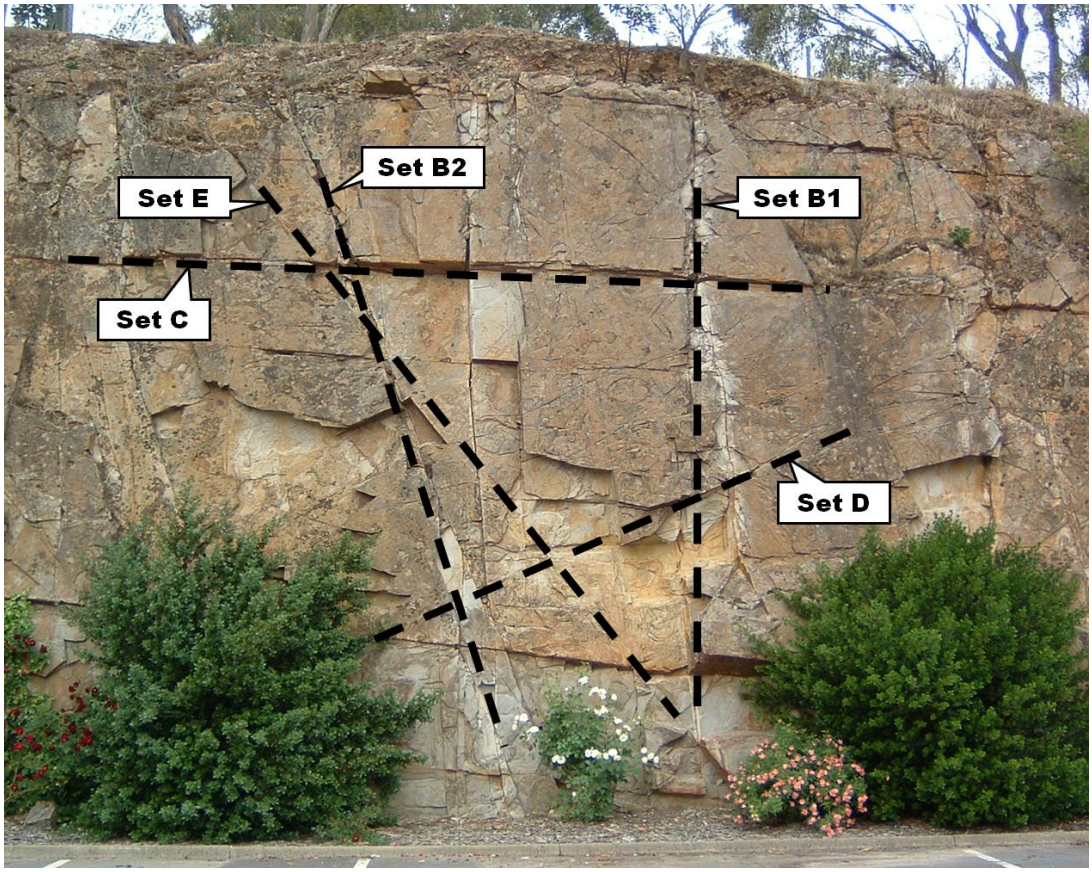

Figure 3.3 ENE-looking, longitudinal section view of a near vertical bedding plane within the Saddleworth Formation (Auburn Dolomite unit) located on the western limb of the Hill River Syncline (~5 m high rock face). This outcrop exposure contains the same rock unit and structures as that intersected in drill holes at the Wendouree site located ~2 km to the SSE. Note the five fracture sets typical of this area: bedding planes (Set A); “ac” (extension) joints (Set B1 and B2); sub-horizontal “bc” (extension) joints (Set C) and conjugate “hk0” (shear) joints (Set D and E).

3.5 Hydrogeological setting

Within the Clare Valley catchment there are relatively consistent and distinctive groundwater patterns. For example, Figure 3.4 is a plot of measured well yield (normalised against the total well depth, L/s/m) for all wells recorded within the catchment versus the total depth of the well. The large majority of these wells are open and used for domestic/agricultural purposes. Compared to near surface (0-10 m depth), median groundwater yields have decreased ~3 fold and ~4 fold at approximately 40 m and 100 m depth below the surface, respectively, suggesting the existence of a hydraulic discontinuity at ~40 m depth below the surface (Figure 3.4). This regional well yield dataset is independent of lithology and position within the overall folded sequence nor can this vertical trend be explained by near-surface weathering. A review of a significant volume (hundreds) of geological water well logs sourced from the State Government online database show that across the catchment the depth of weathering is typically <20 m below the surface (PIRSA 2009). This regional, vertical, groundwater yield trend was also observed at a local scale of the Wendouree site as demonstrated by electromagnetic (EM) flow meter profiles collected as part of this study (Figure 3.5). These EM flow meter profiles reveal the flow distribution entering the well and also show a very sharp decrease to almost negligible groundwater flow rates commencing from approximately 40-60 m depth below the surface (Figure 3.5). Again, this local vertical groundwater flow trend cannot be explained by the near-surface weathering profile (~18 m depth) or by any variance in the uniform carbonaceous silt and dolomite host rocks. These regional- to local-scale field observations suggest that vertical groundwater flow profiles is influenced by some other regional scale factor controlling depth dependent changes in fracture hydraulic connectivity.

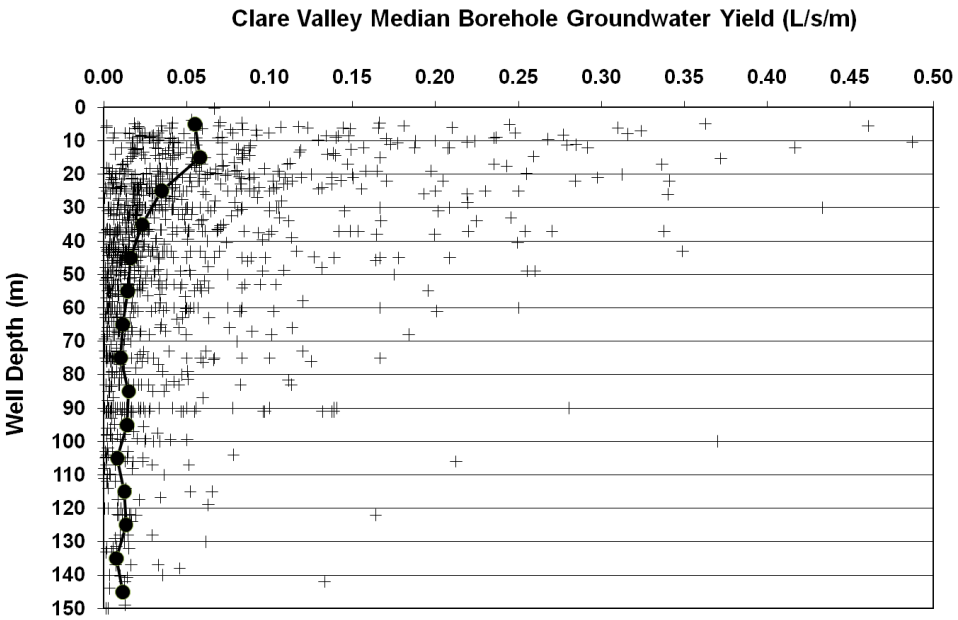

Figure 3.4 Clare Valley catchment-wide well groundwater yields whereby each well yield value was normalised against the total depth of the well then plotted against the total depth of the well (L/s/m, n=1316 drill holes). The "+" symbols represent individual data points whilst the connected solid circles represent the calculated median yield/metre for 10 m thick depth intervals below the surface (PIRSA, 2009). Note that the weathered to fresh rock transition across the catchment generally occurs at <20 m depth below the surface.

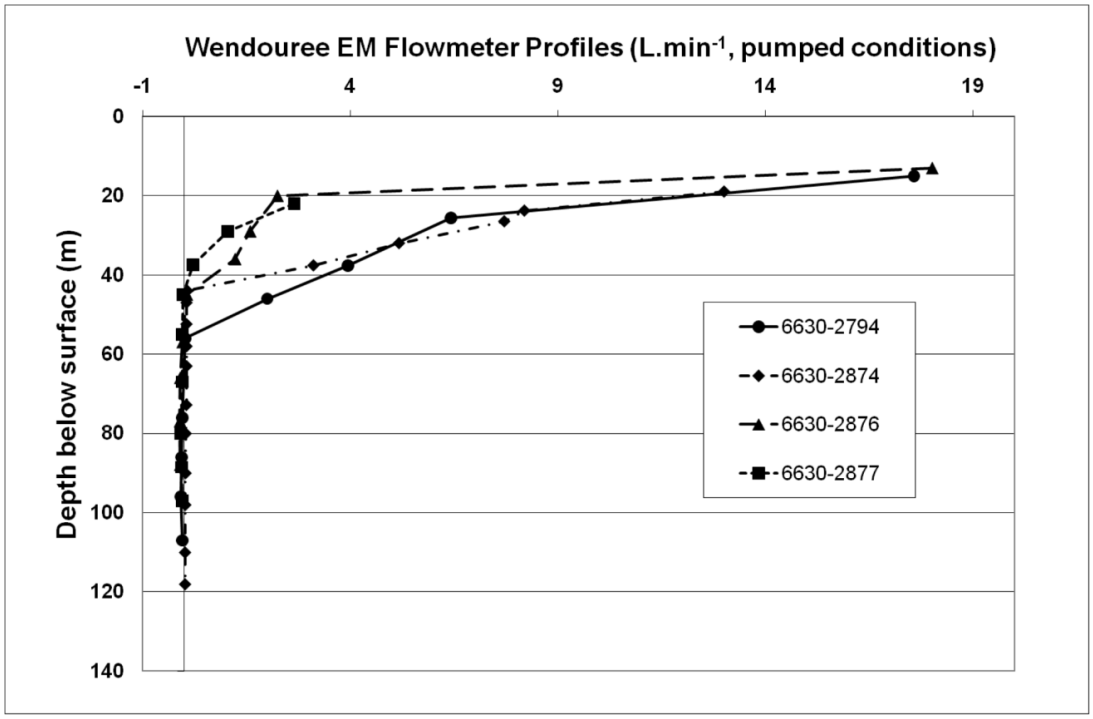

Figure 3.5 EM flow meter profiles under pumped conditions (20 L.min-1) for four Wendouree observation wells (Wells 6630-2794, -2874, -2876 and -2877; see Figure 3.2) located over an area of ~100 m2.

Evidence cited by Love (2003) from piezometer pumping tests and ^{222}Rn concentration depth profiles at Wendouree revealed that the hydrogeology is characterised by high spatial variances in bulk hydraulic conductivity (K_b) values and groundwater flow rates in the upper 100 m depth horizon (Figure 3.6). ^{222}Rn is produced from *in situ* decay of ^{238}U within the aquifer and because of its short half-life (3.83 days) it is used to locate zones of active groundwater flow into wells and as a proxy for lateral flow rates (Love *et al.* 2007). That is, relatively high ^{222}Rn concentrations in groundwater indicates high flow rates within fractures that rapidly transport ^{222}Rn to the well prior to it decaying below detection limits. Together, these Wendouree K_b and ^{222}Rn profiles provide an indication of transmissivities and groundwater flow rates as a function of depth and also suggest the presence of a significant hydraulic discontinuity located at ~40 m depth below the surface that is not coincident with the known weathered to fresh rock transition located at ~18 m depth. The pumping test and ^{222}Rn data are supported by ^{14}C, CFC-12 and ^{3}H data

collected from the same piezometers. These environmental tracers all show modern groundwater ages within the upper 40 m depth horizon indicating rapid vertical circulation whilst more ancient groundwater occurs at > 40 m depth (Love 2003). Estimates of vertical recharge rates at Wendouree from the ^{14}C groundwater age profiles were ~20 $mm.yr^{-1}$ for the upper system (<40 m depth) and <0.2 $mm.yr^{-1}$ for the lower one (>40 m depth) (Love 2003). This suggests that there is minimal hydraulic connection and vertical leakage between these two horizons, a phenomenon also observed elsewhere in the catchment (Cook *et al.* 2005). Regardless of depth, anomalous spikes in ^{222}Rn and ^{14}C concentrations were also found to coincide with major electrical conductivity, temperature and pH discontinuities indicating the presence of significant hydraulically active fractures and advective groundwater flow at specific down hole locations (Love 2003). However, it is clear from the data presented in Figures 3.4-3.6 that at shallow depths (<40 m) the system is hydraulically more active than at greater depths (>40 m).

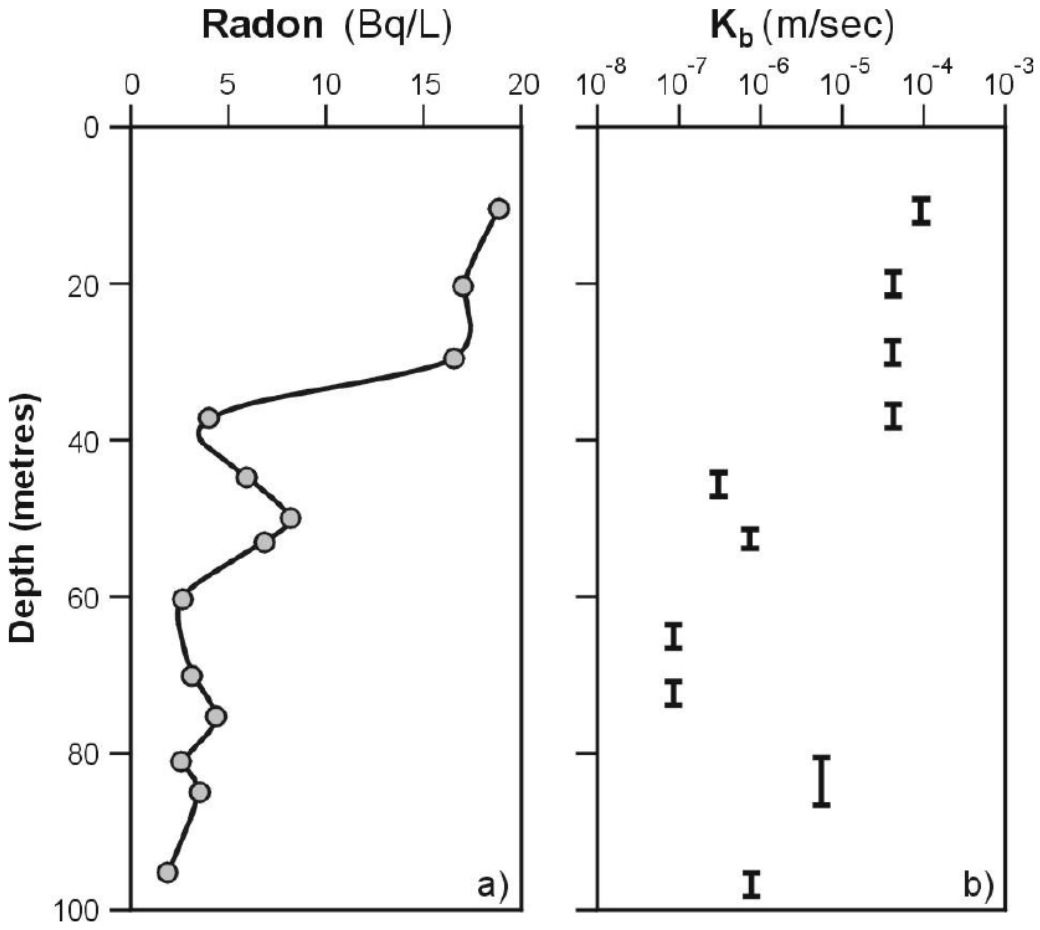

Figure 3.6 An example of ^{222}Rn and bulk hydraulic conductivity (K_b) profiles at Wendouree: (a) ^{222}Rn (Bq.L^{-1}) open well profile (well 6630-2623); and (b) K_b (m.s^{-1}) estimates from piezometer pump test (wells 6630-2623 and -2793). The vertical bars of the K_b profile represent the length of the slotted piezometer interval (Love 2003).

In an attempt to detect hydraulic connection between boreholes at Wendouree, Love *et al.* (2002) conducted a pump-packer test and observed water level changes in a piezometer nest located approximately 14 m to the NE of the pumped borehole (Well 6630-2794; Figure 3.2). This test suggested that a strong vertical connection existed between piezometers located in the upper 0-40 m depth horizon and the packer interval located between 60-65 m depth. At piezometer depths of between 40-75 m, the packer test recorded variable but lower degrees of hydraulic connection whilst at depths >80 m the two deepest piezometers recorded no hydraulic connection. This

pump-packer test data further supports the existence of decreasing levels of hydraulic connectivity with increasing depth and the presence of a significant hydraulic discontinuity located at approximately 40 m depth below the surface.

At Wendouree, Mortimer *et al.* (2011) analysed coincident acoustic BHTV and high resolution temperature logs from four open wells (6630-2794, -2874, -2876 and -2877) ranging from 90 to 222 m depth (see Figure 3.2). The stereographic analysis of the 626 fractures imaged with the BHTV revealed five distinct fracture sets that correlate with bedding and joint set measurements recorded from nearby outcrop and elsewhere within the Clare Valley i.e. the five geological structures typical of the region (Sets A-E; see Figure 3.3). Furthermore, an evaluation of the population distribution and orientations of the interpreted hydraulically active fractures indicated that steeply dipping (>70°) bedding planes and joints are dominantly the most hydraulically active fractures (Mortimer *et al.* 2011). They represented the approximately orthogonal NW-SE striking bedding plane (Set A) and the NE-SW striking "ac" joint set (Set B). This interpretation is plausible given the uplift and unloading stress regime expected at these shallow depths, which should favour steep dipping structures under conditions of isotropic, lateral relaxation of the rock mass.

In a different Clare Valley study, Skinner and Heinson (2004) conducted several electromagnetic (EM) surface and direct current (DC) surface, borehole-to-surface and borehole-to-borehole geophysical surveys at several sites across the catchment including Wendouree. The purpose of their study was to attempt to use electrical and electromagnetic techniques to detect hydraulic pathways within heterogeneous fractured rock aquifers based on the theory that saline fluid saturated fractures are relatively more electrically conductive than their impermeable host rock matrix and can distort the local potential field (Skinner and Heinson 2004).

Specifically at Wendouree, Skinner and Heinson (2004) conducted a surface EM azimuthal survey with EM34 coplanar transmitter-receiver coils in both horizontal and vertical coil orientations (Well 6630-2874; Figure 3.2). This method involved rotating these coils around a selected borehole whilst recording variations in the resistivity of the ground as a function of geographical orientation (azimuth). Figure

3.7 shows a comparison of the results of two surface EM azimuthal resistivity surveys completed at 10 m and 40 m dipole separation distances. The results are depicted as contoured polar plots of calculated apparent electrical conductivity versus azimuth with the calculated apparent conductivity being the weighted average over the penetration depth of the signals, where the weighting depends on the coil orientation and separation. These results reveal that at 10 m dipole separations the direction of maximum apparent electrical conductivity is near symmetrical yet subtly elongated in a NNW-SSE direction. At 40 m dipole separations, this elongation becomes more pronounced with the increased anisotropy being attributed to greater depth penetration and spatial resolution of steeply dipping, conductive fractures, particularly with the vertical coil configuration. A similar asymmetrical-shaped geophysical anomaly was recorded at Wendouree with a DC borehole-to-surface survey, which found the highest electrical potential was oriented NNW-SSE with a down dip direction to the WSW coincident with the strike and dip of the bedding planes (Skinner and Heinson 2004). These methods can be considered analogous to determining the maximum permeability direction of a fractured rock aquifer, which in this case, is aligned with the strike of the bedding planes at the site. This finding was repeated at several other locations throughout the Clare Valley, which suggests that bedding planes are the dominant hydraulically active fractures within the catchment (Skinner and Heinson 2004).

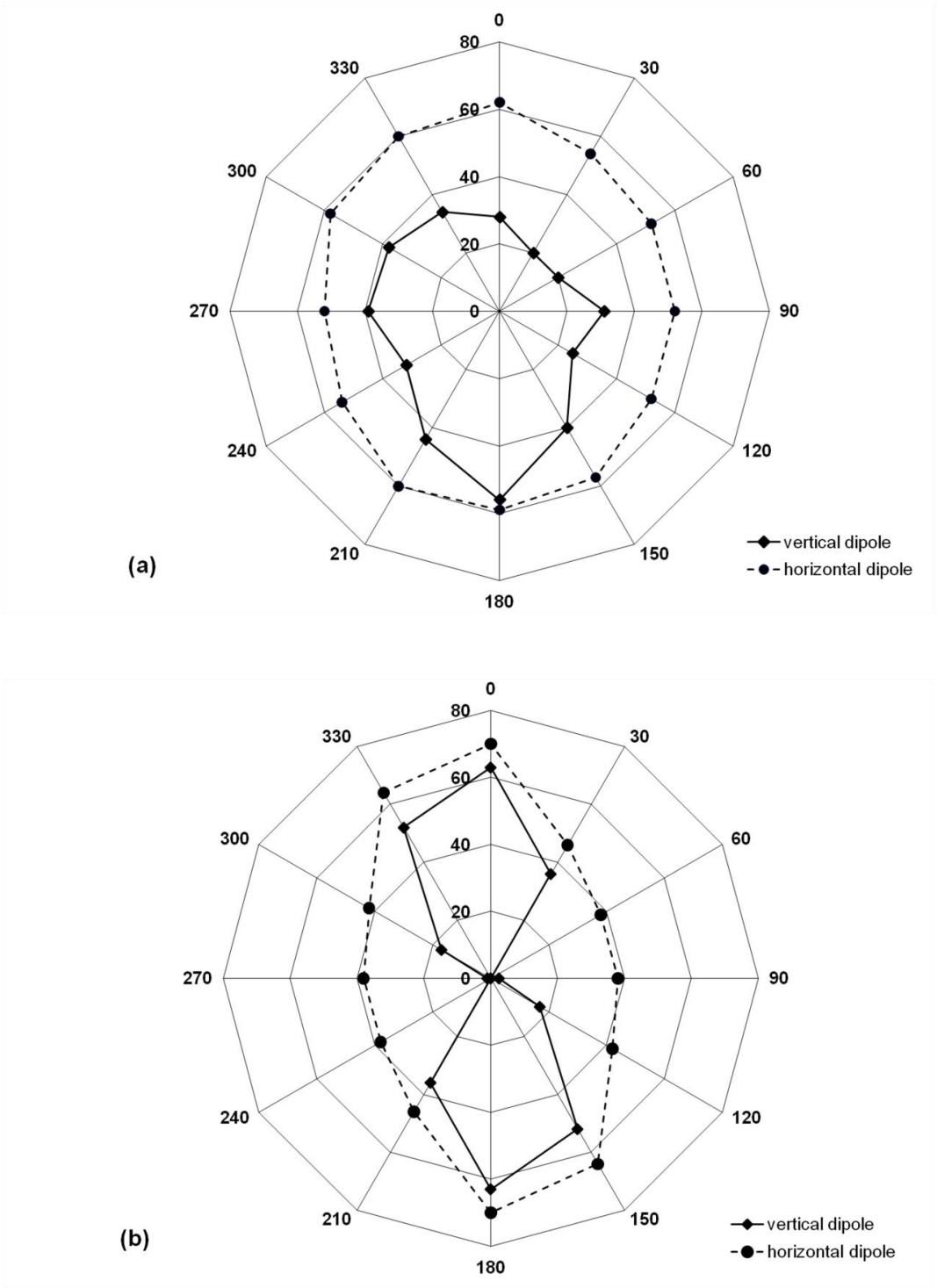

Figure 3.7 Polar plots of surface EM resistivity azimuthal data collected at well 6630-2874 (a) 10 m; and (b) 40 m dipole separations (units of Ωm) for both vertical (diamonds) and horizontal (circles) dipole orientations.

These surface and borehole-to-surface geophysical surveys were used to define the dominant hydraulically conductive fractures at each site. However, to test the hydraulic connectivity between boreholes requires the use of DC cross-borehole surveys. In this method, a known current is individually driven through electrodes at specific down hole positions in one borehole whilst simultaneously measuring the potential voltage at the same intervals down a second borehole as referenced against a zero potential electrode at the surface. At Wendouree and elsewhere within the catchment, these cross-borehole surveys found several extensive, shallow dipping to horizontal conductive structures at depths ranging from ~20-60 m below the surface (Skinner and Heinson 2004). At another Clare Valley site, located ~12 km south of Wendouree, 2.5D inverse modelling of DC cross-borehole data revealed an approximately horizontal fracture of low resistivity extending across the ~60 x 30 m survey area and although it was discernible in all orientations, its anomalous signature was more enhanced where it intersected steep dipping bedding planes (Skinner and Heinson 2004). This conclusion is significant as it highlights that both the electrical and electromagnetic surface and borehole surveys not only found groundwater flow within the catchment being dominated by flow along steep dipping bedding planes but that it also involves lateral flow being facilitated by low angle intersecting fractures. Like the other datasets and conclusions presented in this study, the results of these geophysical studies were consistent across several sites regardless of lithology and position within the Hill River Syncline and helped to define the two distinct upper and lower groundwater flow systems in the Clare Valley (Skinner and Heinson 2004).

3.6 Conceptual model

Mortimer *et al.* (2011) combined all of the above data and field observations to develop the conceptual Wendouree fracture network model consisting of a densely fractured, clay-rich, weathered, upper zone (0-20 m), a less fractured transitional zone (20-40 m) and a low fracture density zone (>40 m) (Figure 3.8). With increasing depth there is a trend of decreasing fracture density based upon a reduction in the number of finite joint sets (Sets B, C, D and E) against a persistent background of high density bedding planes (Set A). This trend has been observed

within the limited amount of diamond drill core samples available plus the BHTV logs. The primary cause of this fracture density trend is attributed to the effects of uplift and unloading. For example, the Wendouree BHTV logs revealed a proportionally greater amount of sub-horizontal joints in the upper 40m depth horizon, which is considered indicative of neotectonic joint formation in response to unloading (Hancock and Engelder 1989). Thus, the increased development of unloading-related, sub-vertical flexural and sub-horizontal sheeting (or relaxation) joints closer to the surface creates a distinct zoning of the vertical fracture density profile throughout the entire aquifer system. In addition, as depth increases so too will the magnitudes of stress resulting in the progressive deformation of fracture apertures. With increasing depth and stress magnitudes progressive fracture aperture deformation will lead to progressive changes in fracture network hydraulics and connectivity. Overall, the most significant hydraulically conductive fractures are expected to be the steeply dipping fractures (Sets A and B), considering that the vertical stress is the major principal stress.

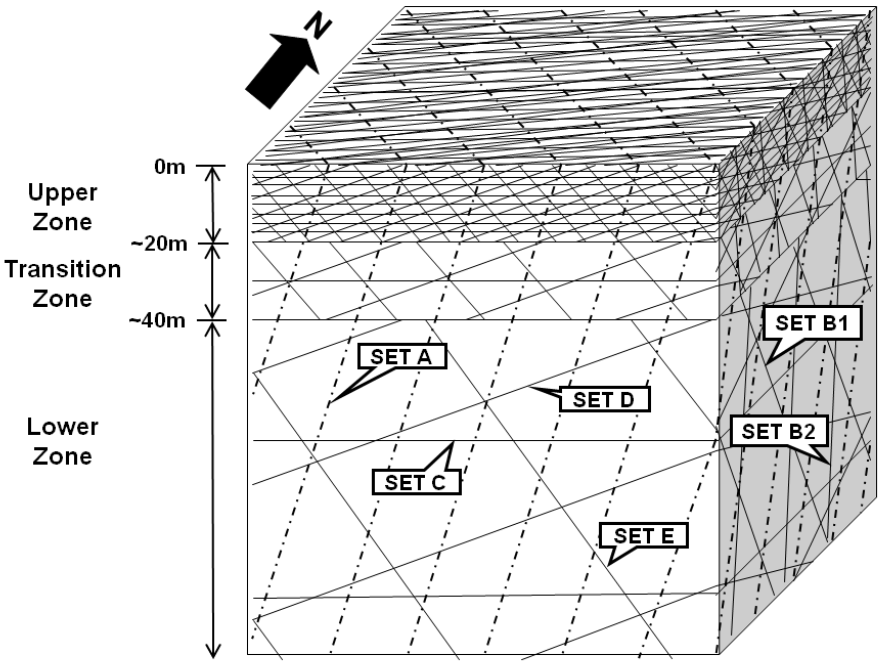

Figure 3.8 A schematic example of the Wendouree conceptual fracture network model showing decreasing joint densities between the upper, transition and lower zones. Dashed lines denote the persistent, dense, bedding planes of Set A whilst the solid lines represent joint sets B, C, D and E.

3.7 Fracture network connectivity models

The philosophy of this HM modelling exercise is to demonstrate the process of fracture deformation and its influence on network hydraulic connectivity with representative, 2D fracture network models under shallow depth conditions. These models are constrained and correlated with known geology and groundwater flow observations, however, these models are not designed to produce a precise match to the field data but to help demonstrate how the process of sub-surface fracture deformation alters fracture network connectivity and fluid flow. This includes the use of stochastic geometrical models based upon real but simplified data inputs that can identify groundwater flow trends and the key features and processes that have the most influence across small to large scales. To identify the key processes that determine fracture network hydraulics and connectivity necessitates the use of HM models at two different scales. Specifically, this study utilised the large-scale (100-200 m block size) stochastic models of Mortimer *et al.* (2011) to demonstrate the effects of depth-dependent changes in fracture density and sub-surface fracture deformation processes on groundwater flow. The addition in this study of small-scale (1 x 1 m block size) models is designed to help visualise how the inherent fracture network connectivity can be altered by secondary processes such as sub-surface fracture deformation as well as to test both quantitatively and qualitatively the observations of Shapiro *et al.* (2007).

3.7.1 Model design

The large scale stochastic, 2D Wendouree UDEC models are based upon the conceptual fracture network model (see Figure 3.8) and are simple 100m to 200 m size, cross-section and planar models built from the surface down (Figure 3.9a and b). The small-scale 1 x 1 m model is a horizontal planar model that represents a sample snapshot of the larger scale models at a depth of 100 m below the surface (Figure 3.9c). These 2D models describe a geometrical reconstruction that consist of 2D vertical or horizontal planar slices of the conceptual fracture network model which incorporate the effects of the 3D stress field (i.e. σ_V, σ_H, and σ_h). The blocks defined by the fracture network generated within UDEC were discretized into a

triangular mesh of constant strain with the nodal distances varying from 1.5 m (large-scale models) to 0.15 m (small-scale models).

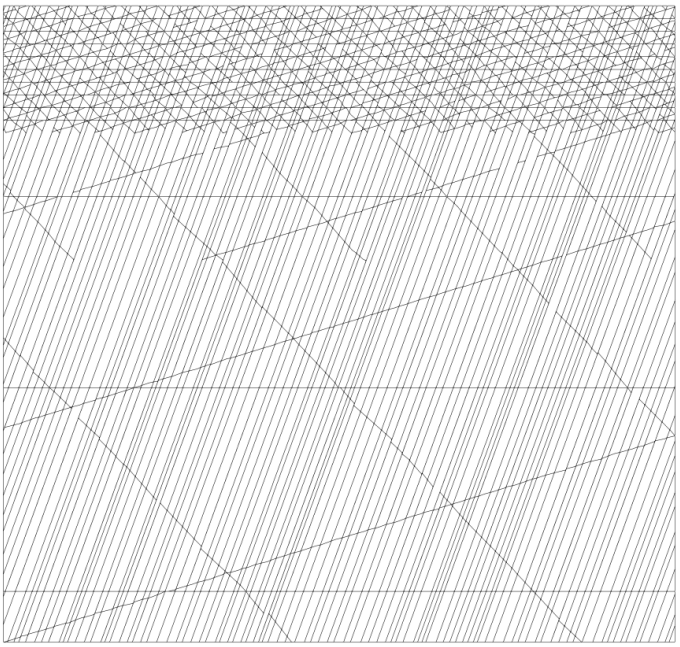

(a)

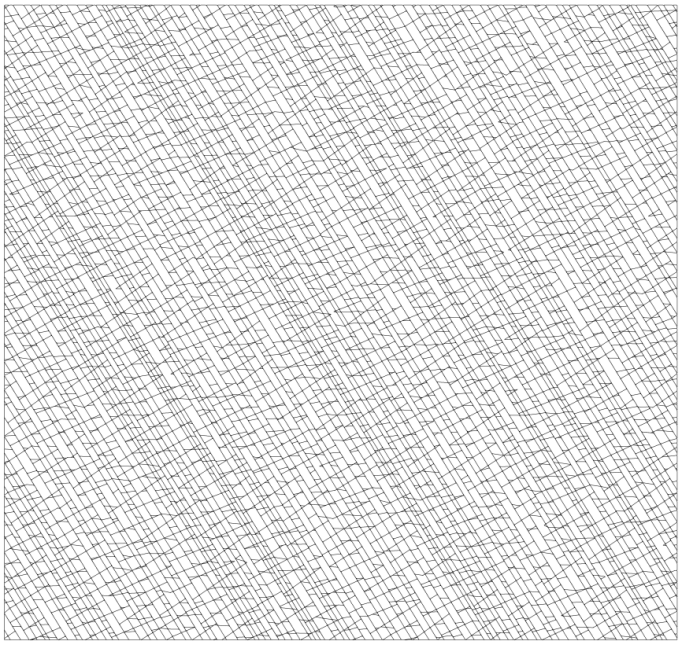

(b)

Figure 3.9 Example stochastic 2D Wendouree UDEC models: (a) the 100 x 100 m NE-SW vertical cross-section model, in the plane of Set B, which is dominated by the dense bedding planes of Set A; (b) the 100 x 100 m horizontal planar model, in the plane of Set C, at 20 m depth below the surface.

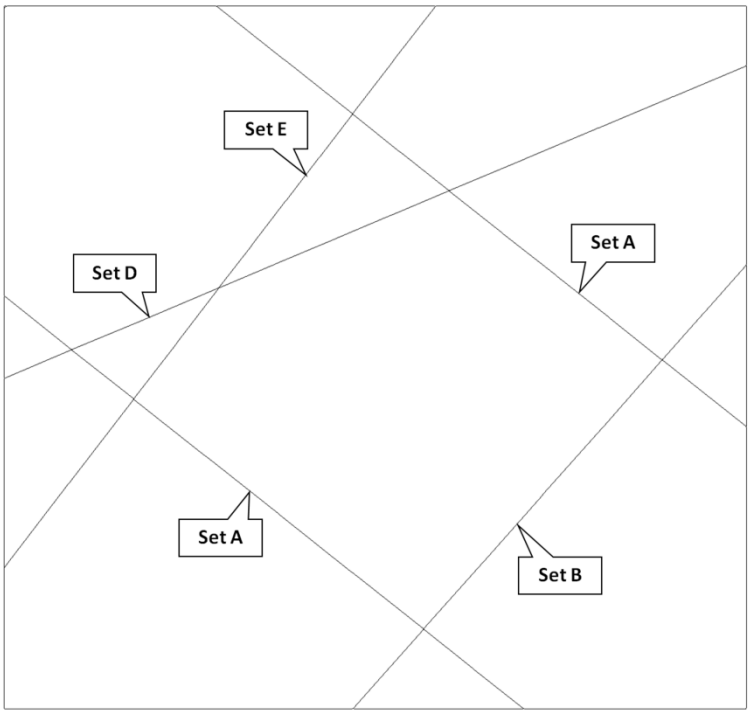

Figure 3.9 (cont.) Example stochastic 2D Wendouree UDEC models: (c) 1 x 1 m horizontal planar model in the plane of Set C at 100 m depth below the surface.

As this study is focussed on the upper 200 m depth horizon, a normal stress regime is employed with the HM models, to simulate isotropic, lateral relaxation of the rock mass consistent with the effects of uplift and unloading (i.e. $\sigma_V > \sigma_H = \sigma_h$). The magnitudes of stress within these models are based upon an estimate of σ_V (i.e. $\rho.g.h$) and applied as a differential stress ratio compatible with the prevailing normal stress regime (i.e. $\sigma_V > \sigma_H = \sigma_h$ at a ratio of 1: 0.5: 0.5). The 2D planar and cross-section models enabled σ_H to be perpendicular to the model boundaries i.e. σ_H at 110°. The cross-section orientation is approximately parallel to the east to west hydraulic gradient recorded at the Wendouree site (Love 2003) and used apparent dips for oblique fracture sets. The principal stress orientations are assumed to be the same as that determined for the far-field (deep) reverse faulting stress regime, which is a reasonable assumption as studies on shallow, neotectonic joint formation within sedimentary sequences found unloading and release joints related to uplift and erosion strike approximately parallel and perpendicular to the regional maximum horizontal stress direction (Endgelder 1985; Hancock and Engelder 1989). The

fracture network was based on the conceptual model (Figure 3.8) whilst other fracture parameters were derived from nearby scanline fracture mapping data (Table 3.1; T Halihan, Flinders University, unpublished data, 1999). The bedding plane to joint set density ratio consists of 2:1 in the upper zone, 16:1 in the transitional zone and 32:1 in the lower zone (see Figure 3.9a). These joint set densities are estimates only as the precise values are unknown due to the limited and biased nature of both the vertical drill core samples and BHTV logs. However, these joint set densities are reasonably comparable to those determined from the BHTV logs and this model design resulted in a reasonable correlation with the known groundwater flow observations (see Section 3.8).

Table 3.1 Mean fracture orientation (std. dev.), classification, mean trace (std. dev.), and mean spacing for the upper, transition and lower zones of the Wendouree stochastic UDEC models. Note that the Set A fractures are designed to transect the entire model with a fixed orientation in order to represent planar, continuous bedding plane surfaces and that the NE-SW cross-section models use modified apparent dips.

Fracture Set	Mean Dip & Dip Dir.	Classification	Mean Trace (m)	Mean Spacing (m)
A	78(0) / 240(0)	Bedding planes ("S_0").	>100	0.5 - 1.5
B1	78(9) / 331(10)	Steep-vertical, "ac" (extension) joints.	6 (5)	2, 16, 32
B2	75(6) / 155(9)	Steep-vertical, "ac" (extension) joints.	6 (5)	2, 16, 32
C	2(6) / 013(33)	Sub-horizontal, "bc" (extension) joints.	11 (18)	2, 16, 32
D	38(4) / 356(13)	D & E - conjugate pair of "hk0" (shear) joints.	2 (1)	2, 16, 32
E	54(5) / 146(9)	D & E - conjugate pair of "hk0" (shear) joints.	6 (5)	2, 16, 32

Fluid pore pressures were based on an assumed hydrostatic gradient with fluid flow allowed to occur in any direction within the fracture network under the imposed hydraulic gradient. Rock mass and fracture parameters were derived from geotechnical logging and ultrasonic velocity testing of limited drill core samples, Mohr circle analysis and other empirical relationships that are compatible with published values (Table 3.2; Kulhawy and Goodman 1980; Norlund *et al.* 1995; Waltham 2002). A comprehensive description of the model conditions and parameters used in this study is provided in Mortimer *et al.* (2011).

Of critical importance to this study is the highly variable joint stiffness distributions recorded for each individual fracture set (Mortimer *et al.* 2011). Therefore, the ranges of normal (jk_n) and shear (jk_s) stiffness values were taken as normally distributed across all fractures within the model (Table 3.2). Specifically, each individual fracture within the model may consist of up to several separate segments, 0.15 m (small-scale models) to 1.5 m (large-scale models), with randomly assigned jk_n and jk_s values. The objective of this approach is to better account for naturally occurring fracture heterogeneity such as asperity and contact area distribution, mineralization, etc and ultimately heterogeneity in deformation and fluid flow along individual fracture planes. Fracture friction and dilation angles were both inferred as zero as these parameters largely dictate the mode of fracture deformation rather than the relative deformation trends occurring across the different fracture sets within the fracture network, which was the main focus of this study. At Wendouree, the mean fracture aperture measured from nearby outcrop was ~100-200 μm and ranged up to a maximum of 1.2 mm (Love *et al.* 2002), however, for the purposes of this modelling exercise a reference aperture value of 0.5 mm is considered appropriate to facilitate the observation of overall fracture network deformation patterns. The choice of this initial aperture value is not considered critical, as the main objective is to explore the relative effects of the *in situ* stress field on individual fracture sets.

Table 3.2 Rock mass and fracture parameters used to construct the Wendouree UDEC HM models. Source: 1 = core sample ultrasonic velocity tests; 2 = Mohr circle analysis; 3 = core sample derived fracture JRC profiles and Elastic Moduli relationships; 4 = Inferred; and 5 = approximate values for fresh water at 20°C.

UDEC Model Parameters	Value	Units	Source
Rock Material Density (ρ)	2732	$kg.m^{-3}$	1
Poisson's Ratio (ν)	0.27	-	1
Young's Modulus (*E*)	77e6	Pa	1
Bulk Modulus (*K*)	96e9	Pa	1
Shear Modulus (*G*)	30e9	Pa	1
Cohesion (c)	19e6	Pa	2
Friction Angle (φ)	54	Degrees	2
Dilation Angle (ψ)	0	Degrees	4
Uniaxial Compressive Strength	128e6	Pa	2
Tensile Strength	8.5e6	Pa	2
Joint Normal Stiffness (jk_n)	7.7 - 35.1e9	$Pa.m^{-1}$	3
Joint Shear Stiffness (jk_s)	3.0 - 13.6e9	$Pa.m^{-1}$	3
Joint Cohesion	0	Pa	4
Joint Tensile Strength	0	Pa	4
Joint Friction Angle	0	Degrees	4
Joint Dilation	0	Degrees	4
Joint Aperture (at zero stress)	0.5	mm	4
Joint Residual Aperture	0.1	mm	4
Joint Permeability Constant (1/12μ)	83.3	$(Pa.s)^{-1}$	5
Water Density	1000	$kg.m^{-3}$	5

3.7.2 Fracture deformation model

To assess the effect of fracture geometry within the applied normal stress regime, the amount of fracture deformation across all individual fracture sets as a function of depth was analysed for a 200 x 200 m Wendouree NE-SW vertical cross-section (see Figs. 3.8 and 3.9a). The deformation patterns of individual fracture sets provide a basis to evaluate the ultimate HM response of a fractured rock mass to the applied stress. UDEC calculates the effective hydraulic aperture of a fracture based upon its initial fracture aperture width at zero stress plus any normal displacement (positive or negative) that has occurred as a result of deformation. This fracture deformation data is depicted for each individual fracture set in terms of the amount of fracture closure normal to fracture walls commencing with an initial hydraulic aperture of 0.5 mm at the surface (Figure 3.10). The fracture deformation profiles of Figure 3.10 show a divergence in the relative amounts of fracture deformation occurring across the individual fracture sets commencing from approximately 50 m depth. In particular, the rate of fracture closure with depth is approximately uniform for the moderate dipping to sub-horizontal joint sets (Sets C, D and E) whilst the steep dipping bedding planes (Set A) close at a lesser rate. Using these closure estimates, the reduction in equivalent parallel-plate hydraulic conductivities for individual fractures can be derived from the Cubic Law (Equation 3.1). For example, at a depth of 185 m the average fracture hydraulic conductivities for the steep dipping bedding planes (Set A) and the moderate dipping to sub-horizontal joint sets (Sets C, D and E) are reduced by ~54% and ~62-71%, respectively. This progressive development with depth of an anisotropic permeability orientation along steep dipping fractures highlights the important role of fracture geometry in regards to stress-dependent fracture permeability. This result is attributed to the fact that the applied normal stress field simulates uplift and unloading through isotropic, lateral relaxation across the entire rock mass, which should result in less deformation occurring along steep dipping fractures. Note, lastly, that the local departures from the general trends are attributable to random assignment of the fracture stiffness values.

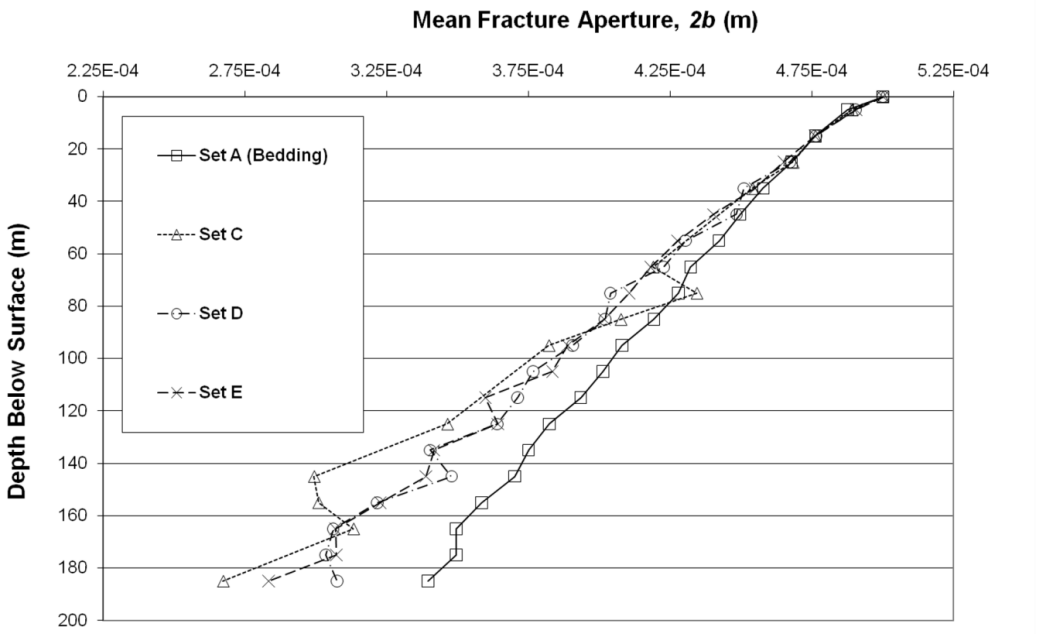

Figure 3.10 UDEC fracture deformation depth profiles of the individual fracture sets that comprise the Wendouree NE-SW cross-sectional model under a normal stress regime. The initial fracture hydraulic apertures were set at 0.5 mm with data points representing the calculated mean fracture aperture for each 10 m thick depth interval.

3.7.3 Groundwater flow models

3.7.3.1 Vertical cross-section flow model

To investigate overall fracture network hydraulics and connectivity, an analysis of groundwater flow through both the deformed (stressed state) and undeformed (zero stress state) Wendouree NE-SW cross-sectional models was completed. For the deformed model, this process involved deforming the model under normal stress regime conditions before subjecting it to steady state, groundwater flow under an east to west oriented hydraulic head gradient of 0.01 and 0.001, which fits with the measured seasonal Wendouree hydraulic gradient of between 0.003 and 0.007 (Love 2003). Like the fracture deformation models, the initial fracture hydraulic aperture for the groundwater flow models was set at 0.5 mm. The process for the undeformed model is identical except that fracture hydraulic apertures are fixed for all depths at 0.5 mm. UDEC assigns equivalent hydraulic conductivities to each uniform aperture

(parallel plate) segment of a fracture according to the Cubic Law (Equation 3.1). The flow rate through each of these segments is calculated using Darcy's Law:

$$q = \frac{(2b)^3}{12\mu}\frac{\Delta P}{L} \qquad (3.2)$$

Where q is the fracture flow rate per unit width normal to flow direction ($m^2.s^{-1}$), ΔP is the pressure difference (Pa), L is the length of each segment (m).

Vertical depth profiles of UDEC derived fracture flow rates ($m^2.s^{-1}$) and field data such as the normalised borehole yields (L/s/m; see Figure 3.4) are not directly comparable; therefore, a comparative analysis of these UDEC results can only be qualitative. The results of the UDEC vertical cross-section flow models are depicted in terms of mean apertures and flow rates for all fractures within 10 m thick horizontal depth intervals with the weathered zone represented by the upper 20 m of the model (Figure 3.11a and b). Figure 3.11a shows a uniform, linear decrease in mean apertures with depth whilst the decrease in mean flow rates is non-linear and resembles the regional well groundwater yield trend of Figure 3.4. When the deformed Wendouree fracture network flow model is compared against an undeformed version of the same model (Figure 3.11b), the applied normal stress regime appears to have had an effect, as the trend of decreasing mean fracture flow rates with depth in the undeformed state is distinctly different and only minimal. As both of these models use an identical fracture network configuration this difference is attributed to stress-related, fracture deformation processes that progressively modify fracture apertures and permeability. Furthermore, this progressive fracture deformation also leads to changes in hydraulic connectivity and flow patterns within the overall fracture network. Although this is difficult to ascertain from this data, particularly as the 2D cross-section model becomes dominated by the relatively higher conductivity, steeply dipping bedding planes with increasing depth.

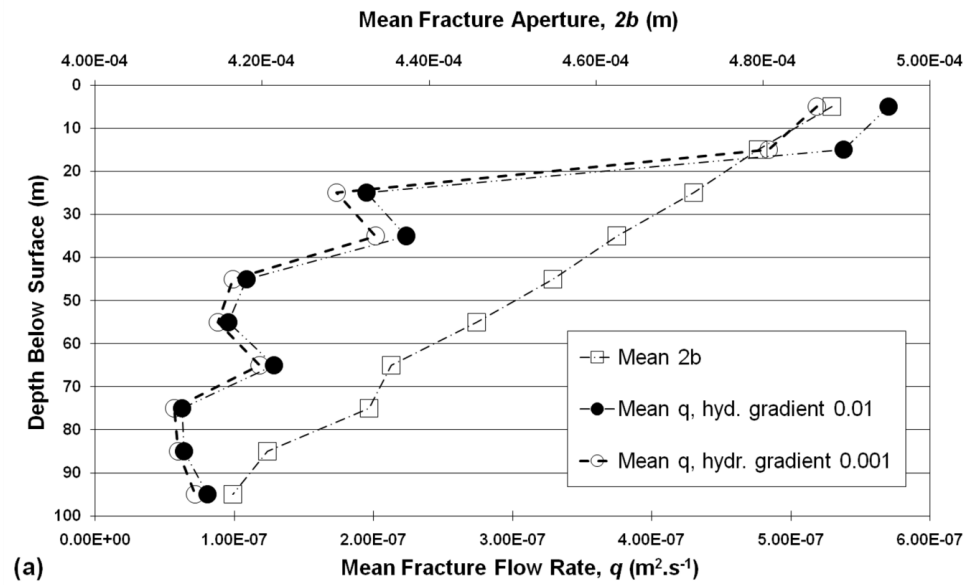

Figure 3.11a UDEC estimated mean fracture flow rates (circles, lower x-axis) and fracture apertures (squares, upper x-axis) for the Wendouree NE-SW cross-section model under a normal stress regime. Closed and open circles equal fracture flow rates calculated at hydraulic gradients of 0.01 and 0.001, respectively. The initial fracture hydraulic apertures were set at 0.5 mm.

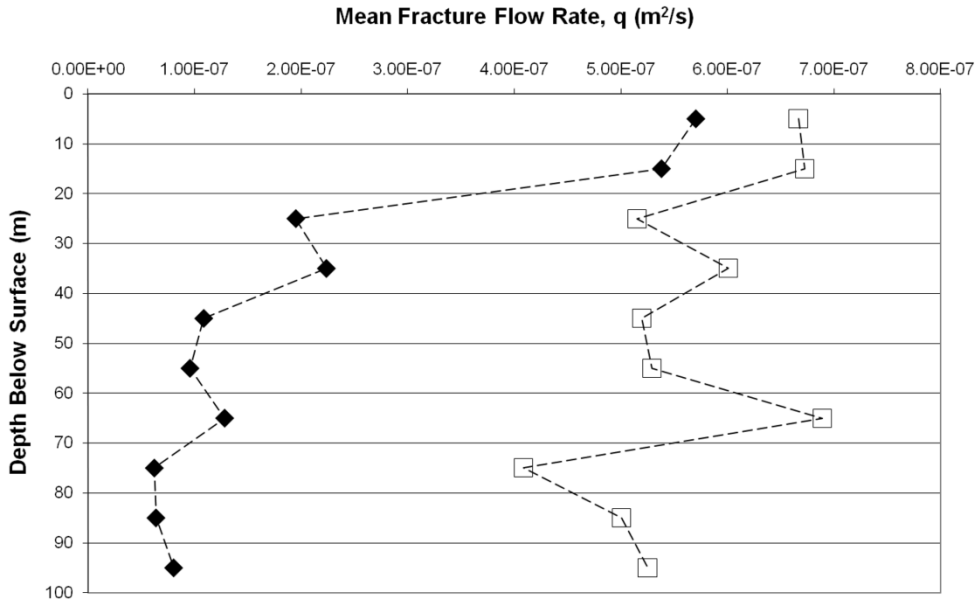

Figure 3.11b Comparison between UDEC estimated mean fracture flow rates for both the deformed (black diamonds) and undeformed (open squares) Wendouree NE-SW cross-section model under a normal stress regime and hydraulic gradient of 0.01. The initial fracture hydraulic aperture for the deformed model is 0.5 mm, which is fixed at all depths for the undeformed model.

3.7.3.2 Hydraulic conductivity ellipses

The potential influence that the imposed stress field may have on the permeability tensor of the Wendouree fracture network model was evaluated by comparing deformed and undeformed models through the estimation of 2D planar hydraulic conductivity ellipses. This process involved slicing the conceptual Wendouree fracture network model into horizontal, planar depth slices at 20 m, 40 m, 75 m and 100 m depths (see Figs. 3.8 and 3.9b). These four depth slices were chosen to capture both the increasing effects of stress and decreasing joint densities that occur with depth. Like the vertical cross-section flow models, these planar models use a normal stress regime to simulate the effects of uplift and unloading. Similar to the methodologies of Min *et al.* (2004) and Zhang *et al.* (1996) each planar model was deformed under their corresponding depth-dependent magnitudes of stress. These deformed models were then subjected to steady-state, fluid flow under an applied east to west hydraulic gradient of 0.01 with the north and south boundaries acting as impermeable, no-flow, barriers. The effective hydraulic conductivity (*K*) of each model is estimated using Darcy's Law below and the UDEC sum of discharge flow rates (*Q*) from each steady-state model:

$$Q = K A i \qquad (3.3)$$

Where *Q* is the sum of discharge flow rates ($m^3.s^{-1}$), *K* is the effective hydraulic conductivity ($m.s^{-1}$), *A* is the cross sectional area normal to the flow direction (m^2) and *i* is the hydraulic gradient.

To estimate the 2D hydraulic conductivity ellipse at a particular depth slice, the value of *K* is calculated for the initial fracture network model using the method described above then this entire process is repeated for 6 x 30° (i.e. 180°) horizontal rotations of the identical model. The 2D hydraulic conductivity ellipse is then constructed by plotting the value of *K* recorded at each 30° horizontal model rotation. For comparison, this exercise is repeated for the same fracture network models but under a zero stress field i.e. the undeformed state with fixed apertures. The initial (and zero stress) fracture aperture was set at 0.5 mm.

The model results show that at each depth slice the hydraulic conductivity ellipses are all elongated in a WNW-ESE direction (i.e. a strike direction of 300°-120°;

Figure 3.12a-d). This elongation direction represents the maximum *K* direction and is close to the strike of the extensive, densely spaced bedding planes (Set A, 330°-150°). The NNE-SSW direction of the minimum *K* direction approximates but is slightly offset to the strike of the less dense, finite length joint sets (Sets B, D and E). The orientation and shape of these *K* ellipses are in agreement with those estimated from the surface EM azimuthal resistivity surveys of Skinner and Heinson (2004; see Figure 3.7). This near coincidence of the maximum and minimum *K* directions with the bedding and joint planes is not a function of the 30° model rotations because one of these model rotations/gradient alignments is exactly coincident with the bedding plane direction. The estimated *K* ellipse at 20 m depth is a relatively smooth oval shape reflecting the overall higher fracture density and permeability of the upper zone of the conceptual model. Commencing from 40m depth (corresponding to the transition to the deeper, low fracture density zone) the strongly asymmetric shape of the *K* ellipses (i.e. the high ratio between the maximum and minimum *K* axes) are reasonably similar reflecting the dominance of the persistent dense bedding planes against a background of decreasing joint set densities.

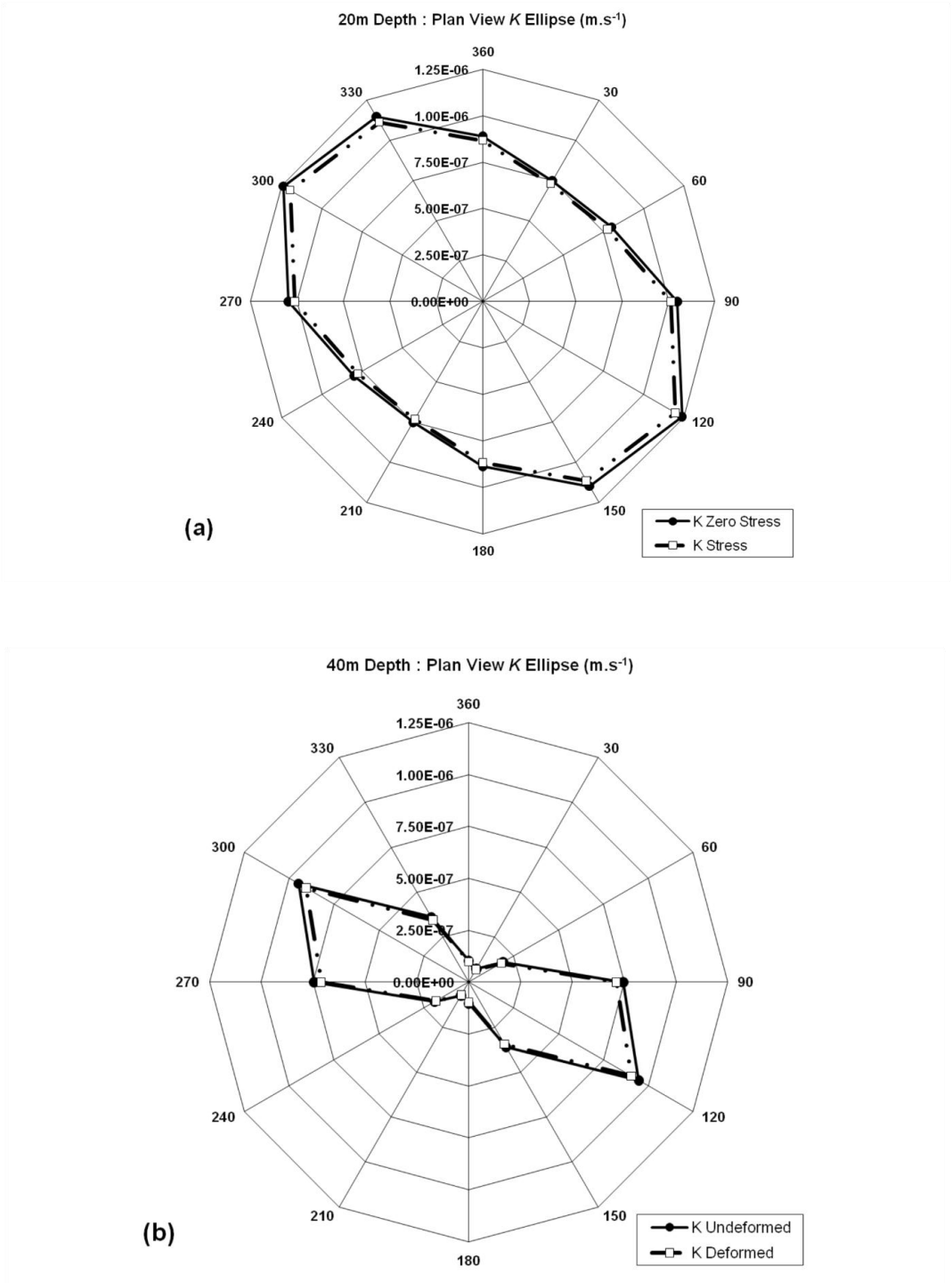

Figure 3.12 Undeformed (solid contour) versus deformed (broken contour) hydraulic conductivity (*K*) ellipses [m.s^{-1}] for Wendouree at (a) 20 m; and (b) 40 m depth below the surface.

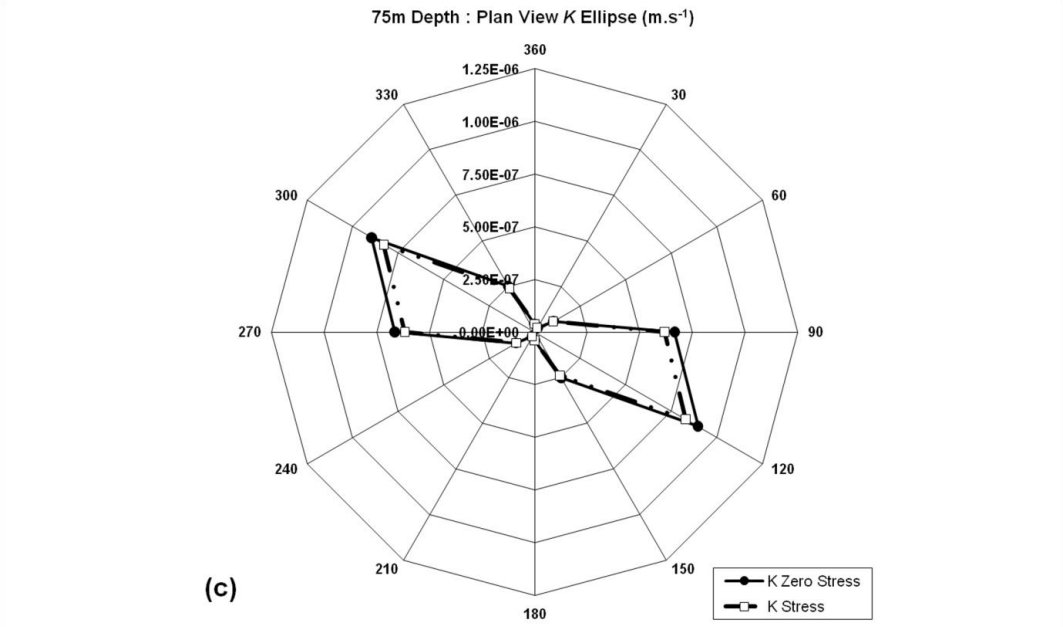

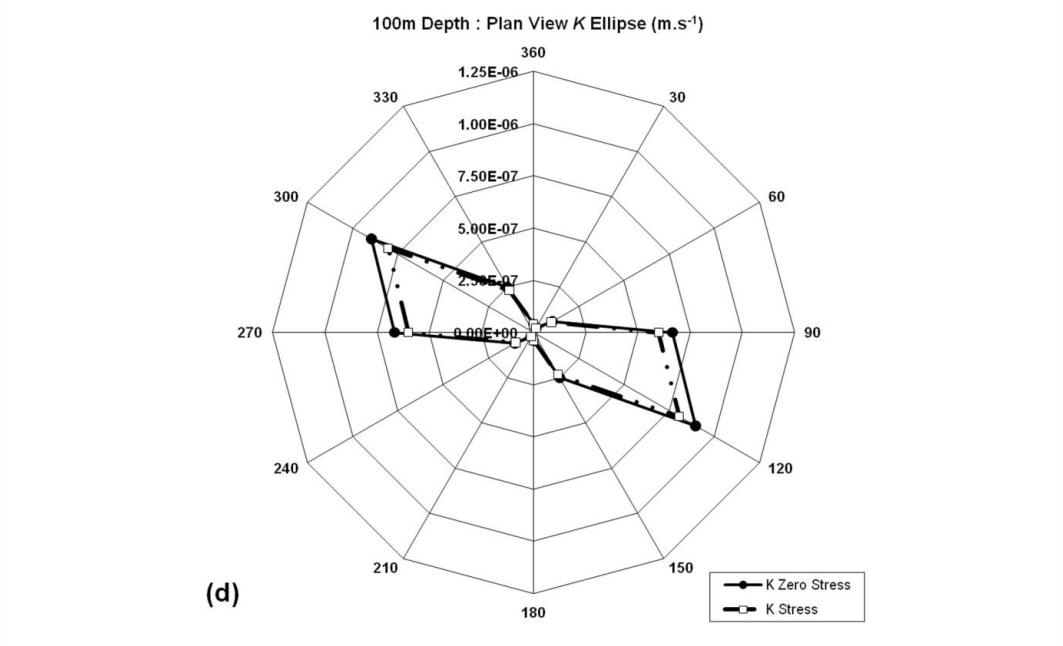

Figure 3.12 (cont.) Undeformed (solid contour) versus deformed (broken contour) hydraulic conductivity (*K*) ellipses [$m.s^{-1}$] for Wendouree at (c) 75 m; and (d) 100 m depth below the surface.

The overall shape of the hydraulic conductivity ellipses for the deformed models closely mimic those of the undeformed models with the exception that they are slightly reduced in their absolute magnitudes of K (Figure 3.12a-d). For example, compared to the undeformed model, the maximum and minimum K values for the identical but deformed model at 100 m depth are reduced by ~10% and ~2.3%, respectively. This implies that the shape and magnitude of the hydraulic conductivity ellipses are controlled by the original structure of the fracture network (i.e. fracture geometry and density) and only marginally influenced by the imposed normal stress regime. Furthermore, the magnitude of the UDEC derived K estimates are in reasonable agreement with those estimated from the pump test derived bulk K_b (see Figure 3.6b), particularly, commencing from >40 m depth. However, at shallower depths of between 0-40 m the UDEC models underestimate the magnitude of K by two orders of magnitude compared to the pump test results. The most likely explanation for this difference lies in the true effects of weathering (increased permeability) and the difficulty in accurately capturing true fracture densities at these shallow depths within the stochastic-based UDEC models. For example, although increased development of unloading-related, sub-vertical flexural and sub-horizontal sheeting (or relaxation) joints closer to the surface is expected, accurately locating and quantifying such features without representative outcrop is difficult.

3.7.3.3 Small-scale hydraulic connectivity models

This horizontal planar model represents a simple 1 x 1 m sized snapshot taken from the larger model located at 100 m depth (see Figure 3.9c). This model uses identical model parameters to the large scale models; however, each individual fracture is comprised of segments 0.15 m in length. To demonstrate how fracture network hydraulic connectivity and conductivity can be altered the results are presented in terms of: (1) the amount of fracture normal closure occurring across the model (i.e. $2b$); (2) estimated flow rates for individual deformed versus undeformed fractures that intersect the eastern and western model boundaries (i.e. q); and (3) a comparison of the sum of discharge flow rates between the deformed and undeformed models (i.e. Q). The flow model methodology is the same as that used to estimate the large-scale K ellipses (see section 3.7.3.2). That is, under a normal stress regime corresponding to 100 m depth below the surface, initial (and zero stress) hydraulic apertures set at 0.5 mm and steady-state, fluid flow under an applied east to west

hydraulic gradient of 0.01 with the north and south boundaries acting as impermeable, no-flow, barriers.

Figure 3.13 is a plot of fracture normal closure (i.e. aperture closure) that has occurred within each individual fracture of the network, which depicts the variable distribution of deformation as dictated by fracture orientation and segment stiffness. The maximum recorded joint closure was 0.116 mm (-23.2%) This plot shows how variable fracture deformation along individual fractures can lead to the development of localised hydraulic restrictions or "chokes" within the flow network even if the fracture is favourably oriented within the *in situ* stress field. Figures 3.14a and b compare calculated fracture flow rates for individual fractures that intersect the western (LHS) and eastern (RHS) model boundaries, respectively, for both deformed and undeformed versions of the same model. Figure 3.14a shows significantly decreased fracture flow rates at the western boundary of the deformed model of between 31-35% when compared to the undeformed model. Similarly at the eastern model boundary, Figure 3.14b demonstrates how the network hydraulics and flow is modified by the formation of localised flow path restrictions due to variable fracture closure. For example, when compared to the undeformed model the deformed model shows a significant flow restriction in the uppermost fracture intersection (y intercept = 0.91 m) which allowed only negligible flow to occur resulting in increased flow occurring in the lowermost fracture (y intercept = 0.4 m). In terms of the bulk sum of discharge flow rates occurring at the western (LHS) model boundary, the undeformed versus deformed models recorded 2.4×10^{-6} $m^3.s^{-1}$ and 1.61×10^{-6} $m^3.s^{-1}$, respectively. This shows that the variable fracture deformation and resultant hydraulic chokes led to a bulk flow rate decrease of 32.9% consistent with the flow rate reductions experienced by the individual deformed fractures intersecting the western (LHS) boundary. For the first time, the results of these small-scale models support the findings of Shapiro *et al.* (2007) as well as demonstrate one of the key physical processes involved in the formation of localised "bottlenecks" that impede groundwater flow and limit the bulk hydraulic conductivity to the least hydraulically conductive interconnected fractures within the network.

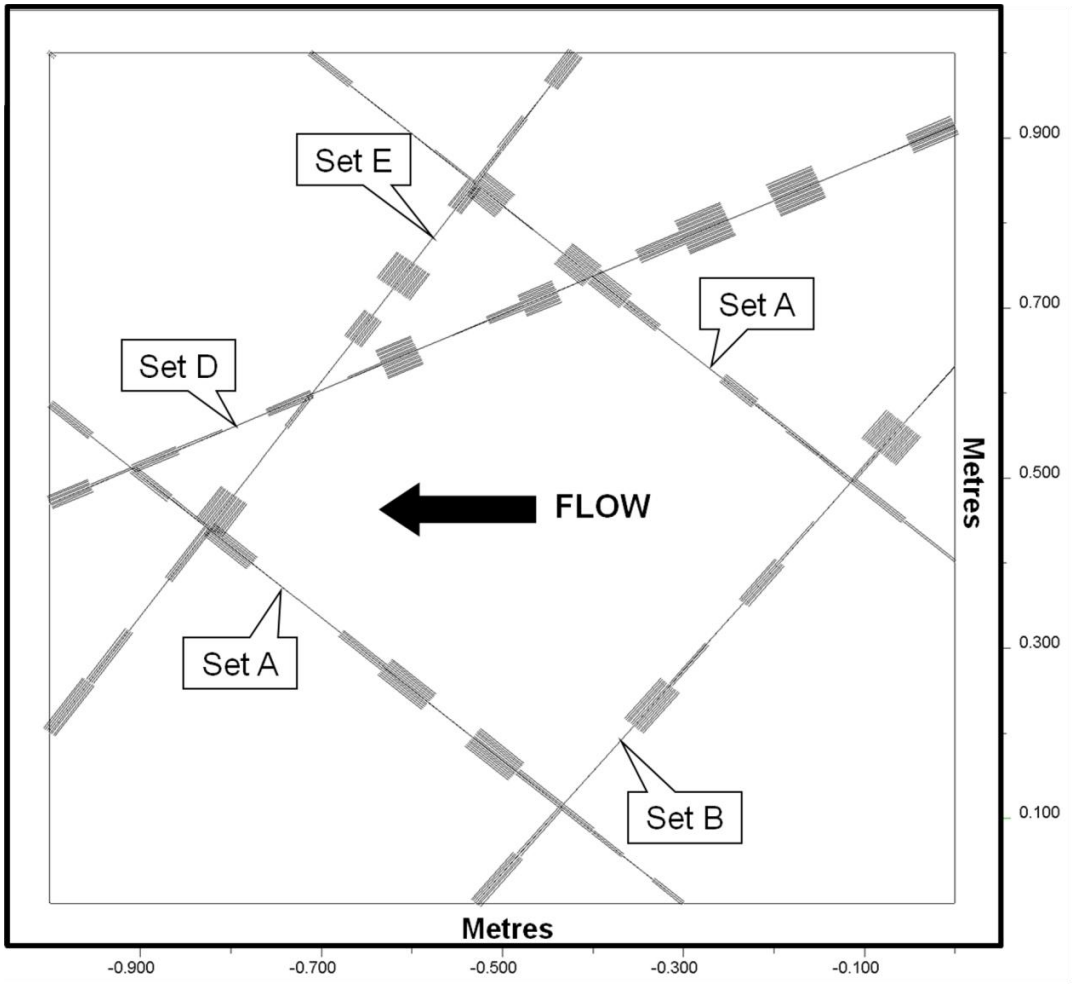

Figure 3.13 Plot of modelled fracture normal (aperture) closure that has occurred along each individual fracture of the 1 x 1 m horizontal planar model located at 100 m depth below the surface (in the plane of Set C). The grey shaded patches represent fracture segments that have experienced aperture closure due to fracture deformation with the magnitude of closure represented by the thickness of the patch. Sets B1 and B2 are represented as a single Set B as their mean strike orientations are approximately equal. The initial reference (undeformed) aperture for all fractures was 0.5 mm and the two bedding planes (Set A) were 0.5 m apart.

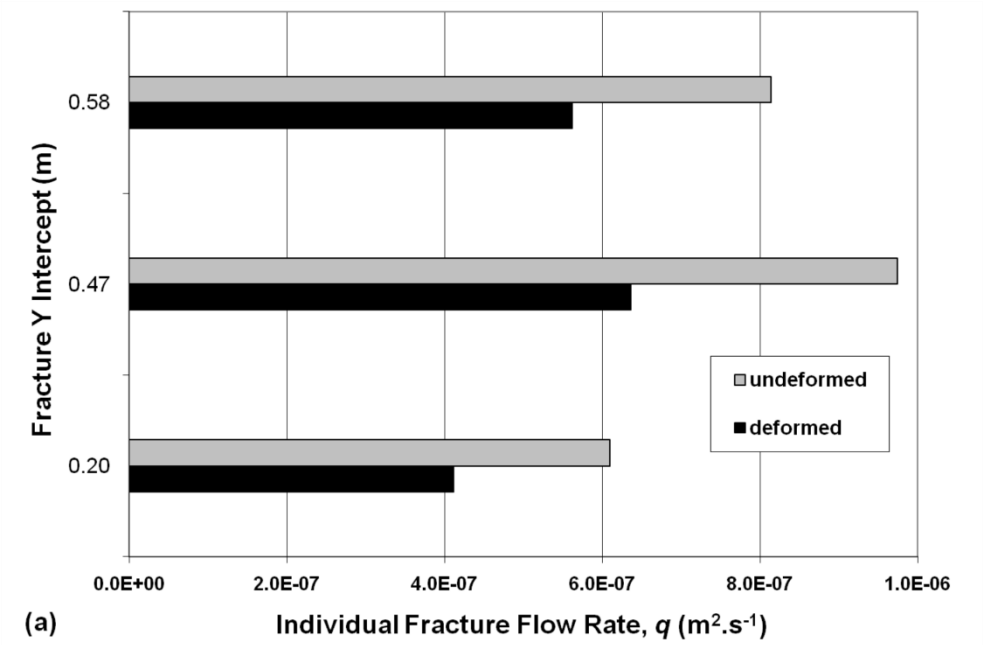

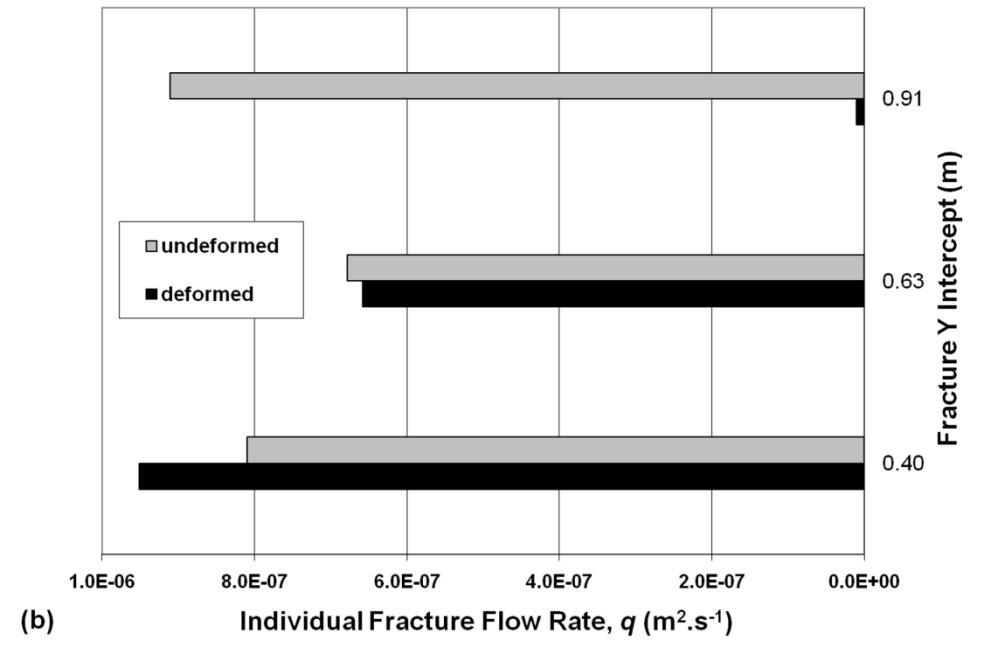

Figure 3.14 Bar chart of fracture flow rates (q, $m^2.s^{-1}$) for individual fractures that intersect (a) the western (LHS) model boundary; and (b) the eastern (RHS) model boundary for both the deformed (black) versus undeformed (grey) 1 x 1m model. Refer to Figure13.3 for the location of fracture intersections (Y intercept) along the eastern and western model boundaries.

3.8 Discussion

Long *et al.* (1982) found that a fractured rock mass will behave like an equivalent porous medium (EPM) if: (1) fracture density is high; (2) apertures are constant and not distributed; (3) orientations are distributed and not constant; and (4) large sample sizes are tested. With respect to hydraulic connectivity, this conclusion by Long *et al.* (1982) highlights two important points. Firstly, the bulk permeability of a fractured rock aquifer is dependent upon hydraulic connectivity as determined by the distribution of fracture densities, extents, orientations and hydraulic apertures. Secondly, as these fracture properties are inherently heterogeneous within an aquifer, hydraulic connectivity is best evaluated as a bulk property at a large enough scale to be representative of the fractured rock mass. However, identifying the key parameters that dictate fracture network connectivity is complex and needs to be addressed at various scales. This study found that the direct and indirect identification of the key determinants of fracture network connectivity required investigation at scales ranging from sub-metre to >100 metres. Small scale features include sub-surface fracture deformation, aperture and stiffness distributions as well as methodologies that involve the *in situ* hydraulic characterisation of individual fractures. Large scale features include the original structural framework within the host rock sequence, depth-dependent fracture density changes and the effects of the present-day *in situ* stress field.

A fracture network with constant fracture apertures (i.e. undeformed) has a permeability tensor that is determined by the primary features of the fracture network such as fracture geometry, density, extents etc. This can be better described as the "inherent permeability" of the fracture network. This study has shown that secondary processes such as the effects of the present-day *in situ* stress field, weathering and uplift and unloading can fundamentally modify this inherent permeability. These processes result in higher degrees of spatial heterogeneity within shallow groundwater systems by modifying the original distribution of fracture densities and hydraulic apertures. When attempting to characterise this spatial variability, HM models are ideal as they can incorporate natural, depth- and stress-dependent changes in fracture density and aperture. In contrast, standard, non-deforming, DFN

modelling techniques typically rely on applying a pre-defined range of estimated fracture hydraulic properties across the fracture network model, which may or not be realistic. The HM models used in this study not only produced results consistent with the field observations but also highlight the strong influence of the *in situ* stress field in determining the final distribution of sub-surface fracture hydraulic apertures and ultimately hydraulic connectivity. Regardless of the scale, geological setting or nature of the *in situ* stress field the physical processes that govern sub-surface fracture deformation and how it can modify the inherent connectivity and permeability of a fracture network is expected to hold true as *in situ* stress is ubiquitous. Locally variable fracture closure along the fracture traces results in hydraulic chokes in the 2D models but in 3D this process also incorporates the effects of: (1) increased tortuosity due to normal and shear deformation; and (2) wedging and intense deformation at block corners (fracture intersections) due to block rotations. The latter process may lead to substantial anisotropy in flow patterns at the scales of individual blocks. Thus, when extrapolating the results of 2D models to 3D flow patterns, one needs to consider possible distributions of constrictions in each fracture plane perpendicular to the general flow direction.

There are many techniques available to measure or infer the physical properties of fractures yet despite being directly linked fracture connectivity remains unquantifiable and difficult to ascertain in the field. Useful methods for detecting hydraulic connection within an aquifer include EM surface and DC surface, borehole-to-surface and cross-borehole surveys, which are relatively less expensive and time consuming than establishing observation wells or conducting hydraulic pump tests. However, on their own these particular geophysical surveys have limited practical use due to their individual resolution limitations with both their shallow depths of effective penetration and their ability to define a broad range of conductive fracture orientations. For example, DC borehole-to-surface surveys are more sensitive to steeply dipping conductive fractures whilst DC cross-borehole surveys are more sensitive to shallow dipping conductive fractures due to the coupling angles involved between the current and potential electrodes (Skinner and Heinson 2004). The accurate interpretation and numerical modelling of these geophysical datasets requires prior knowledge of the structural geology of the study site. In particular, the identification of features that control hydraulic connectivity requires a detailed

knowledge of the distribution of all fracture properties, which can only be gained through a multi-disciplinary methodology aimed at characterising the aquifer both structurally and hydraulically. Furthermore, this process would not be complete without knowledge of other regional scale influences such as the extent of any weathering and the nature of the *in situ* stress field. Conventional methods for detecting hydraulic connection within an aquifer typically include direct borehole hydraulic tests (e.g. pump, tracers etc), which requires the establishment of multiple wells and is restricted to only a limited number of point source locations. In contrast, this study has shown that spatial variations in aquifer hydraulic connectivity can also be identified through single well datasets such as flow meter and environmental tracer profiles as well as catchment-scale groundwater yield profiles. However, the use of these simpler datasets requires a direct comparison with the known geology and geological setting in order to eliminate them as causative factors.

The stochastic HM models used in this study were designed to capture the key processes at various scales and relate them back to the field observations. For example, the individual fracture set deformation profiles of Figure 3.10 shows diverging rates of fracture aperture deformation for each individual fracture set and demonstrates how hydraulic connectivity is progressively modified with increasing depth. The differing rate of deformation for each separate fracture set is a physical process that occurs on a large scale. The greater rate of aperture closure in gently dipping fractures than steeply dipping fractures leads to the progressive restriction of lateral hydraulic connectivity/flow with increasing depth (Figure 3.10). This phenomenon was noted during various field studies such as the pump tests and environmental tracer profiles of Love (2003) and the geophysical surveys of Skinner and Heinson (2004). The comparison between the deformed and undeformed flow models (Figure 3.11) showed that *in situ* stress fields do progressively modify groundwater flow patterns similar to that of the field observations which could not be explained by factors such as weathering and/or lithology.

In contrast, the use of the small scale (1 x 1 m) models was designed to illustrate how localised flow restrictions or "chokes" form within the fracture network through preferential deformation of locally, low stiffness (i.e. weak) fractures or fracture segments regardless of their geometry as normal and shear stiffness can vary

substantially along a single fracture plane (Figure 3.13). This small scale physical process can explain localised departures from expected fracture deformation and flow trends. The significant modification of network connectivity and reduction in both individual fracture and bulk rock mass flow rates in the deformed versus undeformed small scale HM models (see Figs. 3.13 and 3.14) supports the finding of Shapiro *et al.* (2007), that bulk hydraulic conductivity is determined by the least hydraulically conductive interconnected fractures in the network. However, based on this finding, Shapiro *et al.* (2007) inferred that the discrete high *K* fractures identified within their 3-5 m wide packer-isolated sections of single wells must therefore not be connected to the overall fracture network. Our study shows that variable stiffness and resulting restrictions across each fracture plane more convincingly explain why seemingly high *K* fractures do not proportionally contribute to flow rather than their complete isolation from the network. Importantly, this phenomenon was shown to be a widespread phenomenon.

A notable exception to these findings are the departures from overall fracture flow rate trends observed in the relatively deep, localised, hydraulically active fractures as revealed in the hydro-logging profiles of Love (2003) (see Figure 3.6, ~80-85m). Based upon their occurrence at depths much greater than 40 m below the surface, these particular groundwater-active fractures appear to be stress-insensitive and are most likely locked open as a result of other processes such as earlier fracture deformation episodes (e.g. shear dislocation) or partial mineral infill and cementation (e.g. Banks *et al.* 1996; Laubach *et al.* 2004).

The near identical shape and increasing anisotropy of the horizontal planar Wendouree *K* ellipses with depth for both the deformed and undeformed models is attributed to the integrated effects of decreasing joint density with depth against a persistent background of dense, through-going bedding planes. As expected the horizontally isotropic normal stress field ($\sigma_V > \sigma_H = \sigma_h$) had only a minimal effect on the shape of the *K* ellipses other than a minor reduction in the magnitudes of *K*. This demonstrates that *K* ellipses in rock masses with predominant fracture sets are strongly controlled by the original structure of the fracture network (i.e. the inherent permeability). Unlike the vertical cross-section flow model, the stress-related reductions in *K* with depth associated with the horizontal planar models are

approximately linear. This is most likely because these horizontal planar models do not include the sub-horizontal joints of Set C, which in turn implies that these sub-horizontal fractures are critical to overall fracture network connectivity. This fact is supported by the Wendouree borehole-to-borehole geophysical surveys of Skinner and Heinson (2004) which detected lateral flow along a small number of extensive, low angle structures becoming more prevalent at depths >30 m. Considering that the sub-horizontal joints are not favourably oriented (i.e. are preferentially closed) with respect to the *in situ* normal stress regime, their significant role in governing groundwater flow shows their importance to overall network connectivity.

The use of HM models in this study was successful in demonstrating some of the key physical processes that determine fracture network connectivity and its spatial variability. However, it is important to recognise some of the limitations of this approach, which are largely due to the complexities and uncertainties associated with data capture, sample representativeness and spatial confidence. This is particularly true in relation to the geomechanical characterisation of *in situ* rock material and fractures such as, for example, the estimation of fracture stiffness, which ultimately dictates fracture deformation behaviour. Generating statistically significant datasets of rock mass and fracture parameters may not always be possible in areas with little to no outcrop or drill core samples. Similarly, model results are dependent on an accurate definition of the prevailing *in situ* stress field which can vary significantly in regime, orientation and magnitude at shallow depths (Engelder 1993). Without some form of direct or indirect field validation (e.g. *in situ* stress test, measured anisotropic permeability orientation versus fracture orientation) based on a comprehensive practical knowledge of *in situ* stress analysis, the choice of *in situ* stress field should be made considering a range of possibilities so that the model results can bracket the actual conditions. Furthermore, the computational limitations and run time requirements for codes such as UDEC restrict their practical application to either detailed small-scale (<100 m) studies or stochastic representations of larger scale problems. These HM models can reflect regional scale patterns if the aquifer is homogeneous at the scale of the REV although numerous HM models may need to be tested at various scales to ascertain what that is. Generally, HM models offer non-unique solutions and as such they require a parameter sensitivity analysis and, if possible, a direct comparison with field-based observations. Nonetheless, this study

demonstrated that this HM modelling methodology can produce results that are in good agreement with direct field observations and can offer an alternative preliminary approach to standard borehole hydraulic tests without the need for multiple observation wells.

9. Conclusion

The identification of the key determinants of fracture network connectivity requires a multi-disciplinary approach that defines the structural and hydraulic character of the fracture network at sub-metre to hundreds of metres scales. Although difficult to quantify, the influence of hydraulic connectivity on groundwater flow is not only evident in conventional multi-well hydraulic tests but also in single well and catchment-scale datasets such as borehole flow meter, environmental tracer and groundwater yield profiles. The field detection and characterisation of the spatial variability of hydraulic connectivity within a fracture network can also be achieved with electrical and electromagnetic surface and borehole methods. In this study, the use of stochastic HM models at various scales highlighted the significant role of the present day *in situ* stress field in determining overall fracture network connectivity and the localised formation of hydraulic chokes, which for the first time quantitatively and qualitatively support the findings of Shapiro *et al.* (2007).

The key conclusions from this multi-disciplinary study are: (1) the primary control on fracture network connectivity is its inherent permeability as dictated by features such as the distribution of fracture density, orientation, planar dimensions, aperture and roughness; (2) the inherent permeability and connectivity of a fracture network can be modified by secondary processes such as weathering, uplift and unloading and fracture deformation in response to the *in situ* stress field; (3) heterogeneous fracture deformation results in the formation of hydraulic chokes that impede fluid flow; and (4) the bulk hydraulic conductivity of a fracture network is controlled by the least hydraulically conductive interconnected fractures which imposes a physical limit on the overall hydraulic conductivity of a fractured rock aquifer. The results of the small scale HM models suggest that this physical limitation on overall bulk rock mass hydraulic conductivity is a widespread phenomenon.

Acknowledgements

The authors gratefully acknowledge the funding and logistical support received for this research from the Centre for Groundwater Studies, the Department of Water, Land and Biodiversity Conservation South Australia and the University of Hong Kong. The authors would also like to thank Mike Coulthard, James Ward, Steve Chan and Mark Christianson for their assistance with the UDEC models, Todd Halihan for the use of his geological data and Wolfgang Preiss and Tania Wilson for additional project support and advice.

4 Role of mechanical stratigraphy in determining groundwater flow in fractured sedimentary successions

4.1 Introduction

Groundwater flow within fractured rock aquifers is assumed to occur parallel to the gradient of the estimated potentiometric surface, though, this is reasonable only if the hydraulic properties of the lithological units are isotropic (at the scale of flow path characterization) or if the major axis of the permeability tensor is parallel to the gradient (Freeze and Cherry 1979). In a fractured rock aquifer potentiometric surface is defined for its equivalent continuum, which conceals the complexity of actual flow paths, and corresponding distribution of flow velocities and pressures. In addition to the general variability in fracture network heterogeneity and anisotropy, the intercalation of low and high fracture density and permeability units in a sedimentary sequence results in distinct flow domains in each unit. These domains cannot be represented by a single equivalent continuum at the same scale and characteristics. Flow across these juxtaposed domains with different degrees of heterogeneity and directions of anisotropy can be expected to affect groundwater flow patterns that can be approximated at the scales equal to or greater than those of their equivalent continua. The validity of this approximation and hence the loss of details of internal dynamics and processes within and across such sequences varies with the local settings.

Furthermore, the inherent permeability of fracture networks can be modified by secondary processes including weathering, uplift and unloading and other mechanisms that lead to fracture deformation in response to *in situ* stress (Mortimer *et al.* 2011). The amount and rate of fracture deformation within individual lithological units depends on several factors such as the nature of the present-day stress field, depth, rock type, strata thickness, position within the overall stratigraphic sequence, relative mechanical contrasts between adjacent rock units and fracture normal and shear "stiffness" (Price 1966; van der Pluijm and Marshak 2004; Rutqvist and Stephannson 2003). However, no groundwater flow modelling studies are known to the authors that integrate the effects of an intercalated fractured rock

sequence with the effects of the present-day *in situ* stress field and how coupling of these effects can lead to significant modification of groundwater flow.

The primary properties of a fractured rock mass such as fracture density, geometry, extent, aperture and infill determine its "inherent permeability" and are the dominant controls on groundwater flow patterns at shallow (<200 m) depths (Mortimer *et al.* 2011). Generally, this inherent permeability is anisotropic and described graphically by an ellipsoid. In a sedimentary rock sequence individual layers may have contrasting permeabilities if they have contrasting microfabric properties and macroscopic attributes that produce different responses to the same deformation process and eventually distinct fracture network properties in contiguous domains. For example, in fractured sedimentary rock sequences, fractures typically span the thickness of a mechanical rock layer (e.g. bedding) and commonly abut their bounding stratigraphic horizons meaning that the fracture patterns are commonly stratabound in nature (Odling *et al.* 1999; van der Pluijm and Marshak 2004).

To understand fracture patterns and inherent permeability requires an understanding of the primary controls of fracture network development and how they influence groundwater flow behaviour. In fractured sedimentary rock sequences this can be achieved by redefining the sequence in terms of mechanical stratigraphy, which controls joint formation, and/or fracture stratigraphy, which describes fracture characteristics within a horizon (Laubach *et al.* 2009). Mechanical stratigraphy is defined as a subdivision of rock into discrete intervals according to the mechanical properties which determines the response (deformational behaviour) of the interval to an applied force (Laubach *et al.* 2009). A mechanical layer may represent one or more stratigraphic units that have similar response characteristics (Odling *et al.* 1999; Wennberg *et al.* 2006). Fracture stratigraphy is defined as a subdivision of rock formations on the basis of fracture characteristics such as fracture density, extent, clustering etc (Laubach *et al.* 2009; Wennberg *et al.* 2006). Generally, mechanical and fracture stratigraphy are often coincident with stratigraphic layering and stratabound as rock strength is a key determining factor although this relationship is not straightforward as the mechanical properties of rocks may evolve over time with an evolving geotectonic setting and loading history (Laubach *et al.* 2009; Wennberg *et al.* 2006). These stratigraphic methods that map and subdivide

fractured rock aquifers into distinct hydraulic domains and capture relative fracture network permeability and heterogeneity from structural and geomechanical datasets are similar to the delineation of hydrostratigraphic units for porous media. The ultimate aim of these methods is to establish a systematic basis for prediction of variability in fracture distributions within a layered fractured rock sequence and how this variability impacts groundwater flow patterns within the broader succession.

Groundwater flow modelling of fractured rock aquifers is typically conducted under the assumption that permeability is independent of the stress state (i.e. fluid flow is taking place within a non-deforming medium) and that a fracture network with constant fracture aperture has a permeability tensor that is equal to its inherent permeability. Yet the role of secondary processes such as the effects of the *in situ* stress field have also been shown to have a significant effect on groundwater flow patterns by increasing the degree of spatial heterogeneity and anisotropy of the fracture network (Mortimer *et al.* 2011). For example, *in situ* stress fields progressively modify groundwater flow patterns commencing from the near surface via variable fracture deformation and hydraulic aperture distributions leading to the progressive development with depth of anisotropic permeability whilst unloading, erosion and weathering can result in increased near-surface (neotectonic) joint formation and permeability enhancement (Barton *et al.* 1995; Hancock and Engelder 1989; Mortimer *et al.* 2011). Whilst palaeo-stress regimes play a dominant role in the primary development of fracture networks and fracture permeability during episodes of crustal deformation contemporary stress fields and near-surface processes may further influence the fundamental hydraulic nature of fracture networks by altering fracture aperture and depth-dependent fracture density distributions resulting in higher degrees of spatial heterogeneity.

In a homogeneous isotropic system the direction of groundwater flow is predicted to occur parallel to the gradient of the potentiometric surface between any two points in the aquifer. However, potentiometric surface contour maps for fractured rock aquifers based on water level data from a few isolated points do not capture the complexity of the 3D subsurface hydraulic head pattern (Freeze and Cherry 1979). Furthermore, groundwater flow patterns are modified where flow lines cross geologic boundaries between formations of different hydraulic conductivity due to

flow path refraction processes. Therefore, ‘standard’ potentiometric surface maps of fractured rock aquifers are considered unreliable in regards to groundwater flow path prediction. Furthermore, cross-bed flow in stratabound fractured sedimentary systems may be inhibited where bedding contacts act as hydraulic discontinuities and bedding parallel permeability and flow may dominate regardless of the direction of the hydraulic gradient (Hemker *et al.* 2004; Odling *et al.* 1999).

The key questions posed by this study are “how can we apply the concept of mechanical stratigraphy to describe contrasting HM effects on groundwater flow within an intercalated fractured sedimentary sequence?” and “what is the relevant scale at which this description becomes acceptable for a given mechanical stratigraphy?”. With reference to actual field observations and a conceptual representative hydromechanical (HM) fracture network model this study aims to demonstrate:

1. How groundwater flow within an intercalated fractured sedimentary succession is primarily controlled by its mechanical stratigraphy;
2. How mechanical stratigraphy of an intercalated fractured sedimentary sequence governs its response to sub-surface deformation processes which in turn determine the permeability and porosity distribution; and
3. How mechanical stratigraphy can significantly modify and even inhibit cross-bed flow. This influence is postulated as a possible explanation for the formation of natural springs in these types of geological settings.

This study also demonstrates that other practical insights (in terms of determining target locations and depths of wells and managing the groundwater basins) could be gained through discrete fracture network modelling.

4.2 Methodology

The field site chosen for the basis of this investigation is the Clare Quarry located within the Clare Valley, South Australia (Figure 4.1). This field site is a true fractured rock aquifer terrain situated within a near horizontal, WNW-ESE directed regional compressional stress field, is seismically active and undergoing uplift and erosion (Sandiford 2003).

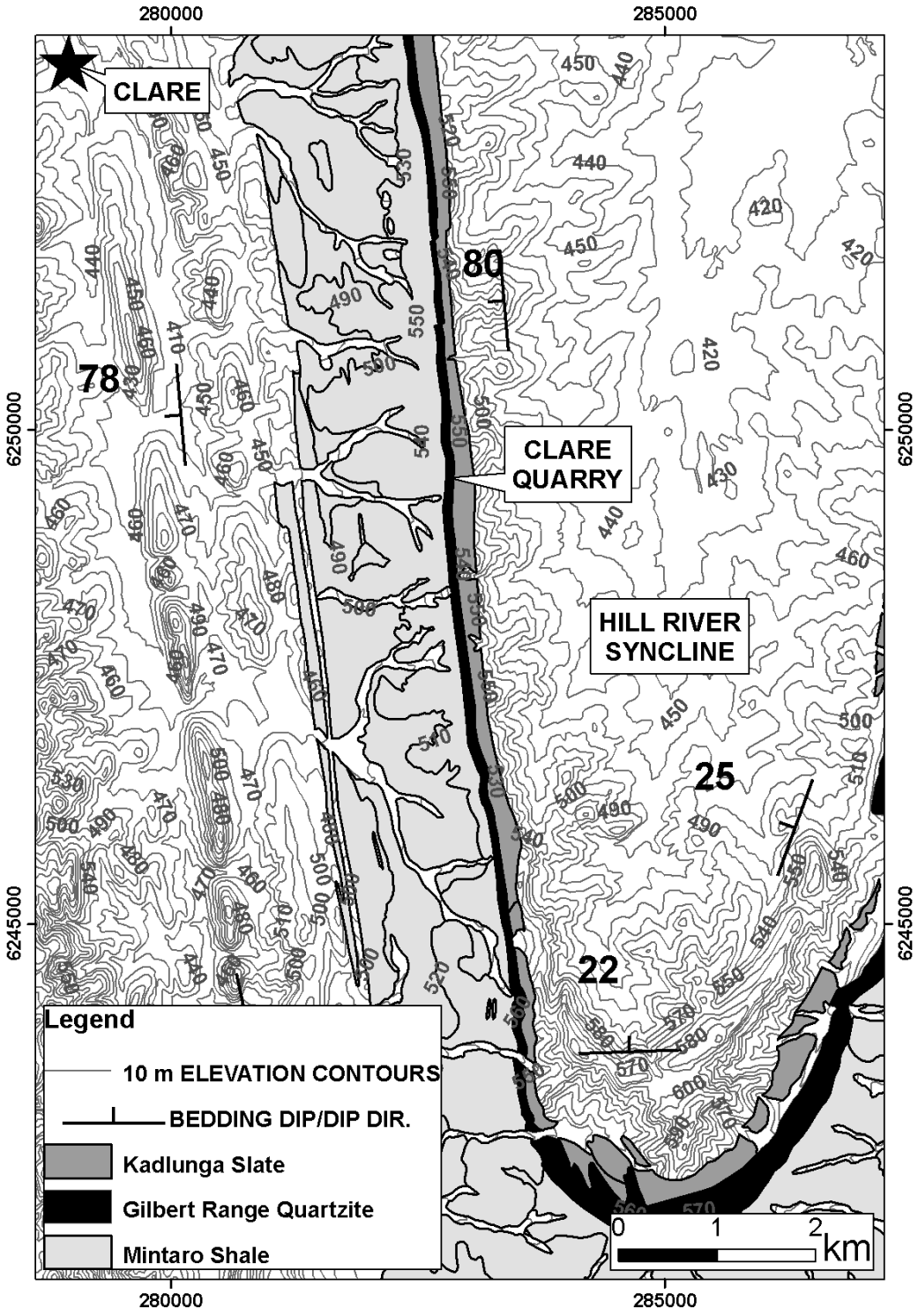

Figure 4.1 Location of the Clare Quarry field site on the overturned, western limb of the "Hill River Syncline" with 10 m topographic contours. The basement geology consists of an intercalated Neoproterozoic to Cambrian sedimentary sequence (Geological Survey of South Australia 2001).

The Clare Quarry is located ~6 km SSE of the township of Clare and is currently being mined for quartzite for industrial purposes. The quartzite is mined from the Gilbert Range Quartzite unit within the near vertical, overturned, western limb of the Hill River Syncline (Figure 4.1). The Gilbert Range Quartzite is ~75 m thick and interbedded between the Kadlunga Slate and Mintaro Shale which are ~120 m and ~900 m thick, respectively (Figure 4.1).

The methodology of this study involves the following key steps:

1. A synthesis of pre-existing data and knowledge of the local- to regional-scale geological setting and history.
2. Fracture network characterisation derived from mapping of selected outcrops within the Clare Quarry and elsewhere within the Hill River Syncline.
3. Development of a conceptual intercalated shale-quartzite-shale model that captures key features of the stratabound fracture networks observed within the Clare Quarry.
4. Based upon the methodology of Mortimer *et al.* (2011) stochastic HM modelling of a conceptual intercalated shale-quartzite-shale model designed to simulate the effects of mechanical stratigraphy on groundwater flow. Using the 2D Universal Distinct Element Code (UDEC) these HM models capture the inherent fracture network properties unique to each rock unit that comprises the mechanical stratigraphy such as fracture density and stiffness. Variable fracture deformation behaviour within each individual mechanical stratigraphic unit in response to the present-day *in situ* stress field is determined by their respective rock mass and fracture network properties. The basic HM model predicts the physical response of a fractured rock mass to an imposed stress field and the stress-displacement relationship of the medium, while satisfying the conservation of momentum and energy in its dynamic simulations with fluid flow calculations derived from Darcy's Law (for a comprehensive review of the UDEC governing equations see Itasca 2004). In these models, rock mass was assumed to deform as a Mohr-Coulomb material and fractures to shear according to the Coulomb-Slip criterion that assigns elastic stiffness, tensile strength, frictional, cohesive and dilational characteristics to a fracture (Itasca 2004).

5. Comparison between undeformed and deformed versions of the conceptual shale-quartzite-shale HM model for quantification of the effects of the *in situ* stress field.

4.3 Geological setting

The Clare Valley catchment (~500 km^2) is located approximately 100 km north of Adelaide, South Australia, and lies within the northern Mount Lofty Ranges (Figure 4.1). The Mount Lofty Ranges forms part of the "Adelaide Geosyncline", which is a Neoproterozoic to Cambrian age (~827–500 Ma), thick (>10 km), rift-related, sedimentary basin complex comprising of thinly laminated (mm) to thick (m) layered sedimentary strata (Preiss 2000). During the Middle-Late Cambrian "Delamerian Orogeny", the rocks of the Clare Valley were subjected to low-grade, greenschist facies metamorphism and three deformation events. This was a major episode of crustal shortening leading to strongly contractional, west-verging, thrust faulting and NNW-trending folding (Preiss 2000). From the Delamerian Orogeny until the late Miocene period the Adelaide Geosyncline remained relatively tectonically stable (Preiss 1995). As southern Australia entered the late Miocene period (<10 Ma) a new phase of tectonic activity commenced, which was initiated by coupling and/or convergence between the Pacific and Australian plates (Hillis and Reynolds 2000; Sandiford *et al.* 2004). As a consequence, the Clare Valley is currently under near horizontal, approximately WNW-ESE directed compression and related seismic activity, which correlates both spatially and temporally with ongoing fault activity along major range bounding faults of the Adelaide Geosyncline (Sandiford 2003). Evidence found on some of these major range bounding faults suggest that the vertical component of their slip rates are in excess of tens of metres Myr^{-1} over the past 5 Myr leading to widespread uplift, erosion and the present-day topography of the Mount Lofty Ranges (Sandiford 2003).

4.3.1 Examples of mechanical stratigraphy in the Clare Valley

Factors that determine rock deformation and strain accommodation throughout a layered sedimentary sequence include strain rate, confining stress, pore fluid pressure, unit thickness and position within the overall sequence. In the case of the

Clare Valley, the various layered sedimentary rocks responded to the Delamerian Orogeny via different deformation mechanisms resulting in dissimilar strain distributions across and within the units. For example, during folding relatively strong, stiff rock units tended to deform via macroscopic (km) folding and brittle fracturing whilst weak, more compliant rock units tended to deform via mesoscopic (m) folding, bedding plane flexural slip and/or the development of a foliation. The development of joint sets during fold deformation depends upon several factors including the type and size of fold, the relative competency contrasts between layers, the extent of joint planes and rock layer thicknesses (Price 1966). As part of this study outcrop mapping exercises conducted at several locations across the Clare Valley found a consistent joint set pattern present within the various layered rock units of the Hill River Syncline. In addition to bedding planes, there are four joint set structures including sub-vertical "ac" (extension) joints, sub-horizontal "bc" (extension) joints and two moderately dipping conjugate "hk0" (shear) joints, which together produced a pattern typical of jointing in response to simple folding of a layered sedimentary sequence during the Delamerian Orogeny (Figure 4.2; Price 1966; van der Pluijm and Marshak 2004). Only the joint density varied at each outcrop as determined by each rock type, thickness and position within the sequence i.e. a stratabound joint formation pattern.

Within the Clare Valley, these different deformation mechanisms have ultimately determined the development of primary structures that dictate many of the hydrogeological patterns observed across the catchment today. A good example of these different deformation mechanisms can be observed within two adjacent rock units exposed at the Clare Quarry located within the steeply dipping, overturned, western limb of the Hill River Syncline (Figure 4.3). Figures 4.3 shows the light coloured, stiff rocks of the Gilbert Range Quartzite (lower formation) adjacent to the purple-coloured, relatively weaker and compliant Kadlunga Slate unit (upper formation). At this location, the stiff rocks of the Gilbert Range Quartzite contain four strongly developed joints sets typical of fold deformation i.e. sub-vertical "ac" joints, sub-horizontal "bc" joints and two conjugate "hk0" joints. Comparatively, joint set formation within the adjacent, more compliant Kadlunga Slate is significantly less developed (Figs. 4.3 and 4.4). This is attributed to differences in the

deformation mechanisms as described above. These two adjacent units are in effect mechanically decoupled (Figure 4.5).

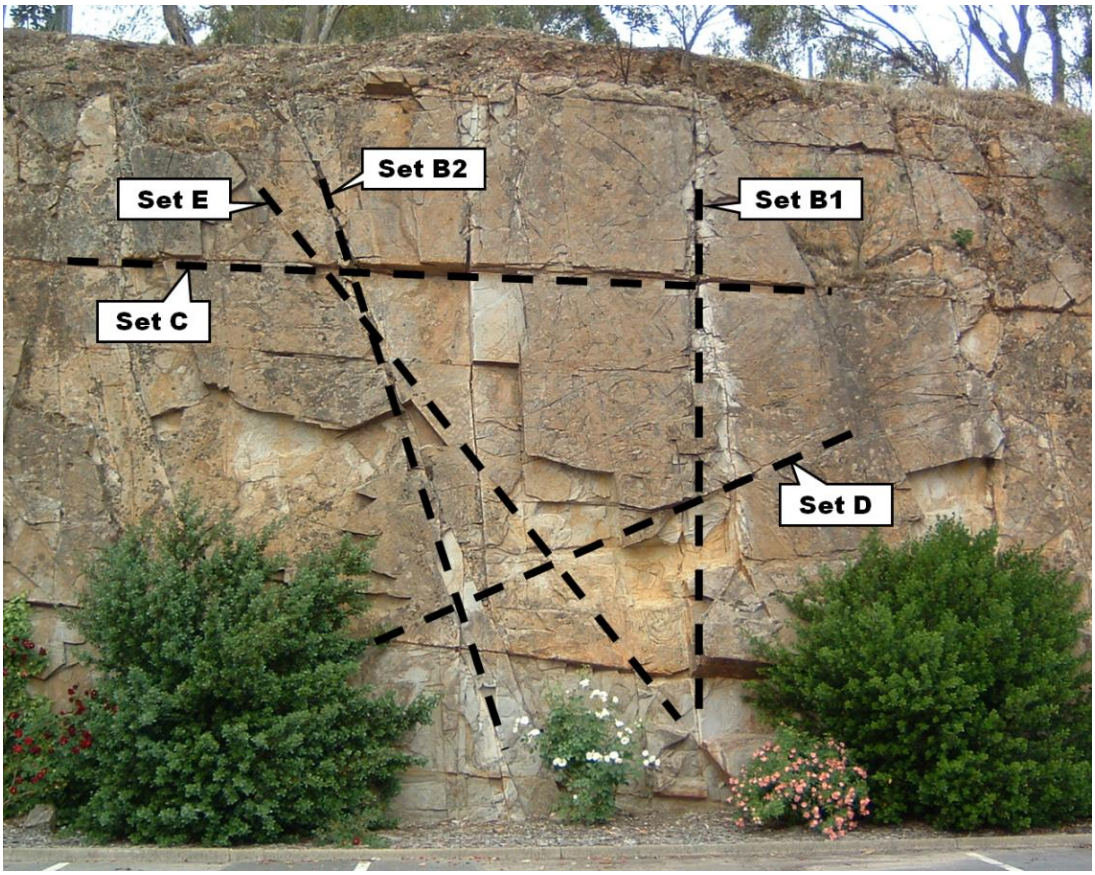

Figure 4.2 ENE-looking, longitudinal section view of a near vertical bedding plane within the Saddleworth Formation (Auburn Dolomite unit) located on the western limb of the Hill River Syncline (~5 m high rock face). Note the five fracture sets typical of this area: bedding plane (Set A, plane of rock face); "ac" (extension) joints (Set B1 and B2); sub-horizontal "bc" (extension) joints (Set C) and conjugate "hk0" (shear) joints (Set D and E).

Figure 4.3 Example of different joint set development within two adjacent rock units of significant stiffness contrast. This is an east looking, long section view of the ~N-S striking, steeply dipping bedding planes exposed within the Clare Quarry. In the lower foreground is the light coloured, relatively stiff, Gilbert Range Quartzite whilst the upper background consists of the adjacent purple-brown coloured, more compliant Kadlunga Slate. The approximate position of their stratigraphic contact is denoted by the dashed black line.

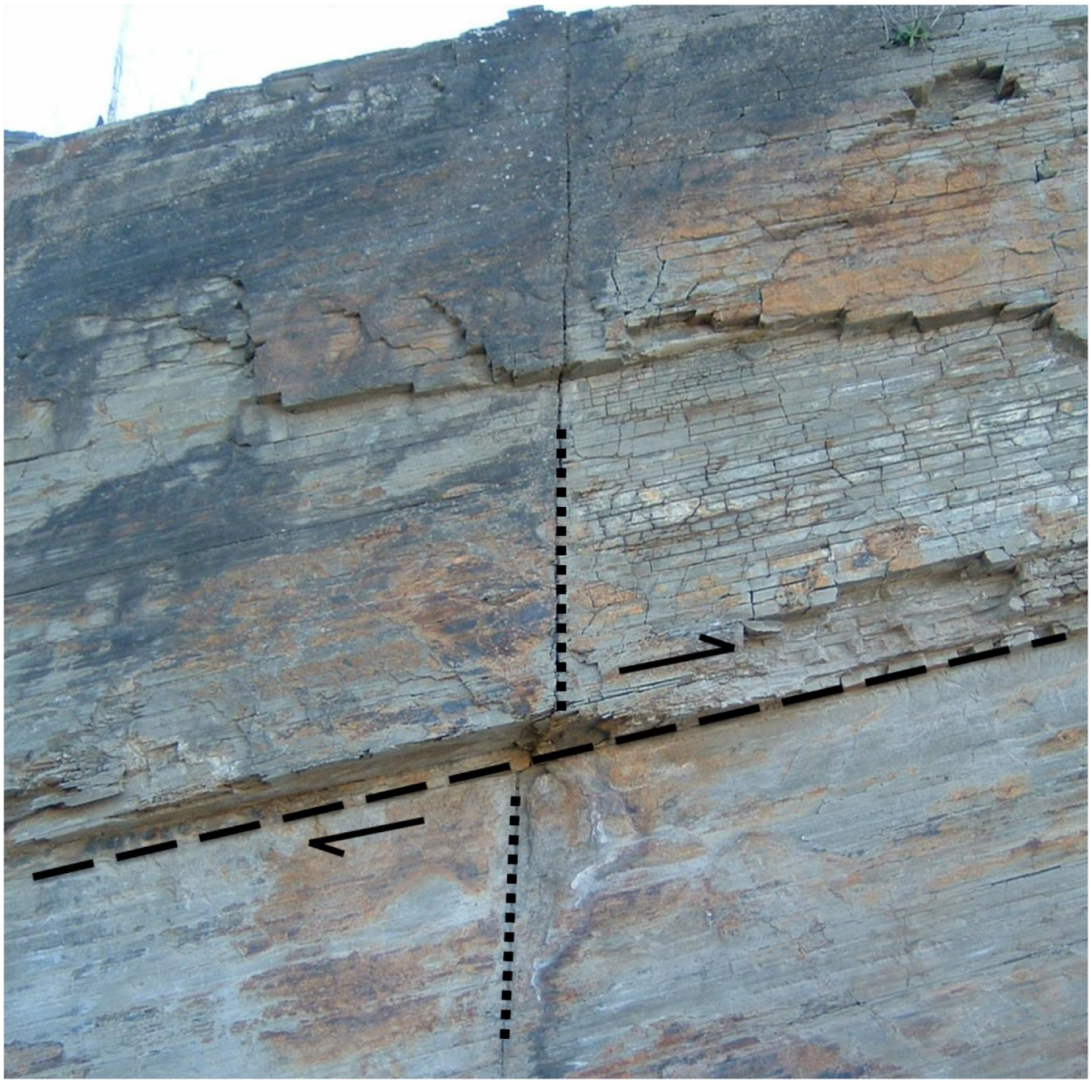

Figure 4.4 Example of bedding plane flexural slip deformation along a shallow dipping, thinly laminated black shales, Mintaro Shale Quarry, evident from offset displacement of an earlier formed joint. Joint offset displacement is approx. 15 cm. Thick dashed black line denotes the trace of bedding. Vertical thin dashed black lines denote the trace of the earlier formed joint.

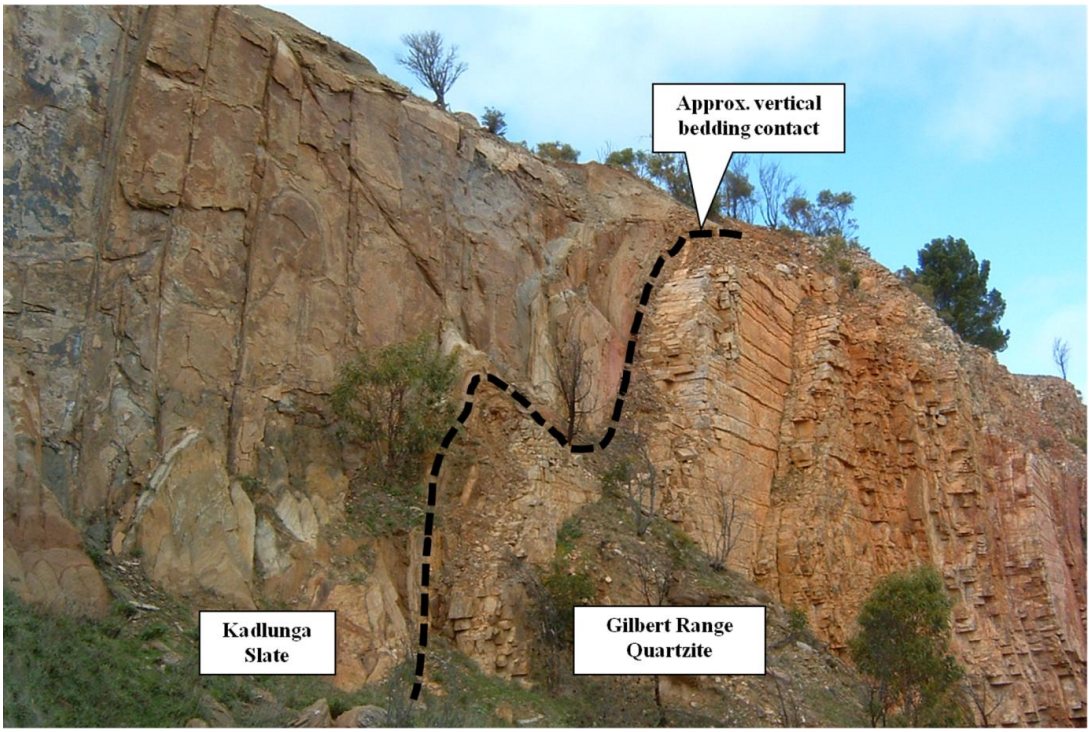

Figure 4.5 View of the near vertical contact between the stiff, light coloured, Gilbert Range Quartzite (RHS) and the adjacent purple-brown coloured, Kadlunga Slate (LHS). The approx. position of their stratigraphic contact is denoted by the dashed black line. Note that the intense fracture pattern of the Gilbert Range Quartzite does not transect across the bedding contact with the Kadlunga Slate indicated that this contact most likely acts as a hydraulic discontinuity.

Several key conclusions can be drawn from the rock exposures within the Clare Quarry. Most importantly, joint set development is dissimilar and strongly stratabound in nature across the various sedimentary units and is more pronounced within the relatively stiff rock types. Within the more compliant laminated sedimentary units, strain accommodation via preferential flexural slip deformation and foliation development allowed these rocks to avoid significant brittle fracturing with only minimal joint development. This suggests that bulk rock mass permeability and fracture network connectivity within the stiff units is greater than within the more compliant units. Fracture network connectivity across adjacent rock units of significant competency contrast is severely restricted with their contacts having the potential to act as significant hydraulic discontinuities. Overall, these intercalated

high and low fracture density and permeability units are expected to exert a significant control on groundwater flow paths regardless of the direction of the regional hydraulic gradient.

4.4 Simulating HM behaviour of mechanical stratigraphy

Understanding the relationships between the effects of stratigraphic position, lithology, fracture network characteristics and stress field forms the primary goal of investigating the role of mechanical stratigraphy. The following example of a stochastic, representative HM model are based upon real but simplified fracture network observations from the Clare Quarry and are designed to demonstrate the key effects of mechanical stratigraphy on groundwater flow. Specifically, comparisons between an undeformed (zero stress state) and deformed (stressed state) HM model differentiate not only between the effects of the inherent stratabound fracture networks (within each mechanical stratigraphy unit) but also responses of these units to the present-day *in situ* stress field.

4.4.1 Conceptual model

In this study we used a conceptual, stochastic, horizontal planar 50 m x 50 m block size model consisting of a central 10 m thick quartzite unit hosted within shale aligned perpendicular to an imposed west to east hydraulic gradient. This is a simplification of the Mintaro Shale-Gilbert Range Quartzite-Kadlunga Slate exposure in the Clare Quarry as this study is focussed on demonstrating the relative HM responses across the mechanical stratigraphy. This 2D UDEC model describes a geometrical reconstruction that consists of a 2D horizontal planar slice of a representative fracture network model situated at 200 m depth which incorporate the effects of the 3D stress field (i.e. σ_V, σ_H, and σ_h). As per the methodologies and results of Mortimer *et al.* (2011), these models were subjected to a normal stress regime equivalent to 200 m of overburden to simulate isotropic, lateral relaxation of the rock mass consistent with the effects of uplift and unloading in the Clare Valley (i.e. $\sigma_V > \sigma_H = \sigma_h$). The magnitudes of stress within these models are based upon an estimate of σ_V (i.e. $\rho.g.h$) and applied as a differential stress ratio compatible with the prevailing normal stress regime (i.e. $\sigma_V > \sigma_H = \sigma_h$ at a ratio of 1: 0.5: 0.5). Fluid

pore pressures were based on an assumed hydrostatic gradient from the surface (i.e. 200 m of head) with fluid flow allowed to occur in any direction within the fracture network under the imposed west (LHS) to east (RHS) oriented hydraulic gradient of 0.01 with the north (upper) and south (lower) boundaries acting as impermeable, no-flow, barriers. The blocks defined by the fracture network generated within UDEC were discretized into a triangular mesh of constant strain with 1 m nodal distances.

Rock mass and fracture property estimates were sourced from RocData v.4 (Rocscience 2010), Mohr-Coulomb envelope analysis, empirical relationships and basic field observations (Tables 4.1 and 4.2). Outcrop mapping of quarry exposures found the mean fracture aperture for the Gilbert Range Quartzite and the Mintaro Shale was 2.05 mm and 0.15 mm, respectively (T Halihan, Flinders University, unpublished data, 1999). However, for the purposes of this modelling exercise a reference (zero stress) aperture value of 0.5 mm is considered appropriate to facilitate the observation of relative fracture network deformation patterns. The choice of this initial aperture value is not considered critical, as the main objective is to explore the relative effects of the *in situ* stress field on fracture sets that comprise the mechanical stratigraphy and not to exactly replicate field observations. At surface the geometric mean length of fractures in the Gilbert Range Quartzite and Mintaro Shale are ~2 m and ~4 m, respectively (Table 4.1). At surface the ratio of fracture density between the Gilbert Range Quartzite and the Mintaro Shale is ~7:1. Although unknown at 200 m depth, fracture density (i.e. model fracture spacing) is inferred to be half that recorded in surface outcrop to account for decrease in unloading-related fracture densities with depth that are known to occur in the Clare Valley (Mortimer *et al.* 2011). Fracture orientations are assumed identical in both the quartzite and shale units with only the fracture density varying between the two rock units similar to that observed in the field.

Table 4.1 Stochastic UDEC fracture network model parameters based upon simplified Quartzite versus Shale outcrop data of this study and T Halihan (Flinders University, unpublished data, 1999). This includes bedding (Set A) defined by the two shale-quartzite contacts and four joint sets (Sets B1, B2, D and E). Length and spacing values represent ratios between the quartzite and shale units as determined from field observations. Note that sub-horizontal joints (Set C) are omitted from this horizontal planar model.

Quartzite : Shale				
Fracture Set	**Strike (°)**	**Initial Aperture (mm)**	**Length (m)**	**Spacing (m)**
A	0	0.5 : 0.5	continuous	—
B1	86	0.5 : 0.5	2 : 4	2 : 14
B2	76	0.5 : 0.5	2 : 4	2 : 14
D	90	0.5 : 0.5	2 : 4	2 : 14
E	68	0.5 : 0.5	2 : 4	2 : 14

Table 4.2 UDEC rock mass and fracture parameters. Source: 1 = RocData v.4 (mean values); 2 = Mohr-Coulomb envelope analysis; 3 = empirical relationship; 4 = Inferred; and 5 = approximate values for fresh water at 20^{o}C.

Model Parameters	**Quartzite**	**Shale**	**Units**	**Source**
Rock Material Density (ρ)	2600	2400	$kg.m^{-3}$	1
Poisson's Ratio (ν)	0.22	0.27	—	1
Young's Modulus (*E*)	66e9	24e9	Pa	1
Bulk Modulus (*K*)	38e9	17e9	Pa	2
Shear Modulus (*G*)	26e9	9e9	Pa	2
Cohesion (c)	44e6	16e6	Pa	2
Friction Angle (φ)	48.5	51.7	Degrees	2
Dilation Angle (ψ)	0	0	Degrees	4
Uniaxial Compressive Strength	230e6	90e6	Pa	1
Tensile Strength	23e6	9e6	Pa	1
Joint Normal Stiffness (jk_n)	6.4–32.2e9	2.3–11.7e9	$Pa.m^{-1}$	3
Joint Shear Stiffness (jk_s)	2.6–13.2e9	0.9–4.6e9	$Pa.m^{-1}$	3
Joint Cohesion	0	0	Pa	4
Joint Tensile Strength	0	0	Pa	4
Joint Friction Angle	35	35	Degrees	4
Joint Dilation	5	5	Degrees	4
Joint Aperture (at zero stress)	0.5	0.5	mm	4
Joint Residual Aperture	0.1	0.1	mm	4
Joint Permeability Constant (1/12μ)	83.3	83.3	$(Pa.s)^{-1}$	5
Water Density	1000	1000	$kg.m^{-3}$	5

Similar to the methodology of Mortimer *et al.* (2011) each individual fracture within the model may consist of up to several separate 1 m long segments with randomly assigned (from a normal distribution) ranges of normal (jk_n) and shear (jk_s) fracture stiffness values throughout the model (Table 4.2). The objective of this approach is to better account for naturally occurring fracture heterogeneity such as asperity and contact area distribution, mineralization, etc and ultimately heterogeneity in deformation and fluid flow along individual fracture planes. Figure 4.6 shows the modelled fracture normal (aperture) closure that has occurred along individual fracture segments within the deformed conceptual model located at 200 m depth below the surface. The heterogeneous fracture deformation distributions observed throughout this model illustrate how localised flow restrictions or "chokes" form within the fracture network through preferential deformation of locally, low stiffness (i.e. weak) fracture segments regardless of their geometry as normal and shear stiffness can vary substantially along a single fracture plane (Mortimer *et al.* in press).

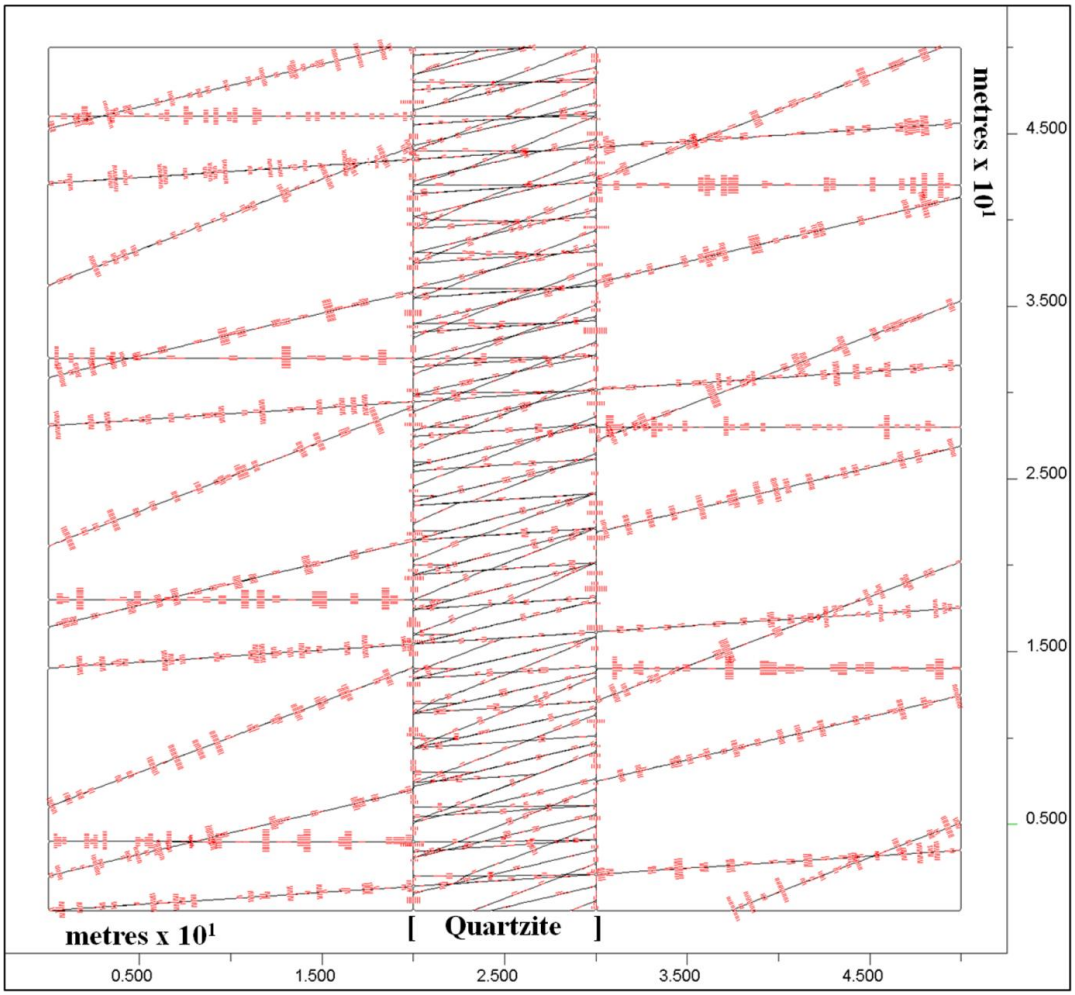

Figure 4.6 Deformed 50 m x 50 m horizontal planar model located at 200 m depth below the surface consisting of a densely fractured, 10 m thick, north-south oriented quartzite (x axis: 20–30 m) within a less densely fractured shale host. This model uses a normal stress regime to simulate the effects of uplift and unloading with an initial reference (i.e. zero stress) aperture of 0.5 mm for all fractures. The red shaded sections represent fracture segments that have experienced aperture normal closure due to fracture deformation with the magnitude of closure represented by the width of the section. Note the greater magnitudes of fracture closure occurring within the host shale.

4.4.2 Relative HM effects between mechanical stratigraphy units

To understand the relative effects of mechanical stratigraphy across different stratigraphic units requires an evaluation of the hydraulic differences occurring between the shale and quartzite units within the entire sequence under the imposed hydraulic gradient. UDEC assigns equivalent hydraulic conductivities to each uniform aperture (parallel plate) segment of a fracture according to the Cubic Law. The flow rate through each of these segments is calculated using Darcy's Law:

$$q = \frac{(2b)^3}{12\mu}\frac{\Delta P}{L} \qquad (4.1)$$

Where q is the fracture flow rate per unit width normal to flow direction ($m^2.s^{-1}$), $2b$ is fracture aperture (m), ΔP is the pressure difference (Pa), L is the length of each segment (m). Mean fracture fluid velocities (v, $m.s^{-1}$) are equivalent to the fluid flow rate divided by the aperture of each fracture segment.

Similar to the methodologies of Min *et al.* (2004) and Zhang *et al.* (1996) the conceptual model (see Figure 4.6) was deformed under a normal stress regime corresponding to 200 m depth. This deformed model was then subjected to steady-state, fluid flow under an applied west to east hydraulic gradient of 0.01 with the north and south boundaries acting as impermeable, no-flow, barriers. For comparison this flow simulation methodology is repeated for an undeformed (i.e. fixed aperture) version of the same model.

Table 4.3 shows the comparison between the undeformed and deformed conceptual model in terms of mean fracture apertures, flow rates and fluid velocities within the quartzite and its host shale units. Figures 4.7 and 4.8 depict the resultant fracture fluid flow rate and velocity distributions in the deformed model which are near identical in pattern for the undeformed model except for the reduction in magnitudes (Table 4.3). The reduction in flow rate and velocity magnitudes within the deformed model is attributed to the fact that compared to the undeformed model mean fracture apertures in the deformed model have reduced in the quartzite and shale units by 8.6% and 23%, respectively (Table 4.3; Figure 4.6). The lower amount of fracture closure occurring within the quartzite is attributed to its greater normal and shear stiffness.

Table 4.3 Undeformed versus deformed conceptual model mean fracture apertures (*2b*), mean fracture flow rates (*q*) and mean fracture fluid velocities (*v*) (see Figures 4.6, 4.7 and 4.8).

Model Parameters	Western (LHS) Shale	Central Quartzite	Eastern (RHS) Shale
Undeformed model			
Aperture, *2b* (mm)	0.5	0.5	0.5
Mean fracture flow rate, *q* ($m^2.s^{-1}$)	9.67e-07	1.76e-07	1.08e-06
Mean fracture fluid velocity, *v* ($m.s^{-1}$)	1.95e-03	3.62e-04	2.17e-03
Deformed model			
Aperture, *2b* (mm)	0.385	0.457	0.385
Mean fracture flow rate, *q* ($m^2.s^{-1}$)	6.68e-08	1.79e-08	7.69e-08
Mean fracture fluid velocity, *v* ($m.s^{-1}$)	2.28e-04	4.09e-05	2.53e-04

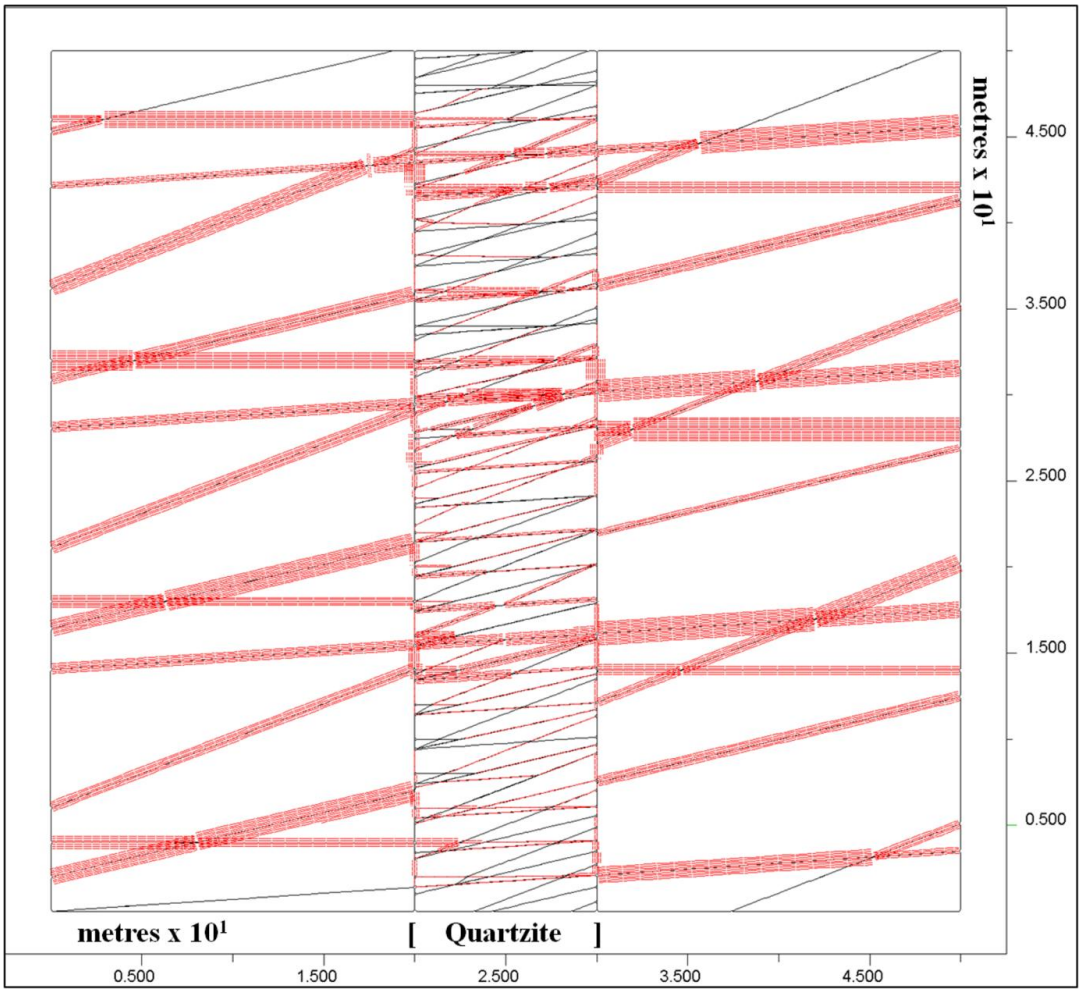

Figure 4.7 Deformed conceptual model fracture fluid flow rates. The red shaded sections represent the magnitude of flow rate within fractures as represented by the relative width of the section. Flow is occurring from west (LHS) to east (RHS) under the imposed hydraulic gradient. Note the greater magnitudes of fluid flow rates occurring within the host shale.

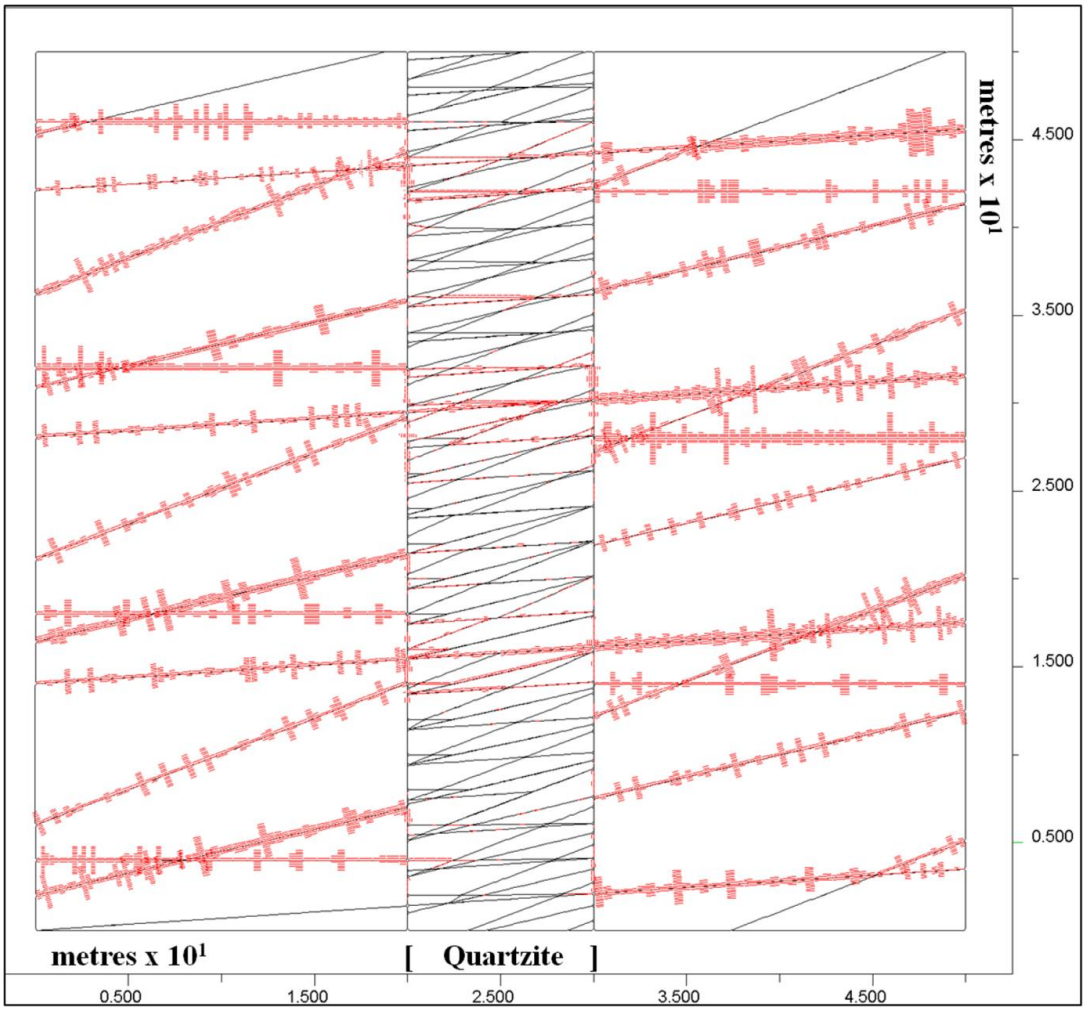

Figure 4.8 Deformed conceptual model fracture fluid velocities. The red shaded sections represent the magnitude of fluid velocities occurring between adjoining fractures as represented by the relative width of the section. Flow is occurring from west (LHS) to east (RHS) under the imposed hydraulic gradient. Note the greater magnitudes of fluid velocities occurring within the host shale.

Regardless of whether it is the undeformed or deformed model, mean fracture flow rates and fluid velocities within the quartzite unit are approximately 80% less than that of its host shale which is largely attributed to the higher fracture density in the quartzite (Table 4.3). In a fractured rock aquifer (with little or no matrix permeability), mean fracture flow rate (q) is related to mean fracture fluid velocity (v) by:

$$q = Q / N \quad (4.2)$$

Where Q is the sum of discharge flow rates ($m^3.s^{-1}$) and N is the total number of fractures; and:

$$v = q / 2b \quad (4.3)$$

Hence, v decreases with increasing fracture density. Therefore the seven fold greater fracture density within the quartzite is expected to result in significantly lower mean fracture flow rates and velocities compared to its host shale units.

4.4.3 HM effects on bulk rock mass permeability

The effect on overall bulk rock mass hydraulic properties can be evaluated in terms of a comparison between the effective hydraulic conductivity (K) of both the undeformed and deformed models estimated from Darcy's Law and the UDEC sum of discharge flow rates (Q) from each steady-state model where:

$$Q = K.A.i \quad (4.4)$$

Where K is the effective hydraulic conductivity ($m.s^{-1}$), A is the cross sectional area normal to the flow direction (m^2) and i is the hydraulic gradient.

Table 4.4 shows that compared to the undeformed conceptual model the bulk rock mass hydraulic conductivity of the deformed conceptual model is reduced by approximately an order of magnitude. This result highlights the significant impact of *in situ* stress and resultant sub-surface fracture deformation on reducing overall bulk rock mass permeability. However, this conclusion is a generalisation as joint stiffness (and aperture) segments are assigned randomly and the ultimate distribution of these segments will have an impact on the results.

Table 4.4 Undeformed versus deformed UDEC sum of discharge flow rates (*Q*) and hydraulic conductivity (*K*) for the conceptual model (see Figures 4.6 and 4.7).

Model	Q ($m^3.s^{-1}$)	K ($m.s^{-1}$)
Undeformed model	1.47e-5	2.94e-5
Deformed model	1.02e-6	2.04e-6

4.5 Discussion

The nature of fracture formation within different mechanical stratigraphy can vary significantly depending largely upon geotectonic setting and history, rock type, thickness and position within the sequence. This is particularly true for the fractured sedimentary succession in the Clare Valley where simple fold-thrust deformation associated with the Delamerian Orogeny produced dissimilar strain distributions and strongly stratabound fracture networks as dictated by the role played by the various mechanical stratigraphy units. At this location, deformation via folding, brittle fracturing, bedding plane flexural slip and/or foliation development was predominantly determined by unit thickness and whether the mechanical stratigraphy was either stiff (e.g. quartzite) or compliant (e.g. shale). For example, brittle fracturing was intense and stratabound within relatively thin and stiff units such as the Gilbert Range Quartzite. The highly intercalated nature of this sedimentary succession resulted in little mechanical coupling between adjacent units of significant competency contrast which tends to favour the formation of strongly stratabound fracture networks in response to deformation (Odling *et al.* 1999). This strong stratabound control on fracture development also results in hydraulic interconnectivity between contrasting mechanical stratigraphy to be significantly restricted (see Figure 4.5).

Mechanical properties of formations such as tensile strength, elastic stiffness, brittleness, fracture mechanics properties, layer thickness and nature of interfaces also affect fracture deformation (Laubach *et al.* 2009). For example, fractures formed within stiff units such as the Gilbert Range Quartzite tend to be rougher and with

increased apertures compared to fractures formed within more compliant units such as the Kadlunga Slate. Subsequent, fracture deformation due to the present-day *in situ* stress field will also be different such that rough fractures experience a greater rate of normal closure but shear at a much lower rate in comparison to smooth fractures.

The conceptual shale-quartzite-shale model of this study is a simplified representation only whilst more detailed predictive models would need to better account for ubiquitous bedding planes within each rock unit as well as the different deformation rules expected for different rock units with different joint roughness and stiffness (e.g. Barton *et al.* 1985). The conceptual model is also based upon limited outcrop observations which cannot fully account for 'undisturbed' fracture apertures and depth-dependent changes in fracture density. Nevertheless, the aims of the conceptual shale-quartzite-shale model of this study were to demonstrate the effects of mechanical stratigraphy on groundwater flow as well as differentiate between the relative effects of the inherent stratabound fracture networks and their individual responses under the influence of the present-day *in situ* stress field. The results of these HM models revealed a near identical ratio of mean fracture flow rates and fluid velocities in the quartzite versus its host shale regardless of whether the model was undeformed or deformed. For example, modelled groundwater flow rates and velocities within the quartzite were ~80% less in the quartzite compared to those within its host shale units regardless of stress state (Table 4.3). This outcome demonstrates that the inherent fracture network properties such as the fracture density of each mechanical stratigraphy unit are the primary control on groundwater flow. Critically, the conceptual model involved joint sets approximately aligned with the imposed west to east oriented hydraulic gradient, however, the results would be expected to differ significantly if the joint sets (i.e. permeability tensor) were either: (1) oriented at a more oblique angle to the hydraulic gradient direction or (2) oriented differently with respect to each adjoining unit. In such scenarios distortion of groundwater flow paths could be expected to be more discernible.

The results of this study are consistent with the findings of Mortimer *et al.* (2011) in that the inherent (i.e. undeformed) permeability tensor of shallow (≤200 m depth) fractured rock aquifers is determined by primary features of the fracture network

such as fracture network density, geometry, connectivity and infill. That is, palaeo-stress regimes play the dominant role in the primary development of fracture networks and fracture permeability (i.e. the inherent permeability) during episodes of crustal deformation. *In situ* stress and related fracture deformation only act to reduce the absolute magnitude of hydraulic parameters such the overall bulk rock mass permeability and groundwater flow rates and velocities within each unit.

The differential hydraulic parameters modelled between the quartzite and shale units of the conceptual model might be expected to affect pressure and head distributions across the sequence which could at the local scale potentially distort potentiometric contours and groundwater flow paths. In reality, actual velocity and pressure head distributions are expected to be complex due to the nature of variable fracture roughness, conduit geometries and intersection effects. However, flow path refraction over small scales is likely to be very difficult to detect. Groundwater flow path orientation is more likely to be discernibly refracted by permeability anisotropy of the inherent fracture network rather than by the effects of *in situ* stress (e.g. Hemker *et al.* 2004, Mortimer *et al.* 2011, Odling *et al.* 1999). Odling *et al.* (1999) found that in stratabound systems the range of fracture sizes is restricted and spacing tends to be regular whereby a rock volume which is large relative to the fracture size and spacing can be assumed to be a representative elementary volume (REV). This suggests that the required scale for observing groundwater flow path behaviour in a fractured sedimentary sequence would need to be sufficiently large to incorporate the permeability tensors of each individual mechanical stratigraphy unit.

Nonetheless mechanical decoupling and poor hydraulic connection between strongly stratabound fracture networks such as that observed between the Gilbert Range Quartzite and its host shale units suggests contacts between significantly contrasting mechanical stratigraphy could modify and even inhibit cross-bed flow. These hydraulic discontinuities could potentially lead to significant changes in vertical head gradients. The Clare Valley catchment at one time was known to contain numerous natural springs although these have largely disappeared through dramatic landscape changes caused by large scale development of farms and vineyards as well as drought-related lowering of the regional water table. It is postulated that hydraulic

discontinuities along contacts between contrasting mechanical stratigraphy could have potentially lead to the formation of natural springs in this area.

4.6 Conclusions

In terms of the question "how can we apply the concept of mechanical stratigraphy to describe contrasting HM effects on groundwater flow within an intercalated fractured sedimentary sequence?" this study found that the key determinant is the inherent permeability of the mechanical stratigraphy and to a lesser extent the effects of *in situ* stress. Therefore, methods that map and subdivide fractured rock aquifers into distinct hydraulic domains which capture relative fracture network permeability and heterogeneity from structural and geomechanical datasets is essential to groundwater flow path analyses. The relevant scale at which this approximation becomes acceptable for a given mechanical stratigraphy is determined by the degree of permeability anisotropy within each unit with respect to the direction of the hydraulic gradient. Mechanical stratigraphy governs sub-surface fracture deformation processes which ultimately affect bulk rock mass permeability and hydraulic behaviour. In general, at shallow (<200 m) depths *in situ* stress and related fracture deformation results in changes in directions and reduction in the magnitudes of the principal components of the permeability tensors of mechanical stratigraphy units. Mechanical decoupling and poor hydraulic connection between significantly contrasting mechanical stratigraphy could potentially modify and even inhibit cross-bed flow. It is postulated that hydraulic discontinuities along contacts between contrasting mechanical stratigraphy may lead to significant changes in vertical head gradients that could potentially produce surface manifestations in the form of natural springs. Understanding and incorporating the effects of mechanical stratigraphy has many practical benefits in terms of the targeting of wells and management of catchment-wide groundwater resources.

Acknowledgements

The authors gratefully acknowledge the funding and logistical support received for this research from the Centre for Groundwater Studies, the Department of Water, Land and Biodiversity Conservation South Australia and the University of Hong Kong. The authors would also like to thank Todd Halihan for the use of his geological data and Wolfgang Preiss and Tania Wilson for additional project support and advice.

5 Targeting faults for geothermal fluid production: exploring for zones of enhanced permeability

5.1 Introduction

Experience in some existing geothermal energy operations (e.g. Dixie Valley, USA; Landau, Germany) shows that faults can boost substantially reservoir permeability and fluid production, making them an attractive geothermal exploration target. However, not all faults have the required level of effective permeability, which is certainly not uniformly distributed over their entire planes. This makes it difficult to characterize them and hence challenging to distinguish between conductive faults and those acting as practically impermeable barriers. Consider also that to achieve sufficiently high production fluid temperatures a fault typically must be intersected at significant depths where the exact hydraulic character of the fault is unknown prior to drilling. Therefore, exploration targeting faults or fault segments with enhanced permeabilities involves significant risks and should be carefully guided to reduce the uncertainty and associated risks prior to drill testing. The main objectives of this discussion paper are to describe the key features that determine fault permeability and to show how the probability of locating zones of enhanced fault permeability can be improved by preliminary fault stress state modelling. For illustrative purposes, hypothetical examples of preliminary fault stress state models are provided.

For the purposes of exploratory drilling targeting faults for geothermal fluid production, "zone of enhanced permeability" can be defined as either: (1) a fault having sufficient natural porosity and permeability with fluid recharge occurring at the optimal fluid temperature (e.g. Dixie Valley, USA); or (2) a zone of enhanced porosity and permeability that may still require some degree of reservoir stimulation (e.g. Landau, Germany). The probability that a given fault has enhanced permeability increases with:

(1) Favourable orientation with respect to the *in situ* stress field; and

(2) Hydraulic connectivity with a significant volume of porous/fractured and permeable reservoir (i.e. fluid mass storage).

For the latter, the fluid mass storage may be provided by the fault itself or an adjoining hydraulically connected rock unit such as a thick layer of porous sandstone. Localized pressure anomalies associated with faults may also be beneficial for advection of fluids from a connected, deeper and potentially hotter reservoir and for lowering the effective stress state of the fault.

5.2 Fault architecture and hydrogeology

The architecture of a fault can vary greatly from a simple structure where strain is accommodated along a narrow plane to more complex structures where strain is distributed over a composite zone that may include numerous faults, small fractures, veins, breccias and cataclastic gouge. Generally, fault structures are subdivided into two simple components being the fault core and the fault damage zone which combined may vary over widths ranging from centimetres to hundreds of metres (Figure 5.1; Caine and Forster 1999; Gudmundsson *et al.* 2010). These two components are distinguishable by their distinct mechanical and hydrogeological properties although these are inherently heterogeneous and can vary significantly along a fault. The fault core refers to the main fault plane that takes up most of the displacement and where the original lithology has been altered through fault-related processes such as grain size reduction, hydrothermal alteration and mineral precipitation in response to mechanical and fluid flow processes (Caine and Forster 1999). The character of the fault core zone is strongly dependent on its protolithology (Caine and Forster 1999). Fault damage zones are defined as the adjacent network of subsidiary structures including small faults, fractures, veins, cleavage, pressure solution seams and folds that laterally decrease in density away from the fault core zone (Figure 5.1; Caine and Forster 1999; Gudmundsson *et al.* 2010).

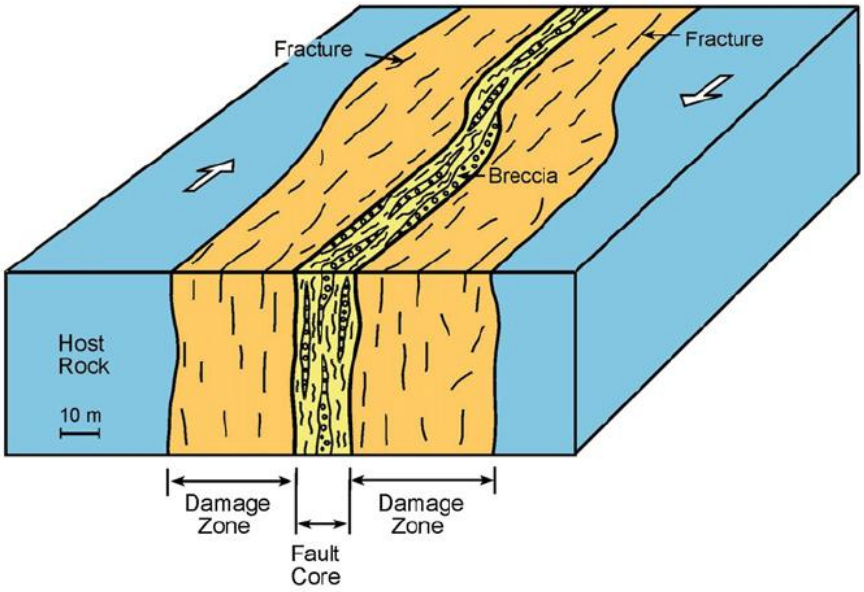

Figure 5.1 Illustrative schematic diagram of a fault including its fault core and damage zone. From Gudmundsson *et al.* (2009).

Depending on the hydromechanical properties of these two structural components, the permeability of a fault can vary considerably ranging from being an impermeable flow barrier to being a significant flow conduit with a high degree of spatial heterogeneity and anisotropy. Generally, faulting in low porosity, competent rock is expected to result in an increase in bulk (rock mass) permeability whilst in high porosity sedimentary rocks it may lead to a general decrease through communition and porosity reduction processes such grain-size reduction and the formation of clay-rich fault gouge and deformation bands (Zoback 2007; Wong and Zhu 1999). Commonly, fault cores are of a relatively lower permeability than their associated damage zones, which is attributed to porosity reducing processes occurring within the cores (Caine *et al.* 2010). For example, at the Mirrors site, Dixie Valley geothermal field, measured core plug permeabilities ranged from 10^{-8} m^2 (10^7 mD) in fault damage zones to 10^{-20} m^2 (10^{-8} mD) in fault cores, however, the permeability of the fault zone as a whole is on the order of 10^{-12} m^2 (1000 mD) (Caine and Forster 1997; Seront *et al.* 1998). In terms of anisotropy, the permeability tensor is expected to be at a maximum parallel to the strike, intermediate down dip and at a minimum perpendicular to the fault plane, which allows for both vertical and lateral flow but may limit cross-fault flow (Ferrill *et al.* 2004). Faults of sufficiently high

permeability can also contribute significantly to both local and regional scale coupled groundwater flow and heat transport via advection/convection processes (e.g. Bachler *et al.* 2003).

5.3 Stress-dependent fault permeability

The link between stress, fault or fracture deformation and permeability is such that as fracture void geometries and the connectivity of a flow network change in response to changing *in situ* stress, the storage, permeability and flow pattern is also expected to change in magnitude, heterogeneity and/or anisotropy. Fracture deformation can result in significant changes in permeability and storage because the ability of a fracture to transmit a fluid is extremely sensitive to its aperture. For example, the transmissivity of an individual fracture (T_f) idealised as an equivalent parallel plate opening can be expressed as:

$$T_f = \frac{(2b)^3 \rho g}{12\mu} \qquad (5.1)$$

Where $2b$ is the fracture aperture width (m), ρ is the fluid density (kg.m^{-3}), g is gravitational acceleration (m.s^{-2}) and μ is the dynamic viscosity of the fluid (kg.m^{-2}.s).

One key aspect of exploring for permeable faults is the theory of stress-dependant fracture permeability in deep-seated, fractured rocks. This theory is supported by studies relating to hydrocarbon and geothermal reservoirs and studies of potential nuclear waste repository sites (e.g. Finkbeiner *et al.* 1997; Gentier *et al.* 2000; Hudson *et al.* 2005). The theory states that the *in situ* stress fields exert a significant control on fluid flow patterns in fractured rocks, particularly, for rocks of low matrix permeability. For example, in a key study of deep (>1.7 km) boreholes, Barton *et al.* (1995) found that permeability manifests itself as fluid flow focused along fractures favourably aligned within the *in situ* stress field, and that if fractures are critically stressed this can impart a significant anisotropy to the permeability of a fractured rock mass. Critically stressed fractures are defined as fractures that are close to frictional failure within the *in situ* stress field (Barton *et al.* 1995). Specifically, the theory of stress-dependent fracture permeability predicts preferential flow occurring along fractures that are oriented orthogonal to the minimum principal stress (σ_3)

direction (due to low normal stress), or inclined ~30° to the maximum principal stress (σ_1) direction (due to shear dilation).

Frictional sliding along a plane of weakness such as a fault occurs when the ratio of shear (τ) to the effective normal stress (σ'_n) equals or exceeds the frictional sliding resistance. This is known as Amonton's Law, which governs fault reactivation:

$$\tau = \mu.\sigma'_n \quad (5.2)$$

Where μ is the coefficient of friction (a rock material property) and σ'_n is equal to the total applied normal stress minus the pore fluid pressure (i.e. $\sigma_n - P_P$). The value of μ has been found to typically range between 0.6 and 1.0 (Byerlee 1978; Zoback 2007). This relationship also shows that pore fluid pressure can have a significant impact as it determines the effective stress and that increasing pore pressures can de-stabilise a fault surface by increasing the ratio of shear to normal stress. The coupling of these hydromechanical (HM) processes means that fluid pressure and flow within faults is linked to tectonic stress and deformation through changes in permeability and storage whilst tectonic stress and deformation is linked to fluid flow through changes in fluid pressure and effective stress (NRC 1996).

How exactly a fault will behave under an applied stress regime depends upon many factors, consequently, investigating stress-dependent fault permeability based solely on fault alignment with respect to the *in situ* stress field is an oversimplification. Just as important are the geomechanical properties of the host rock and its contained faults. Important intact rock material properties include parameters such as density, bulk moduli, uniaxial compressive strength, tensile strength, cohesion and friction angle that are typically estimated from laboratory tests. Fracture stiffness is a function of both fracture wall surface contact (i.e. fracture roughness profile) and the elastic properties of the intact rock material (i.e. bulk rock moduli) where for the same given alignment within an *in situ* stress field relatively stiff fractures deform less than weaker fractures. Fracture normal and shear stiffness are measures of resistance to deformation perpendicular and parallel to fracture walls, respectively, and both increase with increasing effective normal stress. In general, faults tend to exhibit high stiffness if formed within hard, competent rocks or if they become locked open by earlier deformation episodes (e.g. shear dislocation) or mineral infill and cementation, and may even exhibit stress insensitive behaviour when subjected

to high effective normal stresses (Hillis 1998; Laubach *et al.* 2004). In contrast, low stiffness faults can exhibit a wide range of shear and closure behaviour as their alignment with respect to σ_1 changes (Hillis 1998). Ultimately, estimates of fracture stiffness attempt to account for more realistic fracture heterogeneity, asperity contact, deformation and tortuous fluid flow. Equations 5.3 and 5.4 below describe the simplified relationship between fracture stiffness and fracture deformation (Rutqvist and Stephannson 2002):

$$\Delta\mu_n = jk_n \, \Delta\sigma'_n \qquad (5.3)$$

$$\Delta\mu_s = jk_s \, \Delta\sigma_s \qquad (5.4)$$

which states (a) that fracture normal deformation ($\Delta\mu_n$) occurs in response to changes in effective normal stress ($\Delta\sigma'_n$) with the magnitude of opening or closure dependent upon fracture normal stiffness (jk_n); and (b) that the magnitude of shear mode displacement ($\Delta\mu_s$) depends upon the shear stiffness (jk_s) and changes in shear stress ($\Delta\sigma_s$).

Structural permeability within faults is likely to be a transient property as faults often become modified by porosity reducing processes such as hydrothermal mineralisation, hence, fault deformation processes compete with permeability reduction caused by fluid flow (Sibson 1996; Zoback 2007). Active fault slip is typically episodic and can temporarily increase the permeability of a fault zone by as much as many orders of magnitude (Gudmundsson 2000). Therefore, for faults to remain effective permeable structural conduits fault deformation processes must be at least intermittent to continual. For example, in the Dixie Valley geothermal field fluid production is sourced from high permeability faults and fractures that are favourably aligned and critically stressed whilst it is inferred that the formation of fault permeability associated with active deformation competes with permeability destroying hydrothermal quartz precipitation processes (Zoback 2007).

5.4 Preliminary modelling of fault stress states

The numerical modelling of fault stress states has previously been employed by several researchers to identify zones of potential fault enhanced permeability and fluid flux (e.g. Ferrill *et al.* 2004; Gudmundsson 2000; Moeck *et al.* 2009; Zhang and Sanderson 1996). In a similar methodology, this study uses the Universal Distinct Element Code (UDEC) to simulate the coupled HM response of deformable faulted rock masses under a specified *in situ* stress field to derive preliminary indications of fault stress states and, by corollary, their potential permeability. UDEC represents a rock mass as an assembly of discrete rigid or deformable, impermeable blocks separated by discontinuities (faults, joints etc) and can reproduce fully coupled HM behaviour (Itasca 2004). Fluid pressure and fracture conductivity are dependent upon mechanical deformation whilst simultaneously fluid pressures modify the mechanical behaviour of the fractures (for a comprehensive review of the UDEC governing equations see Itasca 2004). The 2D UDEC models describe a geometrical reconstruction that consist of 2D horizontal planar and vertical slices of the conceptual faulted rock mass model and incorporates the effects of the 3D stress field (i.e. σ_V, σ_H, and σ_h). That is, the models perform plane strain analyses, which assumes that the model continues indefinitely (and uniformly) out of the plane of analysis with computations performed for a slice that is one unit thick (Itasca 2004). The ultimate aim of this type of modelling is to distinguish which fault or fault segments in a specified area are critically stressed and, therefore, a potential exploration drill target. These models are designed to assist explorers in areas of unknown or complex geology prior to drilling, however, large model parameter uncertainties means that the results are preliminary, representing a limited number of probable realizations of the influence *in situ* stress state on the modelled faults.

To illustrate this methodology, three hypothetical geological models are presented based upon the northern Perth Basin as an example setting. This involves a strike-slip faulting stress regime, stress tensor $\sigma_H > \sigma_V > \sigma_h$ equivalent to 1.25 : 1.0 : 0.75 and an east-west principle horizontal stress (σ_H) orientation (King *et al.* 2008; van Ruth 2006). For the purposes of this illustrative exercise, rock mass parameters (e.g. density, bulk modulus etc) were sourced from the UDEC rock property database

although, where possible, these should be based upon measured representative field samples or global average values. The most difficult part of this process is assigning fault stiffness values, particularly, as they are expected to vary with host lithology. As fracture stiffness is a function of wall contact area, the jk_n for smooth planar surfaces can approximate the value of the Young's Modulus (*E*) whereas the jk_s, for perfectly matching rough surfaces, can approximate the value of the Shear Modulus (*G*). At shallow depths, estimates can be derived based upon jk_n ranging from 1/2 (smooth) to 1/10 (rough) the value of *E* and jk_s ranging from 1/2 (rough) to 1/10 (smooth) the value of *G*, which are compatible with published data and those derived from empirical relationships (Kulhawy and Goodman 1980; Norlund *et al.* 1995). However, prior to drill testing the true nature of the fault at depth is unknown. As the aim is to attempt to evaluate relative fault stress states, possibly across multiple faults and lithologies, a 'smooth' fault stiffness for each respective lithology was chosen along with zero tensile strength, cohesion and dilation angle values. In theory, these geomechanical properties replicate the behaviour of a 'weak' fault plane, which allows each fault segment to potentially deform. This is a reasonable approach as most active fault zones are inferred to be weak (Gudmundsson *et al.* 2001; Gudmundsson *et al.* 2009).

The three hypothetical geological model examples are:
Model 1: 4 km x 4 km horizontal planar model set at -3.5 km depth below the surface comprising of a single fault with jog hosted within sandstone (Figure 5.2).

Model 2: 5 km x 5 km cross-section of a listric fault hosted with a sedimentary sequence comprising of limestone (surface-1 km depth), siltstone (1 km-2.5 km depth), shale (2.5 km-3.5 km depth), sandstone (3.5 km-4 km depth) and granite (4 km–5 km depth) (Figure 5.3).

Model 3: 4 km x 4 km horizontal planar model set at -3.5 km depth below the surface comprising of a central, circular, granite batholith of 1 km radius hosted within a weak shale unit plus three cross-cutting faults of differing orientation (Figure 5.4).

In these models, rock mass deformation was defined by the Mohr-Coulomb model, which is the conventional model used to represent shear failure in rocks and soils

whilst fracture behaviour was defined by the Coulomb-Slip criterion, which assigns elastic stiffness, tensile strength, frictional, cohesive and dilational characteristics to a fracture (Itasca 2004). Mechanical boundaries were defined as fixed velocity (displacement) boundaries and initial *in situ* and boundary fluid pore pressures are assumed hydrostatic.

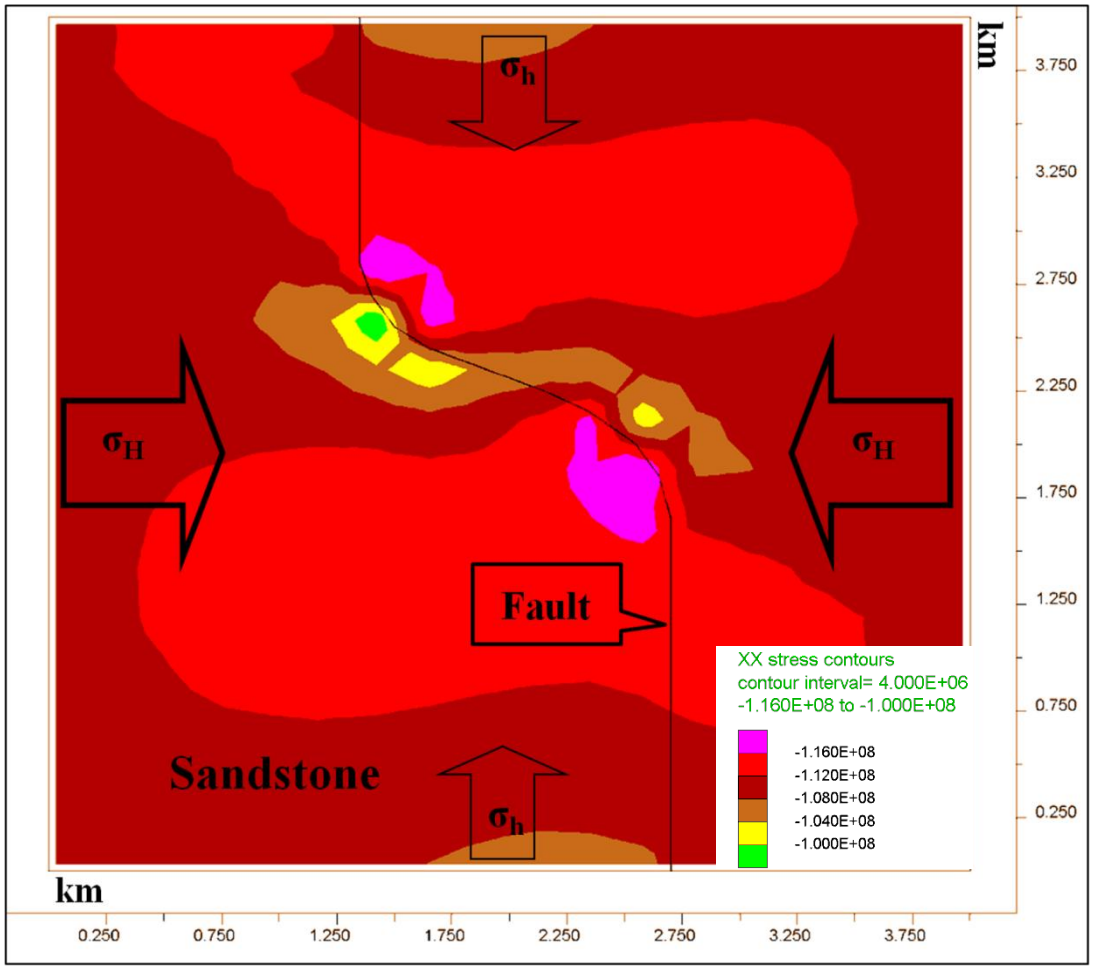

Figure 5.2 Model 1: 4 km x 4 km horizontal planar contour map of x-direction stress magnitudes highlighting the concentration of high and low stress zones into quadrants along the fault jog. This highlights that although fault alignment maybe favourable stress-dependent fault permeability can be segmented and localised. Note that the principle stress (σ_H) direction is east-west (right-left). Legend: purple, red, brown, green and yellow colours represent a decreasing range of high to low stress magnitudes, respectively (negative values are compressive).

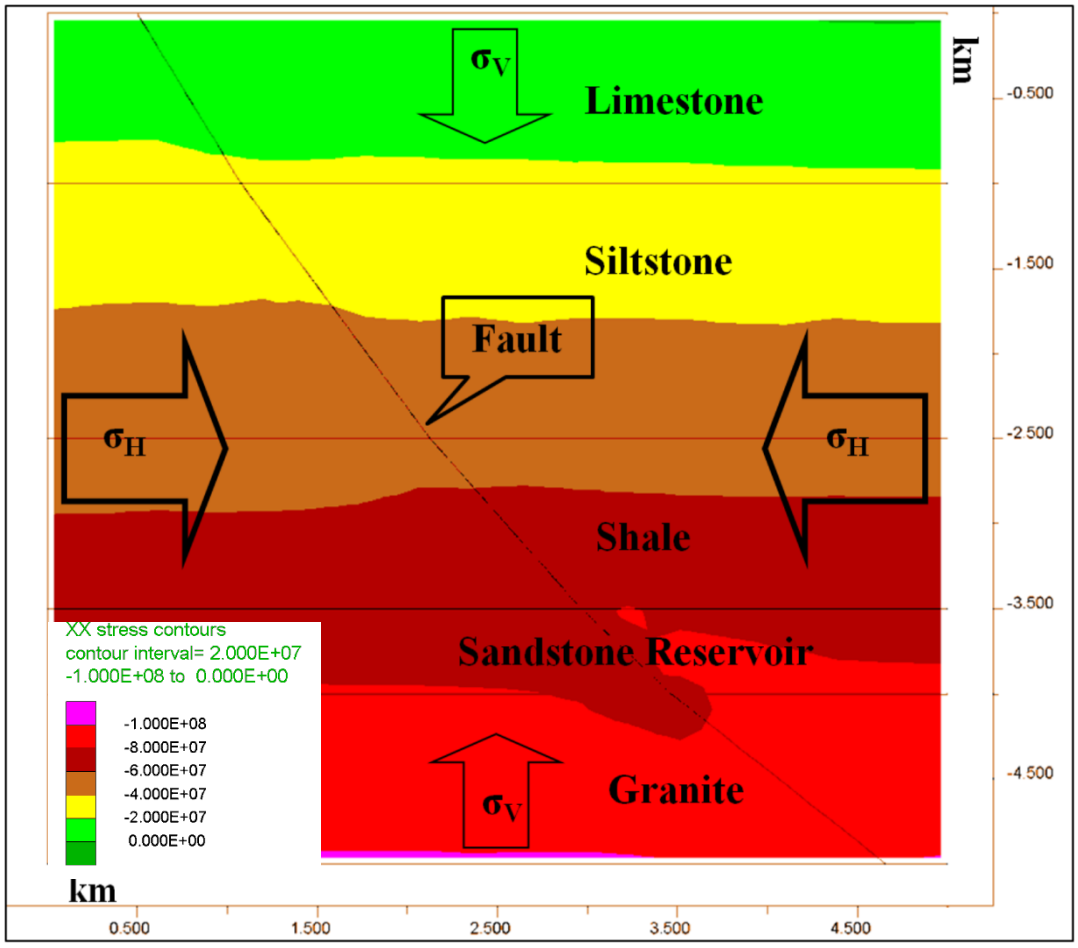

Figure 5.3 Model 2: 5 km x 5 km vertical cross-section profile of contoured y-direction stress magnitudes highlighting a localised low stress field perturbation closely associated with the trace of the listric fault. This indicates low fault plane stress and potentially enhanced fault permeability. Note that the principle stress (σ_H) direction is east-west (right-left). Legend: purple, red, brown, green and yellow colours represent a decreasing range of high to low stress magnitudes, respectively (negative values are compressive).

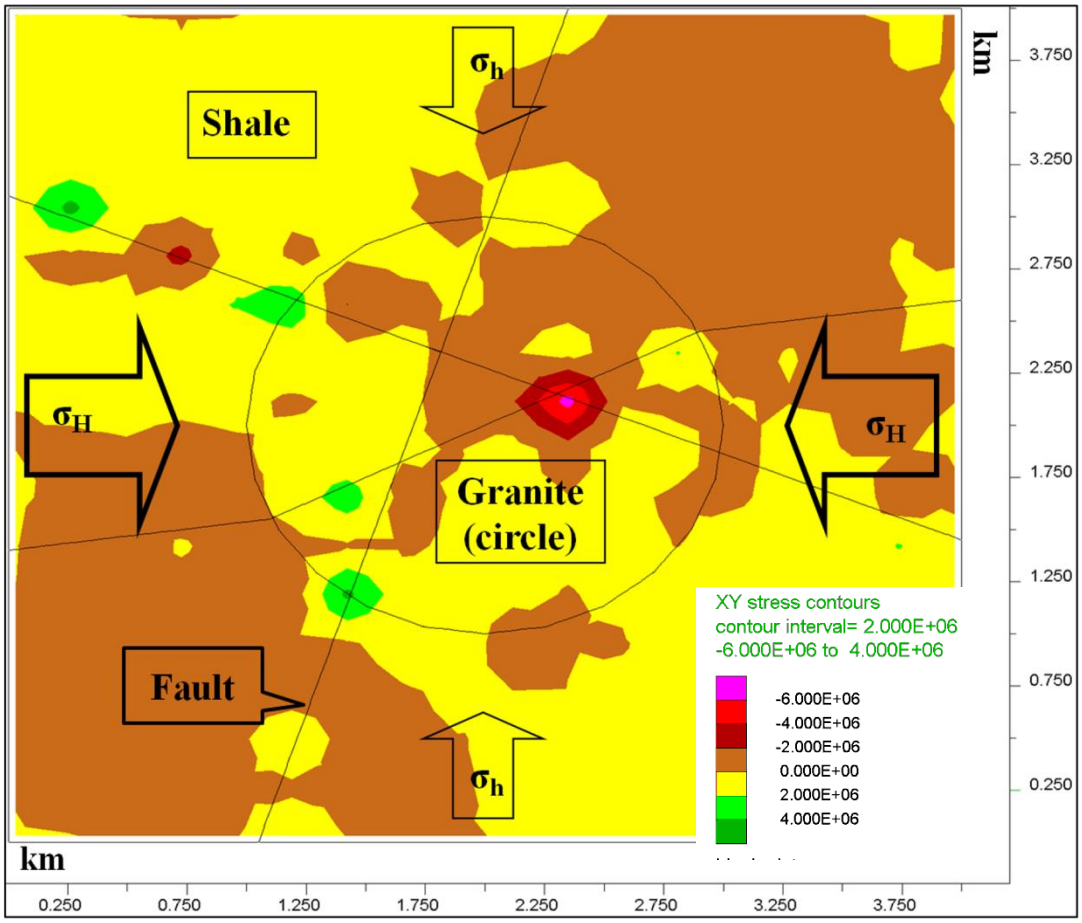

Figure 5.4 Model 3: 4 km x 4 km horizontal planar contour map of x,y-direction stress magnitudes highlighting a critically stressed fault intersection (red) which potentially represents the location of enhanced fault permeability. This intersection is also coincident with a low stress anomaly in the x- and y-direction. Note that the principle stress (σ_H) direction is east-west (right-left). Legend: purple, red, brown, green and yellow colours represent a decreasing range of high to low stress magnitudes, respectively (negative values are compressive).

5.4 Conclusion

The risks of targeting permeable faults to produce from geothermal reservoirs include: (1) a relatively high permeability structure may result in fluid pathway short-circuiting and accelerated rates of reservoir thermal drawdown; (2) multiple fault structures with varying amounts of displacement may truncate and compartmentalise a reservoir thereby reducing accessible reservoir volume; and (3) the targeted fault structure may still be hydraulically sealed and/or stress insensitive as a result of other competing natural processes. The possibility of the changes in the stress regime (and the relative stress magnitudes) with depth is another complicating factor in modelling and reliability of model results. Depending on the geological setting, such changes may occur at depths as shallow as a few hundred metres. These risks can be partially mitigated through interpretation of good quality seismic reflection data and with direct drill testing. The fault stress state models shown in this discussion paper are deliberately simplistic but specifically designed to demonstrate how this method can be used to identify zones of potentially enhanced fault permeability prior to any drill testing in areas of unknown or complex geology. This method may be of benefit to the Australian geothermal exploration sector as target depths are typically in excess of 3 km depth below the surface where natural *in situ* porosity and permeability are typically low and there is a general paucity of data.

Nevertheless, it is important to note that the results of such preliminary models can only be taken to represent possible scenarios of encountering enhanced fault permeability and that these 2D models simplify the 3D reality. Evaluating targets on structural alignment relationships within the *in situ* stress field alone might provide sufficient insight, however, in complex areas, the influence of features such as multiple rock competency and fault stiffness contrasts and fault intersections on perturbing the local stress field should also be taken into account. The results of these numerical models are only as accurate as the quality of the input data and this particular methodology can include a significant amount of model parameter uncertainty (e.g. fault stiffness, estimated or inferred stress field etc). Therefore, this methodology should be viewed as just one tool that can form part of a broader exploration risk management strategy.

Acknowledgements

The authors gratefully acknowledge the funding and logistical support received for this research from the National Centre for Groundwater Research and Training, the Department of Water, Land and Biodiversity Conservation South Australia, University of Hong Kong and University of Mississippi.

References

Anderson EM (1951) The dynamics of faulting and dyke formation with application to Britain. Oliver and Boyd, Edinburgh.

Bachler D, Kohl T, Rybach L (2003) Impact of graben-parallel faults on hydrothermal convection-Rhine Graben case study. Phys Chem Earth 28: 431-441.

Bandis SC (1993) Engineering properties and characterization of rock discontinuities. In: Hudson J (ed) Comprehensive Rock Engineering: Principles, Practice and Project Vol. 1: 155-183. Pergamon Press, Oxford.

Banks D, Odling NE, Skarphagen H, Rhor-Torp E (1996) Permeability and stress in crystalline rocks. Terra Review 8: 223-235.

Barton N, Bandis S, Bakhtar K (1985) Strength, deformation and conductivity coupling of rock joints. Int J Rock Mech Min Sci Geomech Abs 22 (3): 121-140.

Barton NR, Choubey V (1977) The shear strength of rock joints in theory and practice. Rock Mech 10 (1-2): 1-54.

Barton CA, Zoback MD, Moos D (1995) Fluid flow along potentially active faults in crystalline rock. Geology 23: 683-686.

Blum P, Mackay R, Riley MS (2009) Stochastic simulations of regional scale advective transport in fractured rock masses using block upscaled hydro-mechanical rock property data. J Hydrol 369 (3-4): 318-325.

Bour O, Davy P (1998) Connectivity of random fault networks following a power law length distribution. Water Resour Res 33: 1567-1583.

Byerlee J.D (1978) Friction of rocks. Pure App Geophys 116: 615-626.

Caine JS, Bruhn RL, Forster CB (2010) Internal structure, fault rocks and inferences regarding deformation, fluid flow, and mineralisation in the seismogenic Stillwater normal fault, Dixie Valley, Nevada. J Struct Geol 32 (11): 1576-1589.

Caine JS, Evans JP, Forster CB (1996) Fault zone architecture and permeability structure. Geology, 24 (11): 1025-1028.

Caine JS, Forster CB (1999) Fault zone architecture and fluid flow: insights from field data and numerical modelling. In: Haneberg WC, Mozley PS, Moore JC, Goodwin LB (eds) Faults and Subsurface Fluid Flow in the Shallow Crust. AGU Geophys Mono 113: 101-127.

Cappa F, Guglielmi Y, Fenart P, Merrien-Souketchoff V, Thoravel A (2005) Hydromechanical interactions in a fractured carbonate reservoir inferred from hydraulic and mechanical measurements. Int J Rock Mech Min Sci 42: 287-306.

Cook PG (2003) A guide to regional groundwater flow in fractured rock aquifers. Contributions from Williams M, Simmons CT, Love AJ, Halihan T, Herbert G, Heinson G, ISBN 1 74008 233 8, Seaview Press, 108 p

Cook PG, Love AJ, Robinson N, Simmons CT (2005) Groundwater ages in fractured rock aquifers. J Hydrol 308: 285-301.

Davy P, Bour O, De Dreuzy J-R, Darcel C (2006) Flow in multi-scale fractal fracture networks. In: Cello, G and Malamud, B.D (eds.), Fractal Analysis for Natural Hazards. Geological Society, London, Special Publications 261: 31-45.

de Dreuzy J-R., Davy P, Bour (2001) Hydraulic properties of two-dimensional random fracture networks following a power law length distribution: 2. Permeability of networks based on log-normal distribution of apertures. Water Resour Res 37(8): 2079-2095.

Engelder T (1985) Loading paths to joint propagation during a tectonic cycle: an example from the Appalachian Plateau, U.S.A. J Struct Geol 7 (3/4): 459-476.

Engelder T (1993) Stress Regimes in the Lithosphere: Princeton, New Jersey, Princeton University Press, 457 p.

Ferrill DA, Sims DW, Waiting JW, Morris AP, Franklin NM, Schultz AL (2004) Structural framework of the Edwards Aquifer recharge zone in south-central Texas. GSA Bull 116 (3/4): 407-418.

Ferrill DA, Winterle J, Wittmeyer G, Sims D, Colton S, Armstrong A (1999) Stressed rock strains groundwater at Yucca Mountain, Nevada. GSA Today 9: 1-8.

Finkbeiner T, Barton CA, Zoback MD (1997) Relationships among in-situ stress, fractures and faults, and fluid flow: Monterey Formation, Santa Maria Basin, California. AAPG Bull 81 (12): 1975-1999.

Forster CB, Caine JS, Schulz S, Nielson DL (1997) Fault zone architecture and fluid flow. An example from Dixie Valley, Nevada. Proceedings 22nd Workshop on Geothermal Reservoir Engineering, Stanford University, Stanford, California, 27-29 January 1997.

Freeze RA, Cherry JA (1979) Groundwater. Prentice Hall, New Jersey.

Gaffney ES, Damjanac B, Valentine GA (2007) Localization of volcanic activity: 2. Effects of pre-existing structure. Earth Planet Sci Lett 263: 323-338.

Ge S (1998) Estimation of groundwater velocity in localised fracture zones from well temperature profiles. J Volc Geotherm Res 84: 93-101.

Gentier S, Hopkins D, Riss J (2000) Role of Fracture Geometry in the Evolution of Flow Paths under Stress. In: Faybishenko B, Witherspoon PA and Benson SM (eds), Dynamics of Fluids in Fractured Rocks. AGU Geophys Mono 122: 169-184.

Geological Survey of South Australia (2001) South Australia Geoscientific GIS Dataset, Division of Minerals and Energy Resources, Primary Industries and Resources South Australia.

Gudmundsson A (2000) Active faults and groundwater flow. Geophys Res Lett 27 (18): 2993-2996.

Gudmundsson A, Berg SS, Lyslo KB, Skurtveit E (2001) Fracture networks and fluid transport in active fault zones. J Struct Geol 23: 343-353.

Gudmundsson A, Simmenes TH, Larsen B, Philipp SL (2010) Effects of internal structure and local stresses on fracture propagation, deflection and arrest in fault zones. J Struct Geol 32 (11): 1643-1655.

Hancock P, Engelder T (1989) Neotectonic joints. Geol Soc Am Bull 101: 1197-1208.

Hemker K, van den Berg E, Bakker M (2004) Ground Water Whirls. Ground Water 42 (2): 234-242.

Henriksen H, Braathen A (2006) Effects of fracture lineaments and *in situ* rock stresses on groundwater flow in hard rocks: a case study from Sunnfjord, western Norway. Hydrogeol J 14 (4): 444-461.

Hillis RR (1998) The influence of fracture stiffness and the *in situ* stress field on the closure of natural fractures. Pet Geosci 4: 57-65.

Hillis RR, Coblentz DD, Sandiford M, Zhou S (1997) Modelling the Contemporary Stress Field and its Implications for Hydrocarbon Exploration. Expl Geophys 28: 88-93.

Hillis RR, Reynolds D (2000) The Australian Stress Map. J Geol Soc 157**:** 915-921.

Hobbs BE, Means W D, Williams PF (1976) An Outline of Structural Geology. John Wiley & Sons, New York, 571 p.

Hoek E (2007) Practical Rock Engineering. http://www.rocscience.com/hoek/PracticalRockEngineering.asp. Accessed May 2008

Hsieh PA (1998) Scale effects in fluid flow through fractured geologic media. In: Sposito G (ed), Scale dependence and scale independence in hydrology: 59-66. Cambridge University Press.

Hudson J A, Stephansson O, Anderson J (2005) Guidance on numerical modelling of thermo-hydro-mechanical coupled processes for performance assessment of radioactive waste repositories. Int J Rock Mech Min Sci 42: 850-870.

Itasca (2004) UDEC 4.0 Theory and Background. Itasca Consulting Group Inc., Minnesota.

King RC, Hillis RR, Reynolds SD (2008) *In situ* stresses and natural fractures in the Northern Perth Basin, Australia. Aust J Earth Sci 55 (5): 685-701.

Kulhawy FH, Goodman RE (1980) Design of Foundations on Discontinuous Rock, Proceedings of the International Conference on Structural Foundations on Rock. Int Soc Rock Mech 1: 209-220.

Laubach SE, Olsen JE, Gale JFW (2004) Are open fractures necessarily aligned with the maximum horizontal stress? Earth Planet Sci Lett 222: 191-195.

Laubach SE, Olsen JE, Gross MR (2009) Mechanical and fracture stratigtaphy. AAPG Bull 93 (11): 1413-1426.

Long JC, Remer JS, Wilson CR, Witherspoon PA (1982) Porous media equivalents of discontinuous fractures. Water Resour Res 18 (3): 645-658.

Long JC, Witherspoon PA (1985) The relationship of the degree of interconnection to permeability in fracture networks. J Geophys Res 90 (B4): 3087-3098.

Love AJ (2003) Groundwater flow and solute transport dynamics in a fractured rock meta-sedimentary aquifer. PhD Thesis, Flinders University, South Australia.

Love AJ, Cook PG, Harrington GA, Simmons CT (2002) Groundwater flow in the Clare Valley, Report DWR02.03.0002. Department for Water Resources, South Australia.

Love AJ, Simmons CT, Cook P, Herczeg A, Halihan T (2007) Estimating groundwater flow rates in fractured rock metasediments: Clare Valley, South Australia. In: Krasny J, Sharp JM Jr (eds), Groundwater in Fractured Rocks, IAH Selected Paper Series 9: 463-478.

Min KB, Jing L, Stephansson O (2004a) Determining the equivalent permeability tensor for fractured rock masses using a stochastic REV approach: Method and application to the field data from Sellafield, UK. Hydrogeol J 12: 497-510.

Min KB, Rutqvist J, Tsang CF, Jing L (2004b) Stress-dependent permeability of fractured rock masses: a numerical study. Int J Rock Mech Min Sci 41: 1191-1210.

Moeck I, Kwiatek G, Zimmermann G (2009) Slip tendency analysis, fault reactivation potential and induced seismicity in a deep geothermal reservoir. J Struct Geol 31: 1174-1182.

Morin RH, Savage WZ (2003) Effects of crustal stresses on fluid transport in fractured rock: case studies from northeastern and southwestern USA. Hydrogeol J 11: 100-112.

Mortimer L, Aydin A, Simmons CT, Heinson G, Love AJ (in press) The role of *in situ* stress in determining hydraulic connectivity in a fractured rock aquifer. Hydrogeo J. Accepted 22nd May 2011.

Mortimer L, Aydin A, Simmons CT, Love AJ (2011) Is *in situ* stress Important to Groundwater Flow in Shallow Fractured Rock Aquifers? J Hydrol 399 (3-4): 185-200.

National Research Council (NRC) (1996) Rock Fractures and Fluid Flow. Contemporary Understanding and Applications. National Academy of Sciences, Washington D.C.

Neves MA, Morales N (2007) Well productivity controlling factors in crystalline terrains of southeastern Brazil. Hydrogeol J 15: 471-482.

Nordlund E, Radberg G, Jing L (1995) Determination of failure modes in jointed pillars by numerical modelling. In: Fractured and jointed rock masses: 345–350. Balkema, Rotterdam.

Odling N E, Gillespie P, Bourgine B, Castaing C, Chiles J-P, Christensen NP, Fillion E, Genter A, Olsen C, Thrane L, Trice L, Aarseth E, Walsh JJ, Watterson J (1999) Variations in fracture system geometry and their implications for fluid flow in fractured hydrocarbon reservoirs. Pet Geosci 5: 373-384.

Paillet FL (1993) Using borehole geophysics and cross-borehole flow testing to define hydraulic connections between fracture zones in bedrock aquifers. J App Geophys 30: 261-279.

PIRSA, 2009. Drillhole Enquiry System. Online database. Department of Primary Industries and Resources South Australia (PIRSA). https://des.pir.sa.gov.au/deshome.html. Accessed January 2009.

PIRSA Minerals (1999) Earthquakes in South Australia > Magnitude 3, 1995-1999. Online Report. Department of Primary Industries and Resources South Australia (PIRSA). http://www.pir.sa.gov.au/minerals/earthquakes/yearly_earthquake_reports. Accessed May 2006.

PIRSA Minerals (2001) Earthquakes in South Australia 2001. Online Report, Department of Primary Industries and Resources South Australia (PIRSA). http://www.pir.sa.gov.au/minerals/earthquakes/yearly_earthquake_reports. Accessed May 2006.

Preiss WV (1995) Tectonic Evolution of the Mid-North, South Australia. In: Specialist Group in Tectonics and Structural Geology, Clare Valley mid-conference excursion guide. Geol Soc Aust Abs 40.

Preiss WV (2000) The Adelaide Geosyncline of South Australia, and its significance in continental reconstruction. Precamb Res 100: 21-63.

Price NJ (1966). Fault and Joint Development in Brittle and Semi-Brittle Rock, Pergamon Press, 186 p.

Renshaw CE (1996) Influence of subcritical fracture growth on the connectivity of fracture networks. Water Resour Res 32 (6): 1519-1530.

Renshaw CE (1999) Connectivity of joint networks with power law length distributions. Water Resour Res 35 (9): 2661-2670.

Renshaw CE (2000) Fracture spatial density and the anisotropic connectivity of fracture networks. In: Faybishenko, B, Witherspoon, PA, Benson SM (eds), Dynamics of Fluids in Fractured Rocks. AGU Geophys Mono 122: 169-184.

Rocscience (2010) RocData version 4.0, Rock, soil and discontinuity strength analysis. Rocscience Inc., Ontario.

Rutqvist J, Stephansson O (2003) The role of hydromechanical coupling in fractured rock engineering. Hydrogeol J 11: 7-40.

Sandiford M (2003) Neotectonics of southeastern Australia: linking the Quaternary faulting record with seismicity and *in situ* stress. In: Hillis RR, Muller D (eds), Evolution and Dynamics of the Australian Plate. Geol Soc Aust, Spec Pub 22: 107-120.

Sandiford M, Wallace M, Coblentz DD (2004) Origin of the *in situ* stress field of southeastern Australia. Basin Res 16: 325-338.

Seront B, Wong T-F, Caine JS, Forster CB, Bruhn RL, Fredrich JT (1998) Laboratory characterisation of hydromechanical properties of a seismogenic normal fault system. J Struct Geol 20: 865-881.

Shapiro AM, Hsieh PA, Burton WC, Walsh GJ (2007) Integrated multi-scale characterization of ground-water flow and chemical transport in fractured crystalline rock at the Mirror Lake site, New Hampshire. In: Hyndman DW, Day-Lewis FD, Singha K (eds), Sub-surface Hydrology: Data Integration for Properties and Processes. AGU Geophys Mono 171: 201-225.

Sibson, RH (1996) Structural permeability of fluid-driven fault-fracture meshes. J Struct Geol 18 (8): 1031-1042.

Skinner D, Heinson G (2004) A comparison of electrical and electromagnetic methods for the detection of hydraulic pathways in a fractured rock aquifer, Clare Valley, South Australia. Hydrogeol J 12: 576-590.

Snow DT (1969) Anisotropic Permeability of Fractured Media. Water Resour Res 5 (6): 1273-1289.

van der Pluijm BA, Marshak S (2003) Earth Structure: An Introduction to Structural Geology and Tectonics, 2nd edn. New York, WW Norton and Company, 656 p.

van Ruth PJ (2006) Geomechanics: Vlaming Sub-Basin, Western Australia. Cooperative Research Centre for Greenhouse Gas Technologies (CO2CRC), Appendix 9, Report Number RPT06-0043.

Waltham T (2002) Foundations of Engineering Geology. 2nd edition. Taylor and Francis, 92 p.

Wellman TP, Poeter EP (2006) Evaluating uncertainty in predicting spatially variable representative elementary scales in fractured aquifers, with application to Turkey Creek Basin, Colorado. Water Resour Res: 42, W08410, doi:10.1029/2005WR004431

Wennberg OP, Svana T, Azizzadeh M, Aqrawi AMM, Brockbank P, Lyslo KB, Ogilvie S (2006) Fracture intensity vs. mechanical stratigraphy in platform top carbonates: the Aquitanian of the Asmari Formation, Khaviz Anticline, Zagros, SW Iran. Pet Geosci 12: 233-245.

Wong T-F, Zhu W (1999) Brittle faulting and permeability evolution: hydromechanical measurement, microstructural observation, and network modelling. In: Haneberg WC, Mozley PS, Moore JC, Goodwin LB (eds) Faults and Subsurface Fluid Flow in the Shallow Crust, AGU Geophys Mono 113: 83-99.

Zhang X, Sanderson DJ (1996) Numerical modelling of the effects of fault slip on fluid flow around extensional faults. J Struct Geol 18: 109-119.

Zhang X, Sanderson DJ, Harkness RM, Last NC (1996) Evaluation of the 2-D Permeability Tensor for Fractured Rock Masses. Int J Rock Mech Min Sci Geomech Abs 33: 17-37.

Zoback MD (2007) Reservoir Geomechanics. Cambridge University Press, New York, 449 p.